

Notch1-driven T-ALL chromatin landscape is regulated by Tcf1 in hematopoietic progenitors

Présentée le 21 octobre 2021

Faculté des sciences de la vie

Unité du Prof. Radtke

Programme doctoral en approches moléculaires du vivant

pour l'obtention du grade de Docteur ès Sciences

par

Mateusz Waldemar ANTOSZEWSKI

Acceptée sur proposition du jury

Prof. E. Oricchio, présidente du jury

Prof. F. Radtke, Dr U. Koch, directeurs de thèse

Dr E. Laurenti, rapporteuse

Dr J. Meijerink, rapporteur

Prof. B. Deplancke, rapporteur

Abstract

Notch1 receptor signaling is essential for T cell fate specification and physiological thymic T lymphocyte development. Its dysregulation and oncogenic activation are detected in almost 80% of pediatric patients suffering from T cell acute lymphoblastic leukemia (T-ALL). T-ALL is a hematological neoplasm arising from immature thymocytes.

T cell factor 1 (Tcf1) is a crucial well-known transcription factor regulating the early stages of thymocyte maturation and Notch1 directly drives the expression of Tcf1 during normal T cell development. Here we assessed the role of Tcf1 in modulating chromatin topology which enables the initiation of T-ALL at the level of early hematopoietic progenitors. This allows for the discovery of stage-setting epigenetic regulators establishing a leukemia-prone chromatin landscape during Notch1-driven disease initiation.

We found Tcf1 to be an essential mediator of Notch1 signaling during T-ALL induction. Inactivation of Tcf1 prevented leukemogenesis despite oncogenic Notch1 activation. Genomic analysis of hematopoietic progenitors revealed T cell lineage specification to be essential in T-ALL initiation prior to the appearance of phenotypic features of T cells. The expression of genes associated with the T cell lineage was dependent on Notch1 and Tcf1. Chromatin accessibility, chromosome conformation capture and ChIP-seq analysis revealed the co-regulatory epigenetic function of Notch1 and Tcf1 in imprinting a leukemic chromatin landscape.

Epigenetic modulation of distal enhancers which regulate leukemic oncogenes has been well described in patient-derived T-ALL cells. The Notch1-*Myc* enhancer region was shown to be indispensable in the process of leukemogenesis. We have identified a novel regulatory locus, dependent on Tcf1 and Notch1, essential for the expression of *Myc* in pre-T-ALL cells. This genomic region termed Tcf1-regulated *Myc* enhancer (*TMe*) was highly conserved across species. *TMe* was essential for the transition of pre-leukemic cells to a transplantable full-blown T-ALL but was dispensable for the physiological development of T cells. After activation of the enhancer in hematopoietic progenitors, this regulatory site remained accessible and bound by Tcf1 in murine and human T-ALL cells.

Tcf1 is therefore required for shaping the epigenetic landscape of hematopoietic progenitors overexpressing oncogenic Notch1, and thus regulates the expression of genes involved in leukemogenesis.

Keywords: T-ALL, Notch1, Tcf1, Myc, HSC, epigenetic, initiation, chromatin, enhancer, *TMe*.

Résumé

La signalisation du récepteur Notch1 est essentielle à la différenciation des cellules T et au développement physiologique des lymphocytes T thymiques. Son dérèglement et son activation oncogénique sont détectés dans près de 80% des patients pédiatriques souffrant de leucémie lymphoblastique aiguë de type T (LLA-T). La LLA-T est un cancer hématologique provenant de thymocytes immatures.

Le T cell factor 1 (Tcf1) est un facteur de transcription crucial bien connu qui régule les premières étapes de la maturation des thymocytes et Notch1 dirige directement l'expression de Tcf1 au cours du développement normal des cellules T. Dans ce projet, nous avons examiné le rôle du facteur Tcf1 dans la modulation de la topologie de la chromatine qui conduit à l'initiation des LLA-T au niveau des progéniteurs hématopoïétiques précoces. Ceci permet de découvrir les régulateurs épigénétiques qui établissent un paysage chromatinien propice à la leucémie lors de l'initiation de la maladie par Notch1.

Nous avons découvert que Tcf1 est un médiateur essentiel de la signalisation Notch1 pendant l'induction des LLA-T. L'inactivation de Tcf1 a empêché la leucémogénèse malgré l'activation oncogénique de Notch1. L'analyse génomique des progéniteurs hématopoïétiques a révélé que la spécification de la lignée des cellules T est essentielle dans l'initiation de la LLA-T avant l'apparition des caractéristiques phénotypiques de ces cellules. L'expression des gènes associés à la lignée des cellules T dépendait de Notch1 et de Tcf1. L'accessibilité de la chromatine, la capture de la conformation des chromosomes et l'analyse ChIP-seq ont révélé la fonction épigénétique corégulatrice de Notch1 et Tcf1 dans l'empreinte d'un paysage chromatinien leucémique.

La modulation épigénétique des amplificateurs distaux qui régulent les oncogènes leucémiques a été bien décrite dans les cellules LLA-T dérivées de patients. La région de l'amplificateur *Myc* dépendant de Notch1 s'est avérée indispensable dans le processus de leucémogénèse. Nous avons identifié un nouveau locus régulateur, dépendant de Tcf1 et Notch1, essentiel à l'expression de *Myc* dans les cellules pré-LLA-T. Cette région génomique appelée Tcf1-regulated *Myc* enhancer (*TMe*) était hautement conservée à travers les espèces. La *TMe* était essentielle pour

la transition des cellules pré-leucémiques vers une LLA-T transplantable, mais n'était pas nécessaire pour le développement physiologique des lymphocytes T. Après l'activation de l'amplificateur dans les progéniteurs hématopoïétiques, ce site régulateur restait accessible et lié par Tcf1 dans les cellules LLA-T murines et humaines.

Tcf1 est donc nécessaire pour façonner le paysage épigénétique des progéniteurs hématopoïétiques surexprimant l'oncogène Notch1, et régule ainsi l'expression des gènes impliqués dans la leucémogenèse.

Mots-clés: LLA-T, Notch1, Tcf1, Myc, CSH, épigénétique, initiation, chromatine, amplificateur, *TMe*.

Table of contents

Abstract	3
Résumé	5
List of figures	10
List of tables	12
Abbreviations	13
1. Introduction	17
1.1. Regulation of tissue development and homeostasis	17
1.1.1. Notch signaling pathway in development.....	17
1.1.2. Role of the pathological Notch signaling in tumorigenesis	22
1.1.3. Canonical Wnt signaling	22
1.2. Hematopoiesis	24
1.3. T lymphocyte development	29
1.4. T cell acute lymphoblastic leukemia (T-ALL).....	33
1.5. Epigenetic regulation of gene expression	39
2. Aims of the thesis.....	43
3. Materials and methods.....	45
3.1. Animal procedure	45
3.2. Murine models.....	45
3.3. Generation of <i>TMe</i> CRISPR-Cas9-deleted mouse strain.....	46
3.4. Bone marrow chimeras and transplantation assays.....	46
3.5. Isolation of human hematopoietic progenitor cells	46
3.6. Culture of cell lines.....	47
3.7. Retroviral and lentiviral vectors	48
3.8. Production of viral particles and transduction.....	48
3.9. Flow cytometry-based analysis of hematopoietic cells.....	49
3.10. Western blot.....	50
3.11. ATAC-seq	50

3.12.	RNA-seq	51
3.13.	ChIP-seq.....	51
3.14.	ChIP-qPCR	52
3.15.	Reverse ChIP	52
3.16.	In situ Hi-C	53
3.17.	Analysis and visualization software.....	53
3.18.	Quantification and statistics	53
3.19.	Bioinformatic analyses	54
3.19.1.	Evolutionary conservation of genomic sequence	54
3.19.2.	Analysis of RNA-seq	54
3.19.3.	Analysis of ChIP-seq	54
3.19.4.	Analysis of ATAC-seq	55
3.19.5.	Differential analysis and pathway enrichment	55
3.19.6.	Analysis of in situ Hi-C	56
3.20.	Data availability.....	59
4.	Results	61
4.1.	<i>Tcf7</i> loss impairs T cell development downstream of Notch1.....	61
4.2.	<i>Tcf7</i> is essential for Notch1-mediated T-ALL induction	63
4.3.	Oncogenic Notch1 requires Tcf1 to induce a T cell-specific gene expression program in early hematopoietic progenitors.....	67
4.4.	Tcf1 regulates chromatin accessibility in <i>N1/C</i> -expressing LSKs.....	71
4.5.	Dynamic large-scale genomic interactions promoting leukemogenesis rely on Notch1 and Tcf1	75
4.6.	Establishment of enhancer-promoter interactions in T-ALL initiation partly depends on <i>Tcf7</i>	79
4.7.	A novel Tcf1-regulated <i>Myc</i> -enhancer region is essential for Notch1-driven T-ALL progression	84
5.	Conclusion and discussion.....	92

5.1. β -catenin is dispensable for Tcf1-dependent Notch1-driven T-ALL.....	94
5.2. Conditional <i>Tcf7</i> -deficiency impedes T cell development without inducing lymphomagenesis.....	95
5.3. Investigation of early T-ALL initiation events in hematopoietic progenitors .	96
5.4. Epigenetic role of Tcf1 in Notch1-driven T-ALL.....	98
5.5. Analysis of 3D chromatin topology in LSKs.....	99
5.6. Tcf1 and Notch1 activate the novel identified <i>TMe</i> region in leukemia-prone LSKs	101
5.7. Identification of potential therapeutic targets regulating <i>TMe</i>	102
6. Annex.....	104
7. Bibliography	112
Acknowledgments	133
Curriculum Vitae.....	135

List of figures

Figure 1 – Canonical Notch signaling pathway _____	19
Figure 2 – Models of hematopoietic differentiation of HSCs to differentiated cells _	26
Figure 3 – Physiological development of T cells _____	32
Figure 4 – Mutations of NOTCH1 receptor identified in pediatric T-ALL patients __	35
Figure 5 - Cell-specific superenhancer regions of oncogenic MYC _____	37
Figure 6 - Spatial organization of chromatin compaction in the nucleus _____	40
Figure 7 - Physiologic T cell development requires Notch1 and Tcf1 _____	62
Figure 8 – Initiation of Notch1-driven T-ALL is Tcf7-dependent _____	64
Figure 9 – Suppression of erythroid, myeloid and B lineages is mediated by Notch1 _____	65
Figure 10 – β -catenin is dispensable in Notch-driven T-ALL _____	66
Figure 11 - Tcf7 regulates expression of genetic T cell signature in bone marrow progenitors in response to oncogenic Notch1 _____	69
Figure 12 – Notch1 regulates non-T cell developmental process independently of Tcf1 _____	69
Figure 13 – Ectopic expression of Tcf7 in Notch1-proficient BM is not sufficient to induce T-ALL _____	70
Figure 14 - Notch1 and Tcf1 epigenetically establish T lineage specification in early bone marrow progenitors _____	73
Figure 15 – Lineage specification dependent on Notch1 and Tcf1 in early bone marrow progenitors _____	74
Figure 16 – Genome-wide analysis of dynamic compartments A and B by in situ Hi-C _____	77
Figure 17 - Notch1 and Tcf1 regulate 3D organization of chromatin domains ____	78
Figure 18 - Analysis of chromatin loops regarding regulation by Notch1 and Tcf1 _	80
Figure 19 – Activation of chromatin loops is mediated by Notch1 and Tcf1 _____	82
Figure 20 – Notch1 and Tcf1 regulation involving distal elements _____	83
Figure 21 – Tcf1 exerts a crucial regulation within distal Myc enhancers _____	86
Figure 22 – TCF1 with NOTCH1 initiates genetic T cell signature and activates TMe _____	87

Figure 23 – Tcf1 directly regulates NMe and TMe regulatory elements in T-ALL cells	88
Figure 24 - Physiological analysis of hematopoietic lineages in mice with genomic deletion of Tcf1-regulated Myc enhancer (TMe)	89
Figure 25 – Loss of TMe inhibits overexpression of Myc during T-ALL progression	91
Figure 26 - Model of Tcf1-dependent regulation of chromatin accessibility and topology in Notch1-driven T-ALL	94
Annexed Figure 1 – Quality of data generated by <i>in situ</i> Hi-C on <i>ex vivo</i> LSKs	104

List of tables

Table 1 – Cell surface markers allowing for identification of murine and human hematopoietic progenitors _____ 26

Table 2 - Immunophenotype subtypes of T cell acute lymphoblastic leukemia (T-ALL) _____ 34

Annexed Table 1 – Genotyping primers _____ 105

Annexed Table 2 - Antibodies _____ 106

Annexed Table 3 - TPM (Transcripts Per kilobase Million) expression values for selected genes _____ 110

Abbreviations

- AGM – aorta-gonad-mesonephros
- ANOVA – analysis of variance
- ATAC-seq – Assay for Transpose-Accessible Chromatin with high-throughput sequencing
- BM – bone marrow
- BS – binding site
- CB – cord blood
- CD – cluster of differentiation
- ChIP-seq – Chromatin Immunoprecipitation with sequencing
- CLP – common lymphoid progenitors
- CMP – common myeloid progenitors
- CRISPR – Clustered Regularly Interspaced Short Palindromic Repeats
- DLL – delta-like ligand
- DN – double negative (CD4⁻ CD8⁻)
- DNA – deoxyribonucleic acid
- DP – double positive (CD4⁺ CD8⁺)
- E-G – enhancer-gene
- EGF – epidermal growth-factor like
- EPFL – École polytechnique fédérale de Lausanne
- ETP – early thymic progenitors
- FACS – fluorescence-activated cell sorting
- FDR – false discovery rate
- GFP – green fluorescent protein
- GOBP – Gene Ontology (GO) Biological Process
- GoF – gain-of-function
- HD – heterodimeric domains
- HMG – high mobility group
- HSC – hematopoietic stem cell
- IGV – Integrative Genomics Viewer
- IRES – internal ribosome entry site

- KR – Knight-Ruiz
- LFC – logarithmic fold change
- LMPP – lymphoid-primed multipotent progenitors
- LNR – Lin12/Notch repeats
- LoF – loss-of-function
- LSK – lineage⁻ Sca1⁺ cKit⁺
- LT – long term (HSCs)
- MAML – mastermind-like
- MHC – major histocompatibility complex
- MPP – multipotent progenitors
- N1IC – Notch1 intracellular domain, here with truncated PEST domain
- NICD – Notch intracellular domain
- NMe – Notch-*Myc* enhancer
- NRR – negative regulatory region
- ORA – over-representation analysis
- PBL – peripheral blood lymphocytes
- PC – principal component
- PCR – polymerase chain reaction
- poly(I:C) – polyinosinic:polycytidylic acid
- R26 – *Rosa26* promoter
- RBPJ - recombinant signal binding protein for immunoglobulin κ J region
- RNA – ribonucleic acid
- RVP – retroviral particles
- scRNA-seq – single cell RNA sequencing
- SEM – standard error of the mean
- sgRNA – single guide RNA
- SP – single positive
- ST – short term (HSCs)
- TAD – topologically associating domain
- T-ALL – T cell acute lymphoblastic leukemia
- TCD – T cell development
- TCR – T cell receptor

- TF – transcription factor
- TMe – Tcf1-regulated *Myc* enhancer
- TPM – transcript per kilobase million
- TSS – transcription start site

1. Introduction

1.1. Regulation of tissue development and homeostasis

Mammalian development depends on a precisely orchestrated acquisition of different fates by cells in developing tissues. Cellular phenotype and their function in tissue is determined by the expression of genetic programs (1). Differentiation of the most omnipotent cells in the developing zygote to the fully committed mature cells progresses through pluripotent, multipotent, and oligopotent cellular states. Various conserved signaling pathways govern developmental and pathological processes via specific gene expression signatures (2–4). Transcription factors are downstream effector proteins of these signaling pathways that regulate the expression of target genes via binding to the promoters and enhancers. Moreover, modulation of the genomic signatures is further regulated through non-genetic, epigenetic, mechanisms involving modulation of chromatin accessibility and DNA looping which connects distal regulatory elements with promoters (5,6). As demonstrated by the development of induced pluripotent stem cells (iPSC), ectopic expression of a limited number of transcription factors (i.e., Oct4, Sox2, Klf4 and Myc) can fully re-program terminally differentiated cells to an embryonic-like cell state (7). During physiological hematopoiesis the cellular differentiation of blood lineages is governed by master regulators that initiate and assure proper differentiation of diverse cell types of the blood (8). Dysregulation of the physiological signals mediated by these master regulators can lead to the tumorigenesis (9).

Understanding how multicellular organisms develop and how they maintain cellular homeostasis is largely possible due to acquired knowledge about conserved signaling pathways.

1.1.1. Notch signaling pathway in development

Discovered over a century ago in *Drosophila melanogaster*, the Notch signaling pathway is evolutionarily conserved between species and has been studied extensively in mammalian systems (10,11). Although elegant studies reported regulation of biological functions also by non-canonical Notch signaling, the canonical

pathway was reported to have predominant importance in physiological hematopoiesis and T cell development; hence this will be addressed here (12).

Canonical Notch signaling relies on *trans* interactions between two adjacent cells expressing ligands or receptors. Such binding of receptors with ligands is associated with activation of the signaling cascade, while interactions in *cis*, between receptor and ligand on the same cell, are linked to pathway inhibition (13,14). Four Notch receptors were identified in mammalian cells, Notch1 to Notch4, interacting with either Delta-like ligands (Dll1, Dll3, and Dll4) or with Jagged 1/Jagged 2 ligands (15). Notch receptors are transmembrane proteins with a heterodimeric extracellular fragment. We distinguish biomechanically distinct domains of the extracellular part of the receptor: epidermal growth factor-like (EGF) repeats followed by a negative regulatory region (NRR) consisting of Lin12/Notch repeats (LNR) and heterodimeric domains (HD) (14,15). Interaction between ligands and the receptors occurs in antiparallel orientation, involving EGF repeats 10-13 with possible involvement of EGF 8-10 for strengthening of the signal (14). Subsequently, this physical interaction leads to a conformational change in the NRR domain, exposing the cleavage site for ADAM metalloproteinases to release the extracellular domain (Figure 1). Interestingly, the extracellular domain is then degraded not by the receptor-expressing cell but through lysosomal degradation in ligand-expressing cells. In the signal-receiving cell, signal transduction is dependent on the liberation of the Notch intracellular domain (NICD) from a transmembrane fragment of the receptor, which liberation is mediated by γ -secretase. Subsequently, NICD translocates through endosomes to the nucleus and binds to DNA-bound RBPJ (recombinant signal binding protein for immunoglobulin κ J region) to transcriptionally activate the complex with members of the MAML (Mastermind-like) protein family coactivators (Figure 1) (14–18).

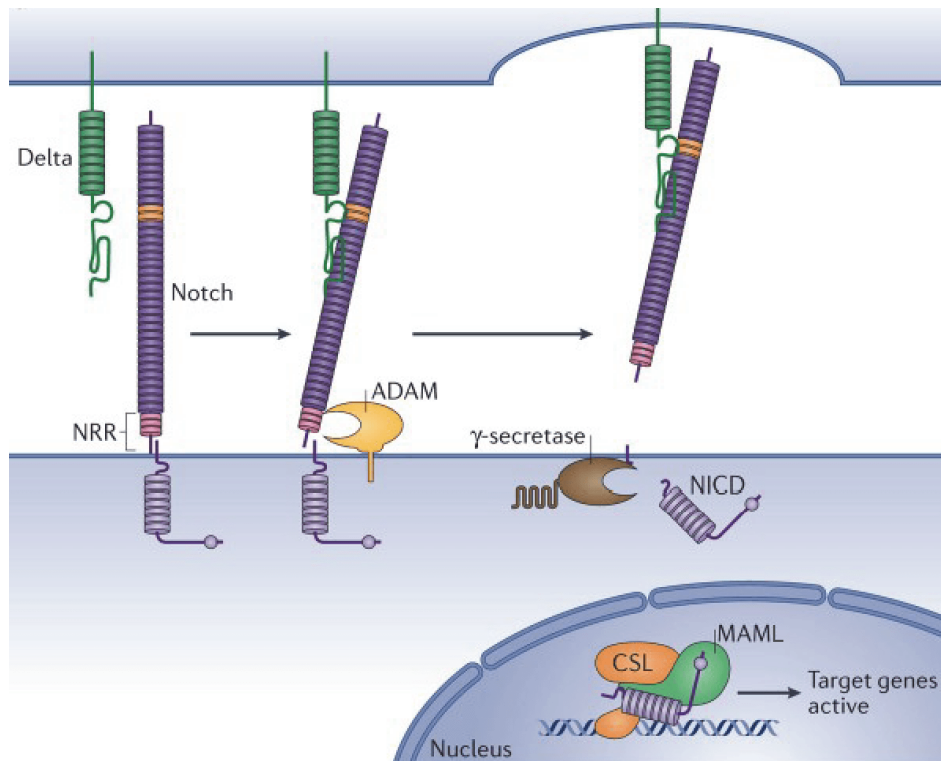


Figure 1 – Canonical Notch signaling pathway

Activation of canonical Notch signaling relies on the interaction between the ligand and the receptor. Amongst mammalian ligands we distinguish Delta-like 1, 3, 4 and Jagged 1, 2 that can bind four mammalian Notch receptors (Notch1-Notch4). Interaction between ligand and the receptor leads to conformational changes at the NRR (negative regulatory region) of the Notch receptor, allowing for proteolytic cleavage by ADAM metalloprotease. This is followed by a subsequent proteolytic cleavage mediated by the γ -secretase protein complex liberating NICD (Notch intracellular domain), which then translocates to the nucleus to form a transcription factor complex with DNA-bound CSL (CBF1, Suppressor of Hairless, Lag-1; also called RBPJ) and MAML (Mastermind-like). Figure adapted from Bray, Nature Reviews Molecular Cell Biology, 2016 (15).

Although Notch signaling relies solely on interaction between ligand and receptor with subsequent translocation of the NICD to the nucleus, the resulting pathway signal amplitude is regulated on multiple levels. First, number of gene copies of ligands and the receptors have proven to be important checkpoints of developmental processes, with a single copy of a gene being insufficient for the development of heart and marginal zone B cells (10,19). As the activation of the pathway relies on *trans* interactions between signal-sending cells and signal-receiving cells, neighboring cells need to express exclusively either ligands or receptors. Regulatory mechanisms for such expression patterns between two neighboring cells were identified as the negative feedback loops (15). The interface of interaction

between the Notch receptor and its ligand has also been directly linked to the affinity and strength of the induced signal; Dll4 exhibiting significantly stronger signal than the weaker Jagged ligands (14). Furthermore, the extracellular domain of the Notch receptor is frequently modified at EGF repeats. Identified O-fucose modifications, mediated by members of Fringe glucosyl-transferases at specific residues of the extracellular domain, play an important role in modulating the affinity between ligand and the receptors. Interestingly, such modifications of the extracellular domain of the receptor enhance interaction between Notch1 and Dll1, while also decreasing the strength of interaction between Notch1 and Jagged1 (14,15,20). Once the extracellular domain of the receptor is successfully cleaved, the intracellular domain is controlled by a regulatory mechanism which affects Notch signaling output. The intracellular domain of Notch receptors contains an important regulatory unit known as the PEST domain. When the modulation of activation strength is required, the PEST domain is first phosphorylated by CDK8 kinase to then be ubiquitinated by FBXW7 E3 ubiquitin ligase, thus targeting the intracellular domain for proteasomal degradation (2,21). Once the nuclear Notch-transcription-activating complex with RBPJ is formed, the final tuning of the signaling output strength occurs. Binding of the N1ICD (Notch1 intracellular domain) to monomeric sites of DNA-bound RBPJ is a predominant mechanism of their interaction at the gene promoters. However, when regulating enhancers N1ICD can form a protein dimer between two head-to-head oriented RBPJ sites spaced by 15 to 17 base pairs. Such dimeric N1ICD-RBPJ complexes are considered the main mechanism that contributes to strong transcriptional activation mediated by N1ICD in pathological cells (22).

As much as Notch signaling is conserved between species, it is involved in an abundance of various physiological processes (10). Notch has overwhelmingly diverse involvement in development, explicitly regulating many processes that can be characterized most broadly as cell stemness and differentiation decisions (2,23). Ligand-expressing cells of particular differentiated phenotype or cellular fate may then affect cellular fate commitment of neighboring receptor-presenting cells. Notch regulates cell fate decisions from early processes in developing embryos to homeostasis in adult organisms. In somitogenesis oscillations are restricted spatiotemporally through expression of genes *Hes7*, *Hes1* and *Hey1*. Their expression is controlled by Notch receptor signaling activated through interaction with Dll1 and

Dll3 ligands (2). Next, vascular formation during angiogenesis has been identified as being dependent on Notch signaling. During branching angiogenesis, the transmission of Notch signals from tip to stalk cells through Dll4 and Jagged1 ligands regulates the levels of VEGF receptors to restrict branching and promote vascular perfusion (2,24). On top of having a prominent role in vasculature development, Notch1 and its downstream effectors *Hey1* and *Hey2* regulate endocardial and myocardial differentiation (2).

The role of the Notch signaling pathway in hematopoiesis was best documented in embryonic hematopoiesis and lymphoid development. Definitive hematopoietic stem cells (HSCs) are generated during mammalian embryogenesis from the hemogenic endothelium at the aorta-gonad-mesonephros (AGM) (25,26). In this biological phenomenon of endothelial to hematopoietic transition, HSCs are generated with full differentiation capacity from endothelial cells. Generated stem cells give rise to lymphoid, myeloid, and erythroid lineages in lethally-irradiated recipients (26). Notch is essential for the development of HSCs in the AGM by regulating the expression of well-established transcription factors such as *Gata2* and *Runx1* (25,27). Genetic loss-of-function (LoF) approaches revealed that canonical Notch signaling during adult hematopoiesis appears to be dispensable for HSC maintenance under physiological conditions *in vivo* (26,28,29). Interestingly, even though loss of *Notch1* and *Notch2* demonstrated a lack of contribution to the self-renewal of HSCs, their deletion led to pronounced inhibition of lymphoid lineage differentiation (28). Genetic manipulation of *Notch2*, in gain-of-function (GoF) and LoF studies, determined its essential role for differentiation of splenic B cells to marginal zone B cells and not to follicular B cells (27,30,31). Finally, the development of T lymphocytes in the thymic microenvironment is strongly dependent on Notch1-signaling, especially during T cell lineage commitment and early development of immature thymocytes (27,32–34). Thymopoiesis and involvement of Notch1 in the development of early T cells will be discussed separately.

1.1.2. Role of the pathological Notch signaling in tumorigenesis

Fine-tuning of the signaling pathway output is essential for maintenance of the cellular homeostasis. Changes in the strength of the signaling output deregulate physiological processes and can lead to the formation of tumors. Cancer stem cells are considered to be the cells of origin for developing tumors and they rely on the signaling from conserved pathways, including Notch (35).

Multiple reports have documented tumor suppressing or oncogenic involvement of Notch signaling in tumor initiation and progression. A tumor suppressive role for the Notch pathway has been described for the first time in skin basal cell carcinoma in tissue-specific Notch1-deficient murine models (36). Moreover, loss of Notch signaling in tumorigenesis also drives, for instance, small-cell lung cancer and hepatocellular carcinoma (37).

An abundance of studies address the oncogenic potential of Notch1 in hematological malignancies, such as T cell acute lymphoblastic leukemia (T-ALL) and B-cell chronic lymphocytic leukemia (B-CLL) (11,38). Oncogenic Notch1 signaling was described extensively as a driver of tumor-initiation processes, but it is also essential for progression and survival of T-ALL leukemic cells, as demonstrated by targeting Notch1 with γ -secretase inhibitors or with competitors for binding with RBPJ (for instance CB-103) (17,39). Moreover, oncogenic dependency on Notch-mediated epigenetic regulation of chromatin topology in tumorigenesis was described in triple negative breast carcinoma (40).

1.1.3. Canonical Wnt signaling

Like Notch signaling, Wnt signaling is implicated in many processes during development and is essential for tissue homeostasis in adults. Wnt signaling pathway in mammals was first identified thanks to detection of a tumor-inducing insertion in a gene called *Int1* (or *Wnt1*) in mouse mammary carcinoma already in 1982. The findings in non-mammalian systems were described even earlier in 1976, with reports describing mutations of *Wnt1* homologs affecting morphogenesis

of *Drosophila melanogaster* (4,41). These alterations of the gene demonstrated strong involvement of the pathway in tissue homeostasis and morphogenesis.

Canonical Wnt signaling is dependent on β -catenin driving the expression of target genes in a transcriptionally active nuclear complex with Tcf/Lef (4,41). In the absence of Wnt signaling, the abundance of β -catenin is controlled by a cytoplasmic destruction complex, enabling the proteasomal degradation of β -catenin (41). The destruction complex is formed by the tumor suppressors Axin1 and Apc, together with kinases such as Ck1 α and Gsk3 β . Ck1 α followed by Gsk3 β phosphorylates the N-terminal domain of β -catenin, which marks the protein for subsequent ubiquitination followed by proteasomal degradation (4,42). Transduction of the signal is initiated by binding of secreted Wnt ligands to the membrane-bound receptor Frizzled and the co-receptors Lrp5 and Lrp6. Subsequently, Lrps are phosphorylated by Ck1 γ and Gsk3 β which mediates membrane translocation of Axin1 to inactivate the destruction complex (4). With the inactivation of the destruction complex, β -catenin is stabilized and accumulates in the cytoplasm. A portion of cytoplasmic β -catenin translocates to the nucleus and binds to the Tcf/Lef family members of transcription factors in order to form a transcriptional activation complex driving gene expression (4,41,42).

Among the many processes dependent on the canonical Wnt signaling pathway, it is vital to recognize the maintenance of intestinal stem cells and hair stem cells, and its involvement in liver homeostasis. The transformation of intestinal crypt cells is associated with LoF mutations of *APC* leading to the formation of adenomas. Moreover, a subset of patients suffering from liver hepatocellular carcinoma carries inactivating mutations of *CTNNB1* (encoding for β -catenin) and *AXIN1* (41,42). On the other hand, the contribution of Wnt signaling in physiological hematopoiesis and T cell development has been reported over many years (43–45). Induction of mutations in *Apc* leading to different Wnt dosages suggest possible involvement of canonical Wnt signaling in the fitness of HSCs (46), but elegant LoF studies definitively demonstrated that β -catenin-mediated Wnt signaling is not essential neither for hematopoiesis nor for thymopoiesis (47–49). Although not essential for physiological hematopoiesis, the pathological Wnt pathway has been linked to the maintenance of leukemic stem cells in T-ALL (50).

1.2. Hematopoiesis

Blood is a one-of-a-kind liquid connective tissue. All its cellular components are suspended in plasma, which allows them to execute necessary biological functions throughout the body. Circulating cells in the blood originate from a specialized microenvironment localized in adult animals in the bone marrow (BM), where HSCs during hematopoiesis give rise to all blood lineages.

Stem cells are a distinguished group of cells identified in most adult human tissues. They possess a unique characteristic of self-renewal paired with an ability to differentiate into progenies (51). Historically, Ernst Haeckel proposed the first hypothetical models of stem cells, while in the context of the blood system the work of Artur Pappenheim described ancestor cells giving rise to differentiated hematopoietic cells (51). However, experimental confirmation of the existence of HSCs residing in the bone marrow – supporting previous speculations – was finally provided over 60 years later. The transplantation of isolated marrow into recipient mice depleted of HSCs by X-ray radiation allowed for reconstitution of progenitors (52). Since then, transplantation-based experiments have been considered the gold standard for *in vivo* assessment of HSCs, as they directly rely on critical characteristics of investigated cells: their abilities to grow and populate depleted hematopoietic niche (self-renewal potential) and to give rise to diverse functional components of the blood (multipotent differentiation). Under physiological conditions, stem cells are known to be quiescent and to divide asymmetrically to maintain the pool of undifferentiated cells (53,54). The self-renewal and multipotency characteristics of stem cells are essential for developmental processes established already in embryos and retained for tissue homeostasis.

Blood formation processes are initiated in HSCs, which subsequently differentiate into erythroid, myeloid, and lymphoid cells. With progressive steps of hematopoiesis, progenies irreversibly lose their ability to generate diverse cell types in favor of specialization. On the very pinnacle of hematopoiesis reside multipotent cells, so-called, long term-HSCs (LT-HSCs) and short term-HSCs (ST-HSCs, also termed MPP1) (Figure 2A) (55). LT-HSCs are the most immature cells, the least actively undergoing cell cycle, but with the highest self-renewal potential that remains unexhausted throughout the life of an organism (55,56). On the other hand, ST-HSCs

are shorter-lived and more actively cycling while remaining multipotent (55,56). Notably, both populations of HSCs provide reconstitution of a recipient bone marrow after transplantation, but ST-HSCs do not contribute to long-term persisting hematopoietic output (57). These minor functional differences between the two types of HSCs with subsequent identification of downstream progenies does not allow to distinguish clearly between the identities of these cells. Therefore, in various models of hematopoietic trees, they are usually referred to in a simplified manner as HSCs (Figure 2B and C) (56,58).

Along with the steps of irreversible differentiation of HSCs in canonical models of hematopoiesis, we can further distinguish three states of multipotent progenitors (MPP2-4) (Figure 2B) (54,56,58). They progressively adopt restricted self-renewing potential with skewing towards differentiated hematopoietic cells (44). MPP2 and MPP3 are considered to be biased toward myeloid lineages with myeloid cells originating from common myeloid progenitors (CMPs), while MPP4 cells differentiate towards lymphoid lineages through the intermediate state of common lymphoid progenitors (CLPs) (Figure 2A and B) (44,54,59). The more recent identification of common progenitors of neutrophils and B, T, NK cells, however introduced an adaptation of the model with lymphoid-primed multipotent progenitors (LMPPs) (Figure 2B) (60). Finally, progenitor output from bone marrow gives rise to all the hematopoietic cell types, such as erythrocytes, megakaryocytes, monocytes, neutrophils, eosinophils, basophils, dendritic cells, NK cells, B cells, and T cells.

The establishment of hematopoiesis models within the hematopoietic tree was predominantly based on the analysis of bulk populations of cells identified by their expression of surface markers (membrane-bound proteins), thus allowing for purification by means of fluorescence-activated cell sorting (FACS) techniques. Then, isolated cells would undergo transplantation-based experimentation *in vivo* or be subjected to *in vitro* assays relying on self-renewal properties of HSCs to create colonies (in colony-forming units experiments). While murine hematopoiesis *bona fide* markers have been identified and associated with each progenitor population, analysis of human HSCs is restricted to rather approximate markers (Table 1) (56,61,62).

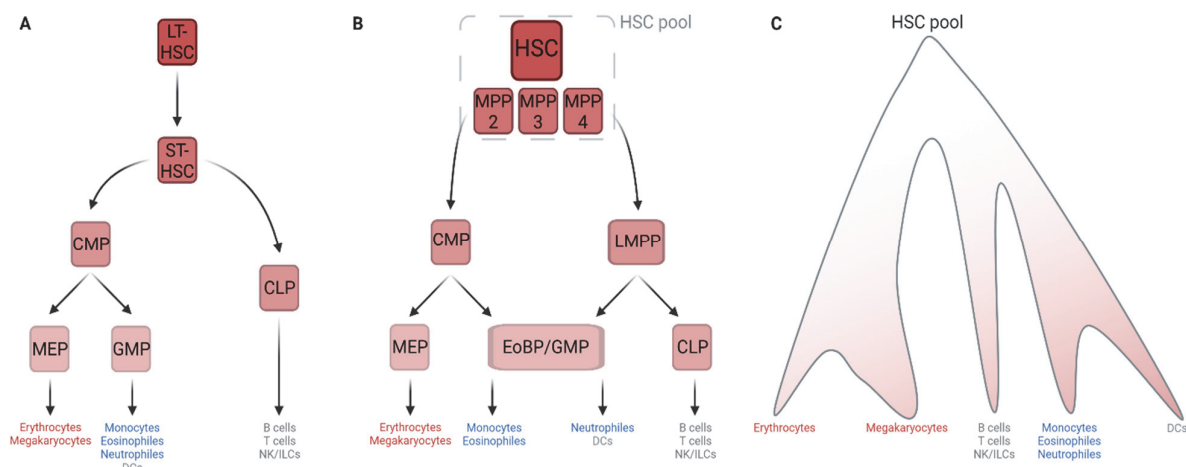


Figure 2 – Models of hematopoietic differentiation of HSCs to differentiated cells

A, The historically first hematopoietic tree showing clear separation between erythroid, myeloid and lymphoid lineages. **B**, Adapted model of hematopoiesis with multipotent progenitors shared between differentiated lineages. **C**, Corrected hematopoietic flux after recent developments from lineage tracing experiments and genomic analysis. A prominent differentiation route from HSCs (hematopoietic stem cells) to megakaryocytes is depicted with distinct flux towards myeloid and lymphoid lineages. Created with BioRender with figure from Laurenti and Göttgens, Nature, 2018 (54).

The most immature hematopoietic progenitors in the murine bone marrow are commonly identified in a population of LSK cells, i.e., lineage⁻ (Lin⁻) Sca1⁺ CD117⁺ (cKit⁺), with human HSCs enriched in a population of Lin⁻ CD34⁺ CD38⁻ cells (Table 1).

	Murine markers	Human markers
HSCs	CD150 ⁺ CD135 ⁻ CD48 ⁻ CD34 ^{+/-}	CD90 ⁺ CD49f ⁺ CD45RA ⁻ CD35 ⁺ (CD11A ⁻) CD10 ⁻
MPP2	CD150 ⁺ CD135 ⁻ CD48 ⁺ CD34 ⁺	CD90 ⁻ CD49f ⁻ CD45RA ⁻ CD35 ⁻ (CD11A ⁺) CD10 ⁻
MPP3	CD150 ⁻ CD135 ⁻ CD48 ⁺ CD34 ⁺	
MPP4	CD150 ⁻ CD135 ⁺ CD48 ⁺ CD34 ⁺	

Table 1 – Cell surface markers allowing for identification of murine and human hematopoietic progenitors

HSCs (hematopoietic stem cells) are commonly characterized by the absence of hematopoietic lineage-specific markers. Together with multipotent progenitors, HSCs and MPPs (multipotent progenitors) are identified among the cells expressing Sca1 and CD117 in mouse, or expressing CD34 but not CD38 in humans. Table based on information presented in references (56,61–64).

In opposition to the classical hematopoietic tree with self-renewal HSCs at the hematopoiesis apex, came recent findings from single cell *ex vivo* experiments (65). Despite relatively well-defined surface markers, multiple reports showed that transplantation of FACS-purified single HSC cells into recipient mice resulted in a spectrum of reconstitution outcomes (54,57,65). Therefore, there is still considerable heterogeneity among HSCs in their self-renewal potential. On top of that, *in vivo* cell tracing experiments with intrinsic barcodes suggest that HSCs have minimal contribution to adult hematopoiesis, with a significant contribution of MPPs in hematopoietic output during post-embryonic life (8,66). Of note, selected single cell RNA-seq (scRNA-seq) data of *naïve* hematopoiesis and lineage barcoding studies disagree with models proposing rather limited hematopoietic contribution of HSCs, demonstrating the unmet need for further research (67–69).

As discussed above, HSCs are ought to have multipotent function – giving rise to all the blood cell types. This characteristic was also recently challenged in transplantation-based experiments and in lineage-tracing barcoding experiments *in vivo* combined with transcriptomic analysis (65,66). Undifferentiated populations of HSCs seem to possess early imprinted bias for their terminal cellular state, with a significant immature subset of HSCs biased towards megakaryocytes posing an essential route of differentiation in case of emergency hematopoiesis (Figure 2C) (57,65,66,70). Importantly, these revisited hematopoiesis models provided different perspectives for the process, where clear-cut delimitation of cellular states is impossible due to continuous changes throughout the process, as demonstrated with single cell multi-omics data and *in vivo* experiments with cellular barcoding (57,62,71). Not only do hematopoietic progenitors seem to have well-defined roles imprinted early in the differentiation, they can also adapt to environmental stimuli and adapt their lineage-bias to meet current output needs (8,57,70).

Adult HSC fate is dependent on genetic regulators driving the expression of genes involved in stemness and differentiation of progenitors. TFs controlling the gene expression of HSCs and their progenies are also dependent on other regulatory mechanisms, such as chromatin topology and post-transcriptional modifications (54,57). Furthermore, even though associations have been made between specific TFs and either ‘stemness’ (immature, most multipotent state of progenitors) or differentiation of HSCs, the continuity of current models of hematopoiesis does not

allow for clean separation of different TFs between differentiation ‘states’ (65,70,72). Indeed, multiple TFs previously associated with HSCs or MPPs are also found to be involved in lineage determinations, e.g., RUNX1 or GATA2 (70,72). Nevertheless, recent developments in single cell genomics and development of murine genetic reporter models demonstrated particular specificity for expression of α -*catulin* and *Hlf* to the most immature HSCs (70,73). Along the branches of the hematopoietic tree, bifurcation of MPPs towards erythroid lineages and lympho-myeloid lineages was also detected on the transcriptome level (Figure 1C). Specification of multipotent progenitors towards erythroid cells is associated with the expression of *CAR1*, *GATA2*, and *APOE*, while lympho-myeloid bias is regulated via, e.g., *FLT3*, *CD34*, *MPO*, and *IGH* (70). It is important to be aware of the plethora of genes showing shared and dynamic expression levels between lineage-specific progenitors, emphasizing the need for further research addressing the regulation of hematopoiesis with ‘omic’ approaches (62,74).

Physiological hematopoiesis towards lymphoid progenitors is dominant shortly after birth, with skewing of the hematopoietic output to myeloid lineages observed during ageing (72). Development of LMPP and CLP has been attributed to a specific set of TFs that are also involved in B cell and T cell development, providing evidence for imprinted bias at very immature hematopoietic progenitors. Investigation of bulk populations of progenitors *ex vivo* revealed lymphoid identity to be established by spatial regulation at different genetic loci and temporal regulation of binding at the regulatory sequences by TFs, e.g., BCL11A, EBF1, LEF1, RAG2, TCF1, and GATA3 (62,75–77). Unfortunately, recently reported scRNA-seq and multi-omic studies addressing *naïve* hematopoiesis, while focusing on myeloid development, do not specifically address lymphoid progenitors. Therefore, the investigation of T lymphocyte development focuses on the differentiation of bone marrow-derived CLP progenitors in the thymic microenvironment.

1.3. T lymphocyte development

T cells with B lymphocytes make up distinctive parts of the cell-adaptive immune response. T cell lymphoid progenitors undergo specific recombination of their surface receptors to develop specificity against peptides presented by major histocompatibility complexes (MHC) (78). Furthermore, development of T lymphocytes is locally restricted to thymus and aberration of this multifactorial process is associated with the development of leukemias (79–81).

The thymic epithelium is a unique biological structure supporting homing and lineage commitment of BM-derived oligopotent progenitors. Assessment of lineage potential of lymphoid progenitors identified BM-derived CLPs, with lymphoid-restricted potential, as the direct precursor of T lymphocytes (60,81,82). Circulating CLPs in response to chemokine signaling of CCR7 and CCR9 receptors activated by CCL19 and CCL25 ligands, respectively, enter thymus via postcapillary venules (83). They differentiate through stages of immature T cells by sequentially migrating through distinct anatomical thymic compartments: the cortex and subcapsular zone, adopting distinct developmental stages known as CD4⁻ CD8⁻ double negative (DN) cells (78,81). The development of immature T cells encompasses four (DN1-DN4) distinct phenotypical maturation stages (3). Differentiation between DN stages has been established based on the orchestrated expression of distinctive surface markers allowing for flow cytometric-based analysis, such as CD117, CD44, CD25, and CD27.

DN1 immature T cells or early thymic progenitors (ETP), are not yet committed to the T cell genetic program and are identified as CD117⁺ CD44⁺ CD25⁻ cells. Logically, the subsequent stage of immature T cells is defined as DN2 cells expressing CD44 and CD25, with a vital division of this developmental stage into DN2a and DN2b (34). At the transition between DN2a and DN2b, critical commitment to the T cell lineage occurs (34,84). The phenotypic transition marked by downregulation of CD117 antigen expression coincides with upregulation of the *Bcl11b* gene. Expression of *Bcl11b* is possible due to coordinated functions of stage-setting TFs Gata3 and Tcf1 (encoded by *Tcf7*) prior to *Bcl11b* expression and is then maintained due to Runx1 sustaining the expression of *Bcl11b* (85). Committed DN2b immature thymocytes further differentiate into either $\alpha\beta$ T cells or $\gamma\delta$ T cells. Mature $\gamma\delta$ T cells originate from the DN2b IL-7R α^{high} cells and mature at the DN3 stage in an *Id3* and *Egr*-dependent

manner (84,86). On the other hand, $\alpha\beta$ T cells differentiate to the DN3 stage, characterized as CD44⁻ CD25⁺ and then subdivided into DN3a and DN3b states based on either the lack or presence of CD27 expression, respectively. Moreover, a transition from DN3a to DN3b stage of T cell development (TCD) correlates with completed TCR β rearrangement and the so-called β -selection checkpoint. Established TCR β chain binds to pre-T α and CD3 to form a pre-TCR complex promoting survival of the cells (Figure 3) (81,87). The final stage of $\alpha\beta$ T cell development (DN4 immature T cells) before the expression of CD4, CD8 receptors, and before the rearrangement of TCR α , has been characterized by a lack of expression of CD44 and CD25 receptors (80,81,84).

Among maturing T cells, we can easily distinguish two main classes of T cells: those with $\alpha\beta$ TCR and with $\gamma\delta$ TCR rearrangement. Late developmental stages post DN immature thymocytes occur in the thymic cortex and medulla (81). CD4⁺ CD8⁺ double positive (DP) T cells with successful $\alpha\beta$ TCR rearrangement are subjected to the steps of positive and negative selection. In the process of positive selection, maturing T cells are selected for their binding with MHC via functional $\alpha\beta$ TCR. Subsequent negative selection eliminates thymocytes bearing high-affinity TCR β receptors strongly binding with 'self' MHC (33,88,89). Surviving cells develop into either CD4⁺ single positive (SP) T helper cells or CD8⁺ cytotoxic SP T cells. These steps are accompanied by the expression of, for instance, CD5 and selection with recognition of MHC class II or class I, respectively. Cell intrinsic processes leading to CD4 and CD8 bifurcation were attributed to CD4-promoting ThPOK and Foxp3 (necessary for the development of regulatory T cells), with Runx3, Tcf1 and Lef1 promoting CD8 T cells (90–93). On the other hand, tissue-resident $\gamma\delta$ T cells do not rely on classical MHC-mediated antigen recognition during development. $\gamma\delta$ TCR is crucial for the specification between $\alpha\beta$ and $\gamma\delta$ T cells, with the strong TCR-signal promoting $\gamma\delta$ T cells over $\alpha\beta$ T cells (86). Thymic selection of $\gamma\delta$ T cells is subsequently dependent on butyrophilins, thus this developmental route is divergent from $\alpha\beta$ T lymphocytes (86,94).

The successful commitment of lymphoid progenitors towards $\alpha\beta$ T lymphocytes is established by Notch signaling due to the interaction between the highly expressed

Dll4 ligands on the thymic cortex epithelium and Notch1 receptors presented on the surface of thymic seeding progenitors (CLPs) (78,84,95,96). In the absence of Notch signaling, early immature T cell progenitors (up to the DN2a stage) are able to generate NK cells, dendritic cells, granulocytes, or B cells (34,91). Notch signaling is essential for the development of DN cells up to the β -selection checkpoint (33). Expression of *Notch1* is sustained by Notch1 itself, via positive feedback regulation, and by E2A. Just before β -selection, thymocytes will downregulate Notch signaling ensuring proper selection and maturation of T cells (Figure 3) (32). Inhibition of Notch1 signaling is initiated by pre-TCR signaling that indirectly represses the expression of *Notch1* via Id3-mediated inhibition of *E2A* (97). Although Notch signaling is crucial for T cell lineage commitment, development, and maturation, each of the stages of thymocyte development mentioned above is strictly controlled by the complex interactions and activity of many different TFs downstream of Notch (85). Tight co-regulation of *Bcl11b*, *PU.1*, *Gata3*, *Runx1* and *Tcf7*, among others, was reported to be critical for the proper regulation of T cell potential and developmental stage transition. However, the outcome of the signaling cascades is usually strictly time- and context-dependent (Figure 3) (85,98–100).

Tcf1 is best known as a member of the canonical Wnt signaling pathway. The binding of β -catenin to TFs belonging to the Tcf/Lef family of a high mobility group (HMG) box transcription factors drives the expression of Wnt target genes (101). In the hematopoietic system, *Tcf7* is expressed in early thymocytes downstream of Notch1 signaling, without the contribution from β -catenin/Wnt pathway (102). Several studies reported a direct link between Notch signaling and Tcf1, as the Notch1-RBPJ transcription complex drives expression of *Tcf7* by regulation of its upstream enhancer (85,99,102). Tcf1 has been implicated to be a marker of the early thymic progenitor differentiation. Moreover, LoF experiments of *Tcf1*^{-/-} mice showed diminished proliferation of immature T cells, emphasizing the importance of Tcf1 for T cell maturation (103,104). Notably, the few Tcf1-deficient thymic progenitors that successfully mature into T cells generate CD4⁺ or CD8⁺ SP T cells due to increased *Lef1* expression, indicating potential redundancy of Tcf1 and Lef1 for maturation of thymocytes (99,105). Recent findings addressing the physiological role of Tcf1 in TCD at different stages highlighted the importance of Tcf1-related chromatin regulation. It has been suggested that Tcf1 has a pioneering chromatin-activating

function and can also inhibit the expression of Notch1-regulated genes in the late stages of thymopoiesis (106,107).

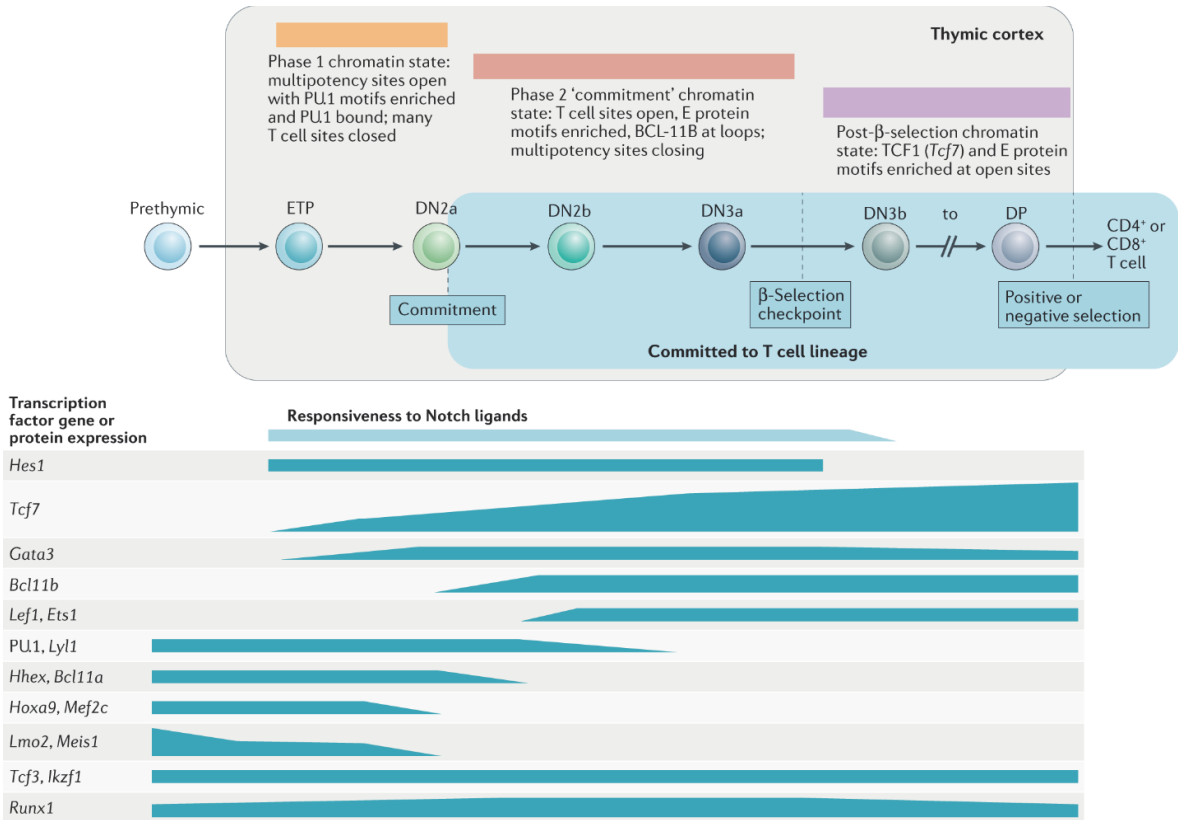


Figure 3 – Physiological development of T cells
 Pre-thymic progenitors from bone marrow (ETPs) differentiate in the thymic microenvironment to CD4⁺ and CD8⁺ T cells. Immature thymocytes pass through T cell lineage commitment phases due to the involvement of TFs and chromatin states in a tightly controlled fashion. The stages of early thymic progenitors to β-selection checkpoint after DN3a stage (double negative CD4⁻ CD8⁻ 3a stage) rely on the Notch signaling pathway. Expression profiles of TFs essential for TCD are depicted at the bottom. Figure adapted from Hosokawa and Rothenberg, Nature Review Immunology, 2021 (34).

Thymopoiesis has been scrutinized mainly using genetic mouse models due to limitations in studying human developmental processes, although such might be possible to overcome with recently described 3D thymic organoid cultures (108). Nevertheless, there are noteworthy differences between the physiological development of T cells in mice and humans. First, in humans the development of T cells is initiated already during gestation thus newborns have fully functional T lymphocytes, unlike murine thymopoiesis that is induced after birth. Because of such

discrepancy, thymic ablation in humans does not result in increased infection rates while severely affecting the repertoire of matured thymocytes (109,110). Moreover, mouse T cells are shorter-lived than humans. Finally, the contribution of the cells originating from the thymus compared with those from lymphoid organs shows that humans rely on peripheral turnover in contrast to strong thymic dependency in murine immunity (111).

Dysregulation of physiological processes governing thymic development of T cells initiates a malignant transformation of immature lymphocytes to T cell leukemias and lymphomas. For example, GoF mutations in various domains of the Notch1 receptor have been identified in a majority of pediatric T-ALL cases (112).

1.4. T cell acute lymphoblastic leukemia (T-ALL)

Acute lymphoblastic leukemias (ALL) are rare tumors of lymphoid cells. The estimated yearly incidence in the U.S. is 0.3% and less than 1% in the U.K. among all diagnosed cancer cases. While ALL affects patients in all age groups, it is more prevalent in pediatric population (patients from 0 to 19 years old). The estimated disease-associated 5-year survival ranges from 70 to 80% depending on risk factors and mutation profile (113,114). In particular, adults suffering from ALL have a worse prognosis with a 5-year survival of 40% (115). Thus, the progression of the disease and associated mortality has a more favorable prognosis in pediatric ALL cases.

Typically, patients suffering from ALL present with symptoms linked to infiltration of the bone marrow by the disease: fatigue related to anemia, increased risk of infection and bleeding due to leukopenia and thrombopenia (116,117). Diagnosis of ALL relies on the analysis of the peripheral blood and bone marrow. The presence of more than 25% of leukemic cells, also called blasts, in the bone marrow define T-ALL (115,118). Morphological analysis of cerebrospinal fluid is also frequently performed for the presence of leukemic cells in the nervous system as central nervous system infiltration by the leukemic cells puts patients into higher risk groups (115,119).

Identification of phenotypic subtype of the leukemia is possible with flow cytometric-based analyses, and allows to distinguish first between acute leukemia of B or T lymphocytes. Among all cases of ALL, those arising from T lymphocytes (T-ALL) constitutes only 15% of cases. Within T-ALL, five distinct subtypes can be identified, with cortical T-ALL having the best prognosis and ETP-ALL the worst (Table 2) (115,118,119). Diagnosis of patients also relies on cytogenic or genetic analysis. Genetic rearrangements or abnormalities associated with better prognosis are *TEL-AML1* fusions and mutation of *NOTCH1* and *FBXW7*. On the other hand, high-risk patients are diagnosed with clonal abnormalities, unmutated *NOTCH1/FBXW7* and deletions in chromosome 6, 7, and 17 (115). High-risk adult patients with cytogenetic aberrations have decreased survival at about 20% (118).

Subtypes	Antigens
pro-T ALL	cCD3 ⁺ sCD3 ⁻ CD1a ⁻ CD2 ⁺ CD5 ⁻ CD7 ⁺ CD34 ⁻
pre-T ALL	cCD3 ⁺ sCD3 ⁻ CD1a ⁻ CD2 ⁺ CD5 ⁺ CD7 ⁺ CD34 ⁻
cortical ALL	cCD3 ⁺ sCD3 ^{+/-} CD1a ⁺ CD2 ⁺ CD5 ⁻ CD7 ⁺ CD34 ⁻
mature ALL	cCD3 ⁺ sCD3 ⁺ CD1a ⁻ CD2 ⁺ CD5 ⁺ CD7 ⁺ CD34 ⁻
ETP-ALL	cCD3 ⁺ sCD3 ⁻ CD1a ⁻ CD2 ⁺ CD5 ^{dim} CD13 ⁺ CD33 ⁺ CD34 ⁺ CD117 ⁺

Table 2 - Immunophenotype subtypes of T cell acute lymphoblastic leukemia (T-ALL)

Patients suffering from T cell acute lymphoblastic leukemia are stratified between five subtypes of T-ALL. Pro-T ALL, pre-T ALL, cortical ALL, mature ALL, and ETP-ALL (early thymic progenitor ALL) show distinct expression of markers on the cellular surface (e.g., sCD3) or present in the cytoplasm (cCD3). CD – a cluster of differentiation. Antigens as described in (115,119,120).

The most recently identified subtype of T-ALL is a rare early thymic progenitor ALL (ETP-ALL) (120). It is a disease of transformed hematopoietic progenitors or of the most immature lymphoid cells. Indeed, one of its main immunophenotyping features is the expression of hematopoietic progenitor and myeloid markers (120,121). Pediatric patients suffering from ETP-ALL have a worse prognosis than non-ETP-ALL

patients (122). Efforts towards understanding the underlying biology of ETP-ALL revealed mutations of *ETV6*, *NPM1*, activation of RAS and JAK-STAT signaling pathways, mutations of epigenetic modulators and T cell associated genes with infrequent *NOTCH1* mutations (121,123).

Development of T-ALL is rarely associated with an inherited genetic predisposition. Environmental impacts on developing thymocytes initiating leukemogenesis have been discussed but further investigation of such involvements is needed (124). Genetic and epigenetic studies, however, have extensively addressed molecular determinants of T-ALL initiation and progression. It has been reported that *NOTCH1* is mutated in over 60% of pediatric T-ALL patients, and together with mutations of *FBXW7*, it has been estimated that the overwhelming majority (almost 80%) of pediatric patients suffering from T-ALL carry oncogenic *NOTCH1* activations (112,125,126). Moreover, studies investigating the sequence of events initiating T-ALL in patients have reported *NOTCH1* mutations amongst the first events (11,127). Mutations affecting the *NOTCH1* receptor have been attributed mainly to two domains: those in the HD domain, leading to ligand-independent activation of the signaling pathway, and within the PEST domain, ultimately inhibiting ubiquitin-mediated degradation of the activated domain of the receptor (Figure 4) (112).

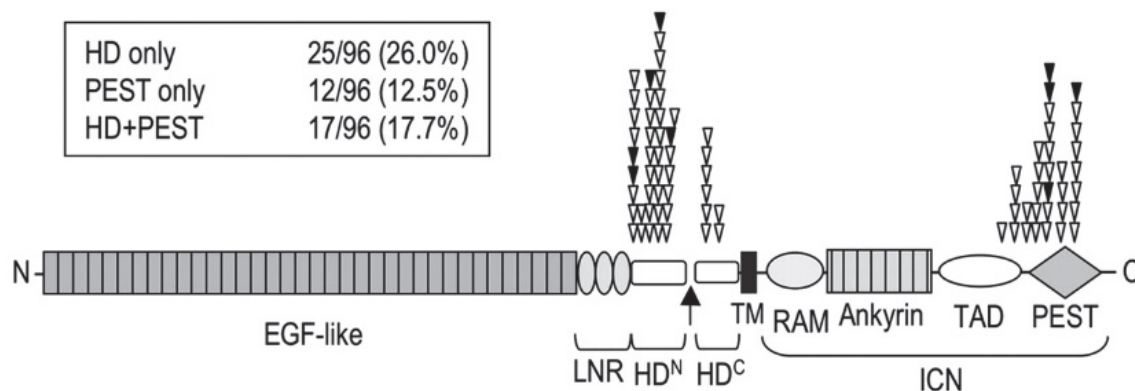


Figure 4 – Mutations of NOTCH1 receptor identified in pediatric T-ALL patients

Heterodimeric domain (HD) and PEST domain are frequently mutated in pediatric patients suffering from T-ALL. Mutations of HD lead to the open configuration of the NOTCH extracellular receptor, leading to constitutive proteolytic cleavage liberating the NOTCH intracellular domain (NICD or ICN). Mutations of the PEST domain inhibit ubiquitination of ICN, thus stabilize the transduction of the signal.

Figure adapted from Weng et al., Science, 2004 (112).

Although Notch1 is the most frequently activated signaling pathway in T-ALL, it is not the only regulator of the disease (128). For example, continuous expression of TAL1 and LMO in developing thymocytes drives T-ALL (129–132). HSC-related factors, like the HOXB genes, were also identified as essential mediators of T-ALL in maturing thymocytes (133). Dysregulation of the cell cycle with mutations of *CDKN2A* is frequently identified in T-ALL and other lymphoid malignancies (128). Moreover, oncogenic signaling from overexpression of TLX and PTEN and RAS pathways are potent initiators of leukemogenesis (131,134,135). Likewise Notch1, Runx1 is essential for physiological thymopoiesis, but in a pathogenic context it drives the expression of oncogenes *Myb* and *Myc* in T-ALL (130,136). In summary, a plethora of oncogenic TFs and signaling pathways have been detected in pediatric patients suffering from T-ALL, as illustrated by genomic analysis of hundreds of primary samples (135).

Treatment of T-ALL relies on intensive chemotherapy. In European clinical guidelines, pediatric and adult T-ALL management plan is firmly based on the BFM (Berlin-Frankfurt-Münster) protocol and its updated versions (137). The BFM describes treatment with vincristine, prednisone or dexamethasone, L-asparaginase, daunomycin, cytarabine, and methotrexate during the Induction Phase. Subsequently, multiple phases of Consolidation, Interim Maintenance, Delayed Intensification, and Maintenance are introduced based on the progression of patients. Blast infiltration of the central nervous system is associated with poor prognoses, therefore prophylaxis in these cases can be achieved with irradiation therapy and intra-thecal methotrexate treatment. It is noteworthy, however, that such therapeutic regimens are highly invasive for the patients (115). Depending on risk factors patients may undergo an allogeneic stem cell transplantation, which shows the best therapeutic outcomes in high risk patients (115).

Chemotherapy and radiation therapy are associated with high toxicities, making them not sustainable for all patients (115,132). Therefore, the development of targeted therapies is the only suitable solution for high-risk patients or relapsing patients. Targeted therapies aim to counteract mutated or overactivated drivers of T-ALL. Due to the activation of the NOTCH signaling pathway in over 80% of T-ALL patients, it has become an attractive therapeutic target. Both ligands and receptors of the signaling

pathway have been targeted with monoclonal antibodies with promising efficiencies in preclinical studies but severe side effects in clinical trial settings. Reported drug-related toxicities included hypertension, liver and gastrointestinal toxicity (132,138,139). Another strategy which abrogates NOTCH1 signaling in T-ALL relies on targeting the γ -secretase complex, the enzyme that liberates the active form of the NOTCH receptor. The efficiency of γ -secretase inhibitors was demonstrated in T-ALL and ETP-ALL patients, again, however, the patients developed severe gastrointestinal toxicities (39,132). Recently, a new inhibitor, known as CB-103, has been introduced to block specific interaction between NICD and RBPJ (17). It has been demonstrated that CB-103 effectively suppresses the growth of T-ALL cells without inducing gut toxicities. Finally, T-ALL activated JAK-STAT pathway with mutations of *IL7R α* have been treated with ruxolitinib in combination with dexamethasone (132). The abovementioned and other therapeutic options, alone and in combination with conventional chemotherapy, are extensively researched in preclinical and clinical studies to improve treatment for T-ALL patients.

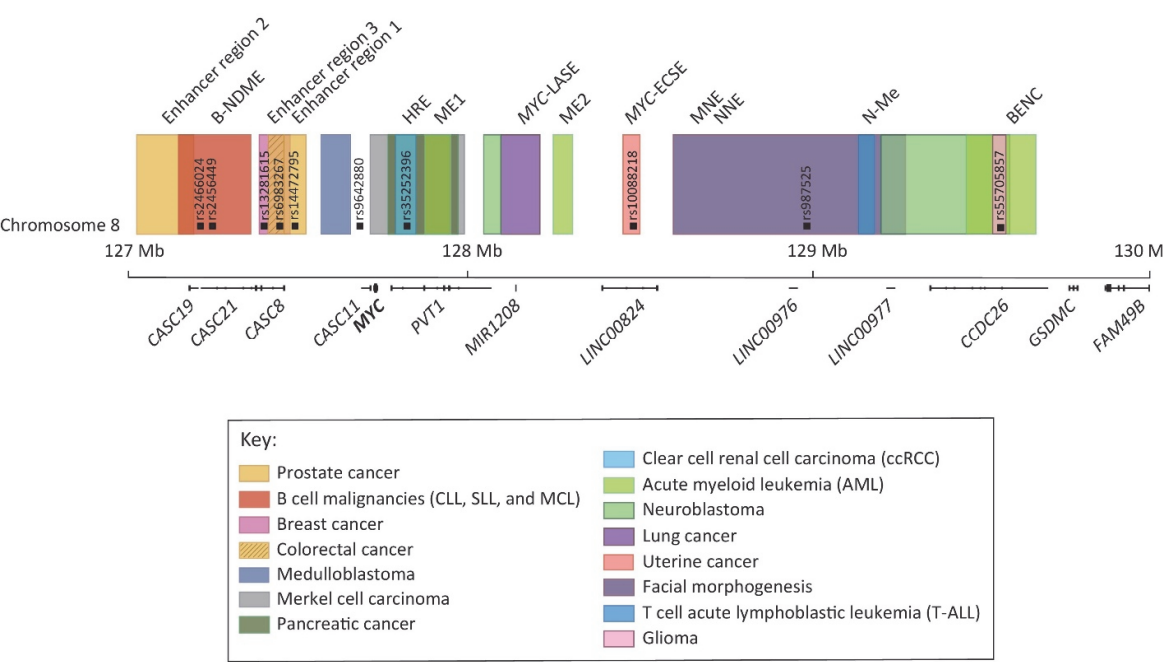


Figure 5 - Cell-specific superenhancer regions of oncogenic *MYC*
Schematic representation of distal regulatory regions driving *MYC* overexpression (highlighted in bold below the representation of genomic localization) in human neoplastic tissues.
Figure adapted from Lancho and Herranz, Trends in Cancer, 2018.

Leukemogenesis initiation, T-ALL progression and response to treatment is strongly dependent on MYC. Initial correlation studies between *Myc* expression and Notch1 signaling revealed binding of Notch1 in proximity to transcription start site (TSS) of the *Myc* promoter (140). Subsequently, Notch1 has been found to drive the expression of *Myc* in murine T-ALL cells by binding to Notch1-dependent *Myc* enhancer site (*NDME*) 1.3 Mb downstream from the promoter (141). In human T-ALL cells and physiological T cells, NOTCH1 regulates the NOTCH-MYC enhancer (*NMe*) localized approximately 1.5 Mb downstream from *MYC*. Deletion of this regulatory region inhibits leukemogenesis, proliferation of T-ALL cells but also impairs physiological TCD (142). The *MYC* oncogene is frequently deregulated in a majority of human neoplasms (143). Distal regulation via context-specific superenhancers has been identified as essential for physiological and pathological expression of *Myc* in hematopoietic stem cells, B cells, T cells and myeloid cells (Figure 5) (144–146). Cellular processes like cell cycle progression, ribosome biogenesis and translation are attributed to positive regulation by MYC. Together with regulation of cellular metabolism, MYC promotes the growth of T-ALL cells, through their proliferation and gene transcription downstream of NOTCH pathway and mTOR signaling (147,148). Moreover, ectopic overexpression of *Myc* rescues T-ALL cells from γ -secretase-mediated inhibition of Notch signaling, confirming their growth dependency on *Myc* addiction (140). Downstream of oncogenic Notch signaling, expression of *Myc* is tightly regulated by complex interactions between varied TFs and their enhancer sites. Gata3, essential for the physiological development of T cells, was shown to regulate the expression of *Myc* through the distal regulatory element in proximity to *NMe* enhancer locus (149). Regulation of epigenetic mechanisms in Notch1-driven T-ALL requires an abundance of factors directly modulating the activation status of the leukemia-prone regulatory regions. Indeed, it has been elegantly shown with studies in which genes frequently mutated in T-ALL patients, like *Dnmt3a* and components of the polycomb repressive complex are inactivated. Inhibition of these epigenetic regulators results in the activation of chromatin leading to the inhibition of physiological TCD and Notch1-dependent progression of T-ALL cells (150,151). Together, these results demonstrate the extent of complex epigenetic mechanisms of action in T-ALL and physiological TCD involving distant enhancer-driven activation of *Myc* by Notch1.

1.5. Epigenetic regulation of gene expression

Gene expression is tightly regulated by the sequence of DNA but also by mechanisms distinct from the sequence itself. Processes relying on dynamic chromatin topology, its compaction, interactions of DNA fragments and modifications of histones modulating the binding of TF genomic loci are referred to as epigenetic (152).

Genomic DNA in the nucleus is over two meters long, therefore it has to be compacted to fit in the confined space. The units of chromatin – nucleosomes – are made of DNA strands and associated proteins called histones (153). Crystallographic analysis of nucleosomes structures revealed amino (N)-terminal tails sticking out from the surface of the protein. These tails are frequently modified post-translationally (153,154). Globular domains of the histones are also subjected to modifications at different lysine residues (153–155). The best studied histone modifications in epigenetic regulation are acetylation and methylation. Histone acetylations are synthesized by histone acetyltransferases and removed by histone deacetylases. Acetylation of histone residues weakens the tight interaction between proteins and DNA by affecting the charge of histones, thus histone acetylations are identified as activating epigenetic marks and are associated with transcription of affected genes (154). On the other hand, histone methylations of lysine, correlated with repression of gene expression, can be mono-, di- and trimethylated by methyltransferases. De-methylation of histones is carried out by enzymes called demethylases (154,155). Posttranslational modifications of histones, in general, are controlled by so-called writers and erasers, while the epigenetic state is detected by readers. Analysis of histone modifications allows for the identification of genomic regulatory elements. Histone tails of active gene promoters carry modifications such as H3K4me3 and H3K27ac, while active enhancers are characterized by H3K4me1 and H3K27ac and absence of the H3K4me3 modification (156). Alterations of the methylation status during initiation and progression of tumor development are mediated by frequent mutations in genes coding for *Dnmt3a* and subunits of polycomb repressive complex 2, for instance, *Ezh2* (153,157).

Continuous processes of gene expression require chromatin to be a very dynamic molecule, thus its three-dimensional organization is not random. Chromatin

architecture analysis revealed chromosome territories with large genomic structures constituting compartments A and B, with compartment A being transcriptionally active and compartment B being associated with transcriptional repression (Figure 6) (158). Regions of chromatin within these compartments can be organized with anchors made up by insulator complexes of CTCF and cohesin into topologically associating domains (TADs) (Figure 6) (158,159). DNA regions within TADs frequently interact with each other, while interactions between distinct TADs are infrequent. Regulation of TAD anchors relies on the directional binding of CTCF, imposing a regulatory mechanism for the expression of proximal genes in a 2D linear scale (160). The genomic loci interacting through physical looping of the chromatin anchored by cohesin frequently connect paired regulatory regions (161).

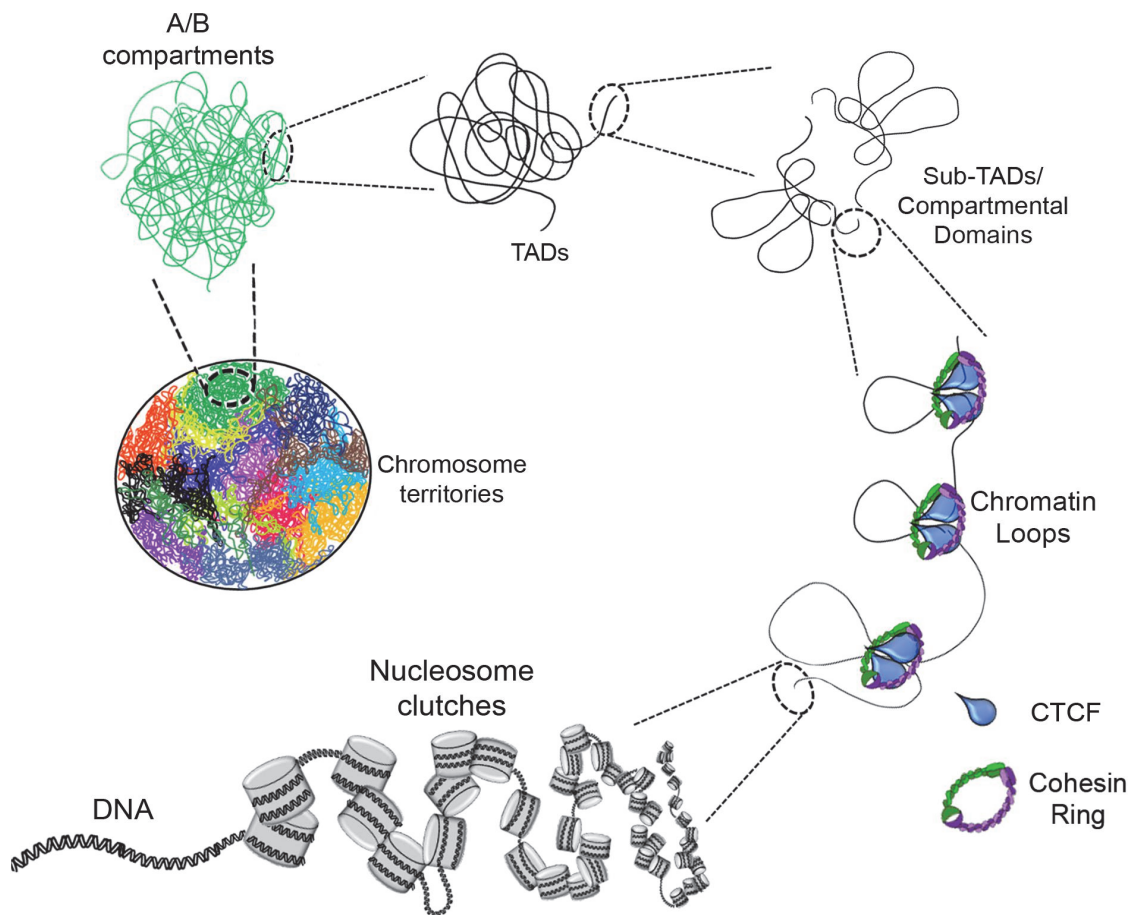


Figure 6 - Spatial organization of chromatin compaction in the nucleus

Genomic DNA is organized in the nucleus in a well-organized structure. DNA is wrapped around the proteins of nucleosomes to form chromatin. Due to the spatial organization of chromatin mediated by cohesin and CTCF, chromatin loops and topologically associating domains (TADs) are formed. Multiple TADs make up active compartments A, or repressive compartments B, with both being organized in chromosome territories. Figure from Magaña-Acosta et al., *Frontiers in Genetics*, 2020 (162).

Assessment of the epigenetic status of a cell can be achieved using distinctive experimental procedures, where each of the methods complements the other. First, chromatin immunoprecipitation for known histone marks associated with various activation states of gene regulatory network, followed by next-generation sequencing (ChIP-seq), allows for descriptive analysis of loci involved in cellular differentiation (163). Then, accessibility of chromatin regions at specific loci associated with genomic regulatory sites can be assessed by employing an assay for transposase-accessible chromatin with high-throughput sequencing (ATAC-seq), which can reveal the importance of distal regulatory elements that affect cellular specification (164,165). Complementary analysis through *in situ* Hi-C allows investigation into genome-wide proximity of chromatin fragments, thus allowing for the discovery of novel enhancer sites and topologically associated domains (159).

Global chromatin rearrangements in the genome of HSCs differentiating towards any of the lineages are accompanied by activation and repression of lineage-specific gene signatures (75,166). The historical perspective on the role of epigenetic regulation in differentiation of stem cells stipulated that decrease of chromatin accessibility accompanies specification of cells (167). However, this view has been challenged as the identification of novel enhancer sites occurring along differentiation of progenitors has been reported (75). Epigenetic remodeling of chromatin in hematopoietic progenitors preserves their lineage fate memory better than transcriptional programming. Such epigenetic memory is conserved in physiological and stress-induced conditions from HSC clones to their progenies (168). In addition, epigenetic mechanisms involved in thymic TCD were shown to be dynamic, demonstrating the importance of non-genetic regulation in physiological T cell function and during leukemogenesis of immature thymocytes (149,169–171). In T-ALL, disease initiation is not the only process regulated by an epigenetic mechanism. This is best illustrated by the previously mentioned well-characterized induction of *MYC* expression in disease progression. Finally, resistance to targeted therapy emerges due to epigenetic modification of gene expression (172).

Taken together, the formation of cellular components of blood from HSCs is a dynamic process regulated by a plethora of transcription factors affecting the expression of lineage-specific gene signatures through direct or epigenetic

mechanisms. Dysregulation of these regulatory mechanisms has been linked to the transformation and progression of neoplastic cells.

2. Aims of the thesis

Development of thymocytes derived from immature hematopoietic progenitors is regulated by Notch1 receptor signaling and one of its downstream effectors Tcf1. Aberrations of physiological thymopoiesis with hyperactivation of Notch1 signaling leads to malignant transformation of immature thymocytes. Therefore, here we address the potential involvement of Tcf1 in Notch1-driven T-ALL. As Tcf family TFs are known binding partners of β -catenin in the activation cascade of the canonical Wnt signaling pathway, the contribution of the β -catenin-mediated Wnt signaling for the initiation of Notch1 leukemogenesis is also investigated. Based on phenotypic observations of disease initiation we aimed to identify an essential molecular mechanisms in the early events of leukemogenesis from immature hematopoietic cells. In summary, we addressed the following:

- The role of Tcf1 in Notch1-driven T-ALL initiation in genetic mouse models inducibly expressing an active, oncogenic form of the Notch1 receptor,
- The involvement of β -catenin signaling in the initiation of leukemogenesis using a conditional genetic loss-of-function mouse model,
- Gene expression signatures by performing transcriptomic analysis of *ex vivo* sorted hematopoietic progenitors from various compound animals allowing for overexpression of *Notch1* with and without simultaneous deletion of *Tcf7*,
- Epigenetic mechanisms hijacked by Notch1 and Tcf1 at the initiation of leukemogenesis in hematopoietic progenitors. Validation of these findings in a CRISPR-Cas9-edited mouse model deleted for essential epigenetic regulatory element,
- Translation of identified Tcf1- and Notch1-dependent epigenetic dependencies from the mouse model to human T-ALL leukemogenesis.

The major part of presented here data is under revision in a peer-review scientific journal as a Research Article entitled 'Tcf1 is essential for initiation of oncogenic Notch1-driven chromatin topology in T-ALL' authored by Mateusz Antoszewski, Nadine Fournier, Gustavo A. Ruiz Buendía, Joao Lourenco, Tara Sugrue, Christelle Dubey, Marianne Nkosi, Colin E.J. Pritchard, Ivo J. Huijbers, Gabriela C. Segat, Sandra Alonso-Moreno, Elisabeth Serracanta, Laura Belver, Adolfo A. Ferrando, Andrew P. Weng, Ute Koch, Freddy Radtke.

3. Materials and methods

3.1. Animal procedure

All animals were maintained at the Ecole Polytechnique Fédérale de Lausanne (EPFL) animal facility. For experimental analyses, littermates not expressing the *Mx1Cre* transgene were used as control mice (*Controls*). Genotyping of mice was performed on DNA isolated from toe biopsies using standard polymerase chain reaction (PCR) buffer composition and reaction mixes. Conditioning of animals for bone marrow transplantation was performed as approved in study protocol VD1099.8. Donor animals used for subsequent enrichment of hematopoietic progenitors were injected intraperitoneally (i.p.) with 5-fluorouracil (150mg/kg bodyweight, Sigma-Aldrich, Cat# F6627). *Mx1Cre* induced gene inactivation was achieved performing five i.p. injections of 2µg/g body weight polyI:polyC (poly(I:C), Invivogen, Cat# tlr-pic) at 2-day intervals. Genomic deletion of *Tcf7* was assessed by PCR (all primer sequences are listed in Annexed Table 1). Induction of oncogenic *Notch1*-expression was assessed by flow cytometry detecting nuclear-localized enhanced GFP (eGFP).

3.2. Murine models

Mx1Cre, *Gt(ROSA)26Sor^{tm1(Notch1)Dam}/J* (*N1IC^{lox/lox}*), *Notch1^{lox/lox}* and B6.129-*Ctnnb1^{tm2Kem}/KmwJ* (*β-catenin^{lox/lox}*) mouse lines have been previously described (33,173–175). The conditional *Tcf7* mouse line was generated as follows. The gene encoding TCF-1 (*Tcf7*) was conditionally targeted by the International Knockout Mouse Consortium EMMA (Project 37596). Exon 3 of *Tcf7* was flanked by two *loxP* sites and deletion of this exon resulted in a nonsense frameshift mutation. The targeting strategy disrupts the β -catenin binding site deleting the floxed exon 3 upon Cre-mediated recombination, corresponding to amino acid 33 through 69. Possible splicing events from exon 2 to exon 4, 5, 6, and 7 will result in out of frame proteins with premature stop codons, whereas splicing to exon 8 could possibly result in an in-frame protein in which amino acids 33 to 226 including a large portion of the high-mobility-group will be missing. Frozen embryos were shipped by EMMA and transferred into pseudo-pregnant females at the Center of PhenoGenomics EPFL, Lausanne. By crossing offspring with B6.Cg-Tg(ACTFLPe)9205Dym/J Tg mice, the Frt site-flanked LacZ-Neo cassette was excised, giving rise to the *Tcf7*-floxed allele.

The *N1IC*^{lox/lox}, *Tcf7*^{lox/lox}, *β-catenin*^{lox/lox} and *Mx1Cre* lines were backcrossed 3 generations into 129S2/SvPasCrl (Charles River, code 287) to generate the following compound mouse strains: *Notch1*^{lox/lox Mx1Cre}, *Tcf7*^{lox/lox Mx1Cre}, *N1IC*^{lox/+ Mx1Cre}, *N1IC*^{lox/lox Mx1Cre}, *N1IC*^{lox/+ Tcf7}^{lox/lox}, *N1IC*^{lox/+ Tcf7}^{lox/lox Mx1Cre}, *N1IC*^{lox/lox Tcf7}^{lox/lox Mx1Cre}, *N1IC*^{lox/lox β-catenin}^{lox/lox Mx1Cre}. All primer sequences used for genotyping mouse lines are listed in Supplementary Table S1. B6.SJL-*Ptprca*^a*Pepc*^b/BoyJ (B6-CD45.1) (176) (Jackson Laboratories, Cat# 2014) animals were bred and maintained at the EPFL animal facility.

3.3. Generation of *TMe* CRISPR-Cas9-deleted mouse strain

The *TMe* mouse line was created by gene editing using the CRISPR-Cas9 technology in zygotes (177). Briefly, zygotes isolated from *C57Bl/6JRj* mice were injected with a mixture of 2 sgRNAs and Cas9 mRNA. The sgRNAs targeted Cas9 to cut at loci on each side of the *Tcf1*-binding site to induce a deletion mutation thereof. The injected zygotes were cultured overnight and 2-cell stage embryos were transferred to pseudopregnant foster mice (177,178). For the *TMe* mouse line the CRISPR/Cas9 targets were: 5'side-Target_87: GTAGGTCCTAGGACTAGTCTGGG and 3'side-Target_83: GGTGGCAGTTCCTCCTATGCTGG. The targets were evaluated for potential off-targets using E-CRISP (E-CRISP, RRID:SCR_019088) (179). Among the resulting mice a founder carrying a 1068 bp deletion (mm10 chr15: 63270451-63271519) was identified by standard PCR.

3.4. Bone marrow chimeras and transplantation assays

Bone marrow (BM) chimeric mice were generated as previously described (180). Reconstitution of transplanted animals was assessed by peripheral blood lymphocyte (PBL) analysis using flow cytometry 2-6 weeks post transplantation. Overall reconstitution and progression of T-ALL was monitored over time by peripheral blood lymphocyte analysis until the endpoint of each experiment.

3.5. Isolation of human hematopoietic progenitor cells

Anonymized normal human cord blood (CB) samples were obtained with informed consent from women undergoing caesarian deliveries of full-term births

according to protocols approved by the Research Ethics Board of the University of British Columbia and Children's & Women's Hospital of BC. CD34⁺ CB cells were obtained at > 90% purity from pooled collections using a two-step RosetteSep/EasySep human CD34-positive selection kit (StemCell Technologies) according to the manufacturer's protocols. CD34⁺ cells were seeded into 96-well round bottom plates and prestimulated in StemSpan SFEM II (StemCell Technologies Cat# 09655) with 10 ng/mL human SCF Cat# 300-07, 20 ng/mL human TPO Cat# 300-18, 20 ng/mL human IGF2 Cat# 100-12, and 10 ng/mL human FGF α Cat# 100-17A (Peprotech) for 24 h.

3.6. Culture of cell lines

The culture of cell lines was performed under standard conditions in a humidified atmosphere at 37 °C under 5% CO₂. The retroviral packaging cell line BOSC-23 (ATCC Cat# CRL-11270, RRID:CVCL_4401) was purchased from ATCC and maintained in DMEM GlutaMAX Supplement, pyruvate (GIBCO, Cat# 31966047) supplemented with 10% FBS (GIBCO), 25mM HEPES buffer (N-2-hydroxyethylpiperazine-N'-2-ethanesulfonic acid, AMIMED, Cat# 5-31F00-H), 50 μ M 2-mercaptoethanol (Life Technologies, Cat# 31350010) and Gentamicin (10 μ g/mL; Life Technologies, Cat# 15710049), referred to as complete DMEM. The lentiviral packaging cell line HEK293T cells was obtained from D. Trono (RRID:CVCL_0063) and maintained in complete DMEM. All primary tumor T-ALL cells and cell lines DND-41 (RRID:CVCL_2022) and Jurkat (RRID:CVCL_0367) were grown in RPMI 1640 GlutaMAX Supplement (GIBCO, Cat# 61870010) supplemented with 10% FBS (GIBCO), 25mM HEPES buffer, 50 μ M 2-mercaptoethanol and referred to as complete RPMI 1640. Lineage-negative bone marrow cells were cultured in IMDM GlutaMAX Supplement (GIBCO, Cat# 31980022) supplemented with 10% FBS (PAA), 25mM HEPES buffer, 50 μ M 2-mercaptoethanol, Gentamicin and growth factors: 10ng/mL murine recombinant interleukin-1 β (mIL-1 β , Stem Cell Technologies, Cat# 78035), 10ng/mL murine recombinant interleukin-3 (mIL-3, Stem Cell Technologies, Cat# 78042), 100ng/mL murine recombinant Flt3/Flk2-Ligand (mFlt3L, Stem Cell Technologies, Cat# 78011) and 100ng/mL murine recombinant stem cell factor (mSCF, Stem Cell Technologies, Cat# 78064). Transduced CB cells were cultured on confluent monolayers of OP9-DLL1 cells (RRID:CVCL_B218) in α MEM media

supplemented with 20% FBS (GIBCO) plus 10 ng/mL human SCF Cat# 300-07, 5 ng/mL human FLT3L Cat# 300-19 and 3 ng/mL human IL-7 Cat# 200-07 (Peprotech).

3.7. Retroviral and lentiviral vectors

The retroviral packaging plasmid pCL^{ECO} for pCL retroviruses was obtained from Addgene (RRID: Addgene_12371) (181). The coding sequence of the intracellular domain of the mouse Notch1 receptor lacking the PEST domain (corresponding to amino acids 1751–2443) was created by PCR amplification from the mouse *Notch1* cDNA template. The sequence was flanked by EcoRI restriction sites (underlined) by amplification with the following primer pairs:

Forward 5'-CCGGAATTCGCCACCATGGATCCGCGGCCAG-3'

Reverse 5'-CGGGAATTCCTACAGTGATGTTGGTAGGGCTG-3'

The modified N1ICD construct was cloned into the EcoRI site of the Migr1 vector, a pMSCV2.2-based retroviral vector containing an IRES-eGFP cassette (182) and termed RV *N1ICD* IRES *eGFP*. The retroviral vector Migr1 Tcf7-p45 eGFP (RV *Tcf7* IRES *eGFP*) containing the cDNA of Tcf7 (p45 isoform) was obtained from H. H. Xue (University of Iowa). All sequences were verified by DNA Sanger sequencing.

The human NOTCH1 (ΔE allele) was obtained from Dr. J. Aster (Brigham and Women's Hospital), Harvard PlasmID. NOTCH1 ΔE and GFP cDNAs were connected with equine rhinitis A virus 2A (E2A) peptide (183). The polycistronic cDNA was cloned into pRRL-cPPT/CTS-MNDU3-PGK-GFP-WPRE3 immediately downstream of the MNDU3 promoter (184). The construct was verified by sequencing.

3.8. Production of viral particles and transduction

Retroviruses were packed and produced as previously described (185) by transfection of BOSC-23 cells with the retroviral vectors and packaging plasmid pCL^{ECO} (RRID:Addgene_12371) (181). Retroviral titers were determined by serial dilution of concentrated retroviral stock aliquots using the NH10 cell line (186). Retroviral particles (RVP) were transduced into lineage-negative bone marrow cells as previously described (182). Briefly, RVP were transduced (1-5 RVP per cell) by spinoculation (45 min at 34 °C by centrifugation at 800g) into lineage-negative bone

marrow cells in complete IMDM medium supplemented with growth factors (murine recombinant IL-1 β 10ng/mL, IL-3 10ng/mL, Flt3L 100ng/mL and SCF 100ng/mL) and 10 μ g/mL polybrene (Sigma Aldrich, Cat# TR-1003-G).

High-titer lentiviral supernatants were produced by transient transfection of 293T cells with second-generation packaging/envelope vectors pCMV dR8.74 (RRID: Addgene_22036), pRSV-Rev (RRID: Addgene_12253), and pCMV VSV-G (RRID: Addgene_8454), followed by ultracentrifugal concentration (25,000 rpm for 90 min at 4 °C; Beckman SW32Ti rotor). Prestimulated CB cells were treated with Cyclosporin H (8 μ M; C988920, Toronto Research Chemicals) for 16 hours, subsequently transduced in 96-well plates coated with 5 μ g/cm² fibronectin (Stem Cell Technologies) by direct addition of concentrated viral supernatants and transferred to OP9-DLL1 co-cultures 6 h later.

3.9. Flow cytometry-based analysis of hematopoietic cells

Single cell suspensions were prepared from spleen, bone marrow, thymus or PBL of mice as previously described (180). Oncogenic *Notch1*-expressing LSK cells were defined as CD45.2⁺ lineage-negative CD117⁺ Sca1⁺ eGFP⁺. For ATAC-seq, RNA-seq, ChIP-seq and *in situ* Hi-C analysis oncogenic *Notch1*-expressing LSK cells were sorted using a FACSARIA (Becton Dickinson) or MoFlo Astrios EQ (Beckman Coulter) cell sorter. Oncogenic *NOTCH1*-expressing human CB cells were defined as CD45⁺ CD34⁻ CD38⁺ CD5⁻ CD7⁺ eGFP⁺. For ATAC-seq oncogenic *NOTCH1*-expressing cultured human CB cells were sorted using a FACSARIA (Becton Dickinson). For Western blot analysis for Tcf1 and Myc oncogenic *Notch1*-expressing T cells were sorted using MoFlo Astrios EQ (Beckman Coulter) cell sorter. Assessment of genomic deletion of the Tcf7 gene was performed on CD4⁺ CD8⁺ DP thymocytes sorted on MoFlo Astrios EQ (Beckman Coulter) cell sorter. Purity of sorted subsets was > 97%. Flow-cytometric data were acquired on a Gallios cytometer (Beckman Coulter) and analyzed using FlowJo v10.7.1 (FlowJo, RRID:SCR_008520). Cell viability was assessed using either 4',6-diamidino-2-phenylindole (DAPI, Thermo Fisher Scientific, Cat# D1306, RRID:AB_2629482) or Zombie UV dye (Zombie UV Fixable Viability kit, BioLegend, Cat# 423107) for sorting and LIVE/DEAD Fixable Aqua (Invitrogen Cat# L34966) for analysis of lymphoid lineages and leukemic cells. All primary and secondary antibody conjugates are listed in the Annexed Table 2.

3.10. Western blot

Protein expression of Tcf1 (anti-Tcf1 antibody, Cell Signaling Technology, Cat# 2203, RRID:AB_2199302), β -catenin (anti- β -catenin antibody, BD Biosciences, Cat# 610153, RRID:AB_397554) and c-Myc (anti-c-Myc antibody, Abcam, Cat# ab32072, RRID:AB_731658) were analyzed by Western blotting of sorted cells and cell lines. Whole-cell lysates (RIPA buffer) separated on 10% sodium dodecyl sulfate–polyacrylamide gel electrophoresis (Bio-Rad) were transferred to polyvinylidene difluoride membranes and incubated with indicated primary antibodies. Washed membranes were incubated with a secondary sheep anti-mouse IgG HRP conjugate (GE Healthcare, Cat# NXA931, RRID:AB_772209) and developed using Pierce ECL Western Blotting Substrate (Thermo Fisher Scientific, Cat# 32209). β -Actin (anti- β -Actin antibody, Abcam, Cat# ab8226, RRID:AB_306371) expression was analyzed as loading control.

3.11. ATAC-seq

Accessible chromatin mapping was performed using Assay for Transposase-Accessible Chromatin using sequencing (ATAC-seq) as previously described (164,187) using sorted *R26 N1IC^{lox/+} Tcf7^{lox/lox}* (Controls), *R26 N1IC^{Δ/+}* (*N1IC*), *R26 N1IC^{Δ/+} Tcf7^{Δ/Δ}* (*N1IC Tcf7^{Δ/Δ}*), *R26 N1IC^{Δ/+} TMe^{+/-}* (*N1IC TMe^{+/-}*) and *R26 N1IC^{Δ/+} TMe^{-/-}* (*N1IC TMe^{-/-}*) LSK cells in biological replicates (50,000 cells each), and using human cord blood overexpressing *NOTCH1* with minor adaptations as detailed below. Cells were washed twice in 150 μ L and 50 μ L 1xPBS, resuspended in 50 μ L ATAC-seq lysis buffer, incubated for 10min on ice and centrifuged at 400g for 10 min at 4 °C. The pellet was incubated in the transposase reaction mix (25 μ L 2 \times TD buffer (Illumina), 2.5 μ L transposase (Illumina, Cat# FC-121-1030) and 22.5 μ L nuclease-free water) for 30min at 37 °C with gentle agitation. After DNA purification with the MinElute PCR Purification kit (Qiagen, Cat# 28004) library was amplified with NEBNext High-Fidelity PCR Master Mix (NEB, Cat# M0541S) using custom Nextera primers. Library for sequencing was size selected with Agencourt AMPure XP beads (Beckman Coulter, Cat# A63880). DNA concentration was measured with an Invitrogen Qubit fluorometer (Life Technologies) and Agilent Fragment Analyzer. The libraries were sequenced by Gene Expression Core Facility of EPFL using the Illumina NextSeq 500 platform and the 75-bp paired-end configuration to obtain at least 35 million reads per sample, or

for investigation of *TMe* regulatory element in murine cells and human cord blood at Novogene using the Illumina NovaSeq and the 150-bp paired-end configuration to obtain at least 100 million reads per sample.

3.12. RNA-seq

RNA from biological replicates was extracted from sorted cells using PicoPure RNA Isolation Kit (Thermo Fisher Scientific - Applied Biosystems, Cat# KIT0214). cDNA libraries were prepared and sequenced by the Gene Expression Core Facility of EPFL. Libraries were generated using TruSeq RNA Library Prep Kit v2 (Illumina, Cat# FC-122-1001). Strand-specific library construction and Illumina NextSeq 500 sequencing of paired-end 2x79nt or single-end 75nt reads were performed.

3.13. ChIP-seq

Chromatin immunoprecipitation followed by sequencing (ChIP-seq) was performed on chromatin from 20,000 LSK cells from biological replicates. Sorted cells were cross-linked with 1% methanol-free formaldehyde (Pierce Life Technologies, Cat# 28906), quenched with 0.125 M glycine, frozen at -80 °C and stored until further processing. ChIP reaction was performed with Diagenode True MicroChIP Kit (Diagenode, Cat# C01010130) with modifications of the manual detailed below. Lysed samples were sonicated using Diagenode Bioruptor Pico (Diagenode, Cat# B01060010). Sheared chromatin was immunoprecipitated with 1µg of antibodies. Eluted and decross-linked DNA was purified with Diagenode MicroChIP DiaPure columns (Diagenode, Cat# C03040001) and eluted in 30µL of Nuclease-Free water.

ChIP and input libraries for sequencing were prepared with MicroPlex Library Preparation Kit (Diagenode, Cat# C0101134). Size selection steps were performed with Agencourt AMPure XP magnetic beads (Beckman Coulter, Cat# A63880). Subsequently, ChIP-seq library was quantified with Agilent Fragment Analyzer. The libraries were sequenced by Gene Expression Core Facility of EPFL using the Illumina NextSeq 500 platform and the 75-bp paired-end configuration to obtain at least 30 million reads per sample.

3.14. ChIP-qPCR

Briefly, chromatin samples were prepared from 10 million 1% formaldehyde fixed cells, sonicated in 200µL of 1% SDS lysis buffer with Diagenode Bioruptor Plus (Diagenode, Cat# B01020001) and immunoprecipitated with 2µg antibody recognizing Tcf1 (Cell Signaling Technology, Cat# 2203, RRID:AB_2199302) and 2µg of mouse IgG (Diagenode, Cat# C15400001-100, RRID:AB_2722553). Antibody-chromatin complexes were captured with Pierce protein A magnetic beads (Pierce Life Technologies, Cat# 88845), washed with low salt buffer, high salt buffer, LiCl wash buffer, and eluted. After reversal of cross-linking, RNase and proteinase K treatment were performed and DNA was purified with Diagenode MicroChIP DiaPure columns (Diagenode, Cat# C03040001). Enrichment analysis was performed by qPCR with 7900HT Fast qPCR.

3.15. Reverse ChIP

We performed reverse ChIP assays as previously described (149). Briefly, we generated *TMe* DNA bait sequences by PCR from human genomic DNA using a *TMe* biotinylated forward primer (5'- GGTGAAAAGTGCTTAGAAACAG-3') and an unmodified *TMe* reverse primer (5'- CAGTGACTTATCTTATCCCAG-3'). Then, we conjugated DNA baits to streptavidin beads and incubated them with nuclear protein extracts from DND41. We used non-conjugated beads as negative control. *TMe* pulled down proteins were analyzed by mass spectrometry at the Proteomics Unit of the Josep Carreras Leukemia Research Institute. The MS/MS spectra were searched against the Swissprot human database using Andromeda within MaxQuant (v.1.7.6.0). A 1% False Discovery Rate (FDR) cut off was applied at both peptide and protein level using a standard target-decoy database strategy. All the protein groups labeled as "Reverse", "Only identified by Site" and "Potential contaminant" were excluded from the analysis. We recovered 459 proteins from DND41 extracts. Then, we filtered out proteins that were present in more than 2% of the experiments of the Contaminant Repository for Affinity Purification (CRAPome) database (188). We identified 52 *TMe* associated proteins in DND41.

3.16. In situ Hi-C

Low input *in situ* Hi-C was performed on 150,000 LSKs from biological replicates with Arima-HiC Kit (Arima) according to the manufacturers' protocols. DNA fragmentation was performed on Covaris E220 Evolution sonicator (Covaris, Cat# 500429) with default settings for 400bp DNA size distribution. Libraries for sequencing were prepared with Swift Biosciences Accel-NGS 2S Plus DNA Dual Indexing Library Kit (Swift Biosciences, Cat# 21024 and #28096). Size selection steps were performed with Agencourt AMPure XP magnetic beads (Beckman Coulter). Library amplification was performed following DNA quantification with Invitrogen Qubit Fluorometer and KAPA Library Quantification Kit (Roche, Cat# 07958927001). Prepared libraries were sequenced using the sequencing platforms at Novogene with Illumina NovaSeq 6000 S4 and the 150 bp paired-end reads generating around 700 million paired reads per library of biological replicate.

3.17. Analysis and visualization software

Genomic data was visualized with Integrative Genomics Viewer 2.7.2 (IGV, RRID: SCR_011793) and Juicebox 1.11.08 (189). Quantitative data and statistical analysis was performed with GraphPad Prism 9 (RRID: SCR_002798). Flow cytometric data was analyzed with FlowJo v10.7.1 (RRID: SCR_008520). Representation of data was generated in Adobe Illustrator 2021 (RRID: SCR_010279).

3.18. Quantification and statistics

Each experiment discussed herein was performed at least twice independently. p-values were calculated using unpaired two-tailed Student's t-test or one-way ANOVA with GraphPad Prism 9. Statistical difference analyses of Kaplan-Meier survival curves were performed using Log-rank (Mantel-Cox) test. Unless otherwise stated, bioinformatic statistical analyses were performed using R version 4.0.3 (RRID:SCR_001905) and Bioconductor 3.12. To highlight statistical significances in figures, the following annotations for p values: *, p-value<0.05; **, p-value<0.01; ***, p-value<0.001; ****, p-value<0.0001 were used.

3.19. Bioinformatic analyses

3.19.1. Evolutionary conservation of genomic sequence

The evolutionary conservation of *TMe* sequences was analyzed using the DIALIGN TF tool (DIALIGN, RRID:SCR_003041) (190). *TMe* sequences from 26 vertebrate species were aligned and putative transcription factor binding sites were identified in highly conserved regions. Evolutionary conservation scores were calculated at individual alignment sites using PhastCons (191). The *TMe* phylogenetic tree was generated using the iTOL tool (iTOL, RRID:SCR_018174) (192).

3.19.2. Analysis of RNA-seq

Adapter sequences and low-quality ends were removed with cutadapt (1.9.1) and reads were aligned to the mouse genome build mm10 using HISAT2 (2.0.3beta) aligner (193). Raw counts per gene were calculated with featureCounts (1.4.4) and genes with average TPM (Transcripts Per kilobase Million) < 1 were filtered out. Between-sample normalization was performed using the EdgeR (3.28.0) TMM method. Normalized log2 transformed counts (voom) were subsequently analyzed for differential expression (eBayes, limma 3.42.2), p-values were FDR corrected (194). Pathway over-representation analysis (ORA) was performed in the genes significantly (FDR < 0.5) induced (LFC > 1) or repressed (LFC < -1) using GO and KEGG biological pathway database from mSigDB (version 7.0) (195). P-values were computed by hypergeometric test and FDR corrected.

3.19.3. Analysis of ChIP-seq

Adapter sequences and low-quality ends were removed with cutadapt as needed and reads were aligned to the mouse genome build mm10 using BWA-MEM (0.7.17) (196). Properly paired good quality reads were filtered with samtools (1.9) using samtools view -b -h -f 0x2 -q 2. Peaks were called using MACS2 (2.1.1.20160309) (197) using macs2 callpeak -t -f BAMPE -g mm -B --nomodel --nolambda -q 0.05 --keep-dup all --call-summits (for CTCF ChIP) or --broad --broad-cutoff 0.1 (for all histone mark ChIP).

3.19.4. Analysis of ATAC-seq

Mouse ATAC-seq reads were processed as follows: adapter sequences and low-quality ends were removed with cutadapt, and reads were aligned to mouse genome build mm10 using BWA-MEM. Properly paired good quality reads were filtered with samtools view -b -h -f 0x2 -q 2, and subsequently used for peak calling using MACS2 using macs2 callpeak -t -f BAMPE -g mm -B --nomodel --nolambda -q 0.05 --keep-dup all --broad --broad-cutoff 0.1.

Human cord blood ATAC-seq sequencing reads were trimmed using atopos (1.1.21) (198) to remove the Illumina TruSeq adapter sequences. Trimmed reads were aligned to the human genome build hg38 using BWA-MEM. The aligned reads were filtered to include reads from chromosomes 1 - 22, X, and Y using samtools and duplicates were marked using “MarkDuplicates” from Picard (2.18.27). ATAC-seq peaks were called with MACS2 with the same parameters. For the previously published human cord blood CD34+ samples used as control (199), ATAC-seq sequencing reads from patient 1 were trimmed to keep the first 38 bp to match the length of the ATAC-seq reads from patient 3. The subsequent steps until peak calling were performed as for the other human cord blood ATAC-seq data.

Transcription factor binding motif and footprints

Transcription factor footprints were predicted based on the aligned ATAC-seq reads using the TOBIAS (0.12.4) snakemake pipeline (200) with default parameter values and options. Transcription factor motifs were downloaded from JASPAR (JASPAR 2020 non-redundant vertebrate CORE PFMs) (201) and human and mouse evidence-based gene annotations were downloaded from GENCODE (202).

3.19.5. Differential analysis and pathway enrichment

Differential analysis of chromatin accessibility or binding was performed using EdgeR within the Diffbind R package (2.16.2) (203). Chromatin peaks were called significantly changed if FDR was below the cutoff of 0.01. Heatmaps of significantly changed peaks were produced with the genomation R package or EnrichedHeatmap R package version (1.18.2) (204). Pathway enrichment analysis was performed using rGREAT (1.20.0) (205) and the following geneset collections: Gene Ontology

Biological Process, Phenotype Data and Human Disease, KEGG. Ontologies with a fold enrichment > 2 and FDR 0.05 were reported.

3.19.6. Analysis of in situ Hi-C

Creation of Hi-C contact maps

Hi-C paired-end sequencing reads for each sample were filtered and aligned to the mouse genome build mm10 using the Juicer pipeline 1.6 (206) using default parameters and a file containing the restriction site coordinates of the restriction enzymes used in the Arima-HiC kit (cutting at GATC and GANTC) which was generated with the generate_site_positions.py script provided with Juicer. Aligned Hi-C contacts with an alignment score > 30 (MAPQ > 30) from individual replicates were combined using the “mega.sh” script provided with Juicer. Chromatin contact maps from pooled data were created (in .hic format) using the “pre” command. In this step, contact matrices were obtained at multiple resolutions: custom resolutions (2.5 kb and 5 – 25 kb with a 1 kb increase) and at default resolutions (50, 100, 250, 500 kb, 1, and 2.5 Mb). Contact maps were visualized with Juicebox (189).

Correlation between Hi-C contact maps

Contact matrices at 1 Mb resolution with Knight-Ruiz (KR) normalization were obtained for each chromosome from each sample to obtain the correlation between Hi-C contact maps. The contact matrices of each chromosome from the same sample were combined to create genome-wide contact matrices for each sample. The Pearson correlation between the genome-wide, normalized counts of each sample was calculated using R. Hierarchical clustering of the Pearson correlation matrix was performed in R with the hclust function, default parameters, and (1 – Pearson correlation) as the dissimilarity measure.

Chromatin compartment analysis

Chromatin compartments were identified by obtaining the eigenvector of each chromosome from each sample by using the Juicer tools “eigenvector” command. KR-normalized contact matrices at 1 Mb resolution from pooled samples were used as input for the eigenvector Juicer tool. As suggested by (207–209) genomic regions with high gene density were assigned to the compartment A (corresponding to positive PC1

values), and conversely, genomic regions with negative PC1 values were assigned to compartment B.

Identification of chromatin domains

Chromatin contact domains were identified in KR-normalized chromatin contact maps at 5 kb resolution using Arrowhead from Juicer tools (159). To select only chromatin domains anchored by CTCF sites, the JASPAR motif MA0139.1. was identified within CTCF ChIP-seq peak regions, and motif orientation and motif scores were assigned using FIMO from the MEME Suite (4.10.0) (210). Chromatin domains were considered as CTCF anchored if presenting at least one strong CTCF motif (FIMO score > 10) within 50 kb of both boundaries, and with opposite orientations. Condition-specific chromatin domains were identified by using bedtools intersect (2.29.2) (211) using the `-v` option to obtain domains which do not have an overlap with domains from a different condition. Significant differentially expressed genes localized in condition-specific and overlapping domains in pairwise comparisons were selected for pathway analysis using rGREAT.

Chromatin domain boundaries CTCF enrichment analysis

CTCF coverage tracks (bigWig) were generated from ChIP-seq read alignments using the bamCoverage tool from deepTools 2.0 (212) with a bin size set to 10 bp and a RPGC normalization of the number of reads per bin. To draw heatmaps, the left and right boundaries of chromatin domains were retrieved, and the normalizeToMatrix function from EnrichedHeatmap was used to extend the TAD boundaries ± 50 kb, bin to every 1000 bp, and compute mean weighted CTCF signals by bin (mean_mode = "w0").

Identification of chromatin loops

Chromatin loops were identified as previously proposed (213). Chromatin contacts were called at 2.5 and 5 to 25 kb resolutions (with a 1 kb increase) with HiCCUPS from Juicer tools (159) using parameter values as described in Greenwald et al. 2019 for resolutions 5 to 25Kb, and `-p 4`, `-i 7` and `-d 10000` for 2.5 kb resolution. For resolutions between 2.5 and 10 kb, chromatin loops within 20 kb were merged together using pgltools (2.2.0) (214). For resolutions higher than 10 kb, loops which

were called within twice the size of the loop anchors (i.e. resolution) were merged using pgltools. The merged loops called at each resolution were then combined and subsequently merged if they occurred within 20 kb. At each merging event, chromatin loops which were called in at least three different resolutions were retained. Finally, the chromatin loop called at the highest resolution and with the lowest “FDR donut” value was kept for downstream analyses. Condition-specific chromatin loops were identified by using pgltools intersect with the `-v` option to obtain loops that do not overlap with loops from a different condition. For functional annotation of chromatin loops, each anchor of chromatin loops was associated to a gene if the anchor boundary occurred within 2.5 kb either upstream or downstream of a gene TSS. For visualization of chromatin loops, Hi-C contact maps, TADs, RNA-seq, ChIP-seq, ATAC-seq and CTCF binding sites, we used the Sushi R package (1.27.0).

H3K27ac at chromatin loop anchors

We analyzed the H3K27ac levels at chromatin loop which had anchors associated to a gene TSS. For each chromatin loop anchor that was associated to a TSS, we plotted the normalized H3K27ac signal present at the other end of the chromosome loop. H3K27ac heatmaps were produced with the EnrichedHeatmap using the following parameters: `extend = 2500`, `w = 50`, `mean_mode = "w0"`, and `background = 0`.

Enhancer-promoter analysis

H3K4me1 peaks not overlapping with H3K4me3 peaks were selected (H3K4me1⁺/H3K4me3⁻ peak set) using the GenomicRanges R package version 1.42.0. Group specific peak sets were pooled and overlapping peaks (at least one bp) were merged to create a consensus set of enhancer sites. Anchors of TSS annotated chromatin loops were overlapped with consensus enhancer sites. Any pair of TSS and enhancer located in opposite anchors of the same chromatin loop were identified as potential enhancer-promoter interactions. Enhancer activity was determined based on H3K27ac and H3K27me3 histone modifications. To identify enhancer regions with differential H3K27ac and H3K27me3 histone modification between groups, we used DiffBind on the set of enhancer sites, with a cutoff of 0.5 on the absolute log fold change (203). Enhancer activity was considered increased in one group compared to

another when there was an increase in H3K27ac, without increase in H3K27me3; and vice versa.

3.20. Data availability

ATAC-seq, RNA-seq, ChIP-seq and Hi-C data sets of murine LSK and human ATAC-seq were deposited - GSE169121. Publicly available ATAC-seq (GSM4743251 and GSM4743252) data sets from non-infected and non-cultured CD34+ human cord blood cells were used as *Controls*.

4. Results

4.1. *Tcf7* loss impairs T cell development downstream of Notch1

Canonical Notch1 signaling (33) and its downstream target Tcf1 (99,103,104) are shown to be essential in T cell lineage specification. To confirm the function of Tcf1 (encoded by *Tcf7*) in the context of physiological TCD, we generated a conditional gene-targeted mouse line for the *Tcf7* gene. Exon 3 of *Tcf7* gene was flanked by loxP sites and deletion of this exon disrupts the β -catenin binding site (215). *Tcf7*^{lox/lox} mice were crossed with *Mx1Cre* (174) transgenic mice to establish the *Tcf7*^{lox/lox} *Mx1Cre* compound line.

The involvement of Notch1 and Tcf1 in TCD was re-confirmed and assessed by analysis of age-matched *Notch1* ^{Δ/Δ *Mx1Cre*} and *Tcf7* ^{Δ/Δ *Mx1Cre*} animals 4-6 weeks post conditional LoF of *Notch1* and *Tcf7* in thymocytes, compared with poly(I:C)-injected but not recombined controls: *Tcf7*^{lox/lox} and *Notch1*^{lox/lox} (Figure 7A). As expected, activation of *Mx1Cre* with poly(I:C) led to gene inactivation of either *Notch1* or *Tcf7* resulting in impaired total thymocyte count (Figure 7A,B). T cell develop in the thymic microenvironment from BM-derived progenitors through four stages of double negative cells (DN1-4; CD4⁻ CD8⁻) and CD4⁺ CD8⁺ DP T cells into CD4⁺ SP and CD8⁺ SP lymphocytes. Deletion of *Notch1* and *Tcf7* strongly reduced absolute numbers of CD4⁺ SP, CD4⁺ CD8⁺ DP and CD8⁺ SP thymic T cells (Figure 7C,D). The reduction of thymocyte numbers was a result of an early developmental block at the DN1 stage in *Notch1* ^{Δ/Δ *Mx1Cre*} and *Tcf7* ^{Δ/Δ *Mx1Cre*} animals (Figure 7E,F). However, only in *Notch1* ^{Δ/Δ *Mx1Cre*} animals thymic lymphoid progenitors, in the absence of Notch signaling, gave rise to immature B220⁺ IgM^{-/low} B cells (Figure 7G,H).

Taken together, the functionality of the conditional *Tcf7* LoF mouse model was confirmed by re-assessing T cell development.

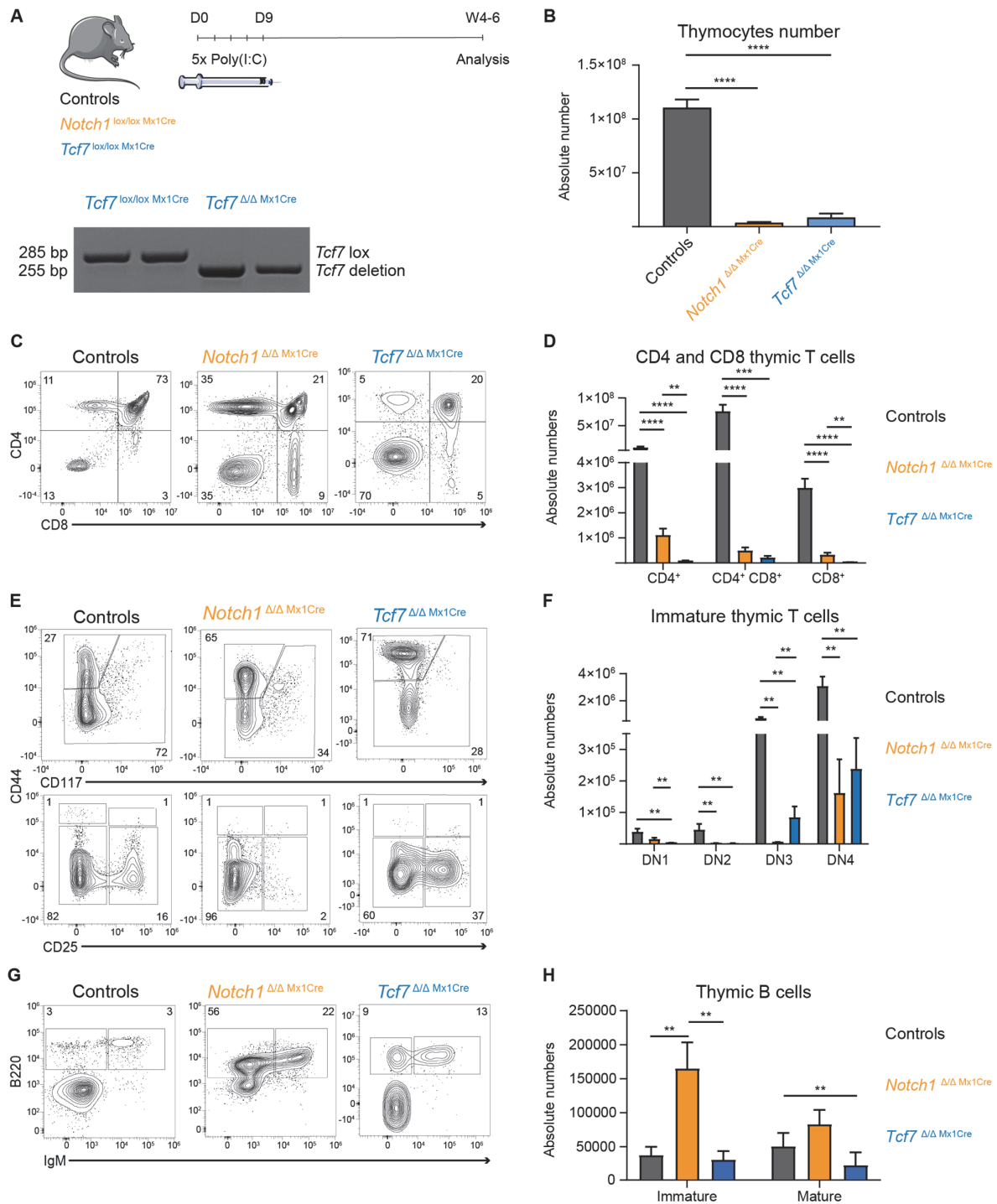


Figure 7 - Physiologic T cell development requires Notch1 and Tcf1

A, Schematic representation of conditional deletion: *Tcf7*^{lox/lox} or *Notch1*^{lox/lox} (Controls, black, n=15), *Notch1*^{lox/lox} *Mx1Cre* (orange, n=9) or *Tcf7*^{lox/lox} *Mx1Cre* (blue, n=11) mice. Lower panel confirms genomic deletion of targeted *Tcf7* locus by PCR. **B**, Quantification of absolute number of thymocytes in all experimental groups. Data are represented as mean \pm SEM. Unpaired t-test, ****, p-value<0.0001. **C-H**, Phenotypic flow cytometric analysis of induced thymic cells. Left panels depict representative plots from Controls, *Notch1* ^{Δ/Δ} *Mx1Cre* and *Tcf7* ^{Δ/Δ} *Mx1Cre*, with quantification of absolute numbers on the right for **(D)** CD4 and CD8 cells, **(F)** immature T cells and **(H)** thymic B cells. Data are represented as mean \pm SEM. Unpaired t-test, **, p-value<0.01; ***, p-value<0.001; ****, p-value<0.0001.

4.2. *Tcf7* is essential for Notch1-mediated T-ALL induction

Having confirmed the importance for *Tcf1* and Notch 1 in TCD, we aimed to assess the function of *Tcf1* in the context of Notch1-driven T-ALL induction. The *R26 N1IC^{lox/+} Mx1Cre* (*N1IC*) genetic Notch1 GoF mouse model was used to induce leukemogenesis in BM chimeras (173). *Mx1Cre*-mediated recombination results in *Rosa26*-driven (*R26*) expression of a dominant active form of *Notch1* (*N1IC*) linked to an *eGFP* fluorescent reporter allowing for detection of induced and recombined cells by flow cytometry. *R26 N1IC^{lox/+} Tcf7^{lox/lox} Mx1Cre* (*N1IC Tcf7^{Δ/Δ}*) compound animals were used to interrogate LoF of *Tcf7* in an oncogenic Notch1-driven T-ALL setting (Figure 8A). In addition to *N1IC*-expression, activation of the *Mx1Cre* recombinase drove efficient inactivation of *Tcf7* leading to loss of *Tcf1* protein in induced BM cells (Figure 8B).

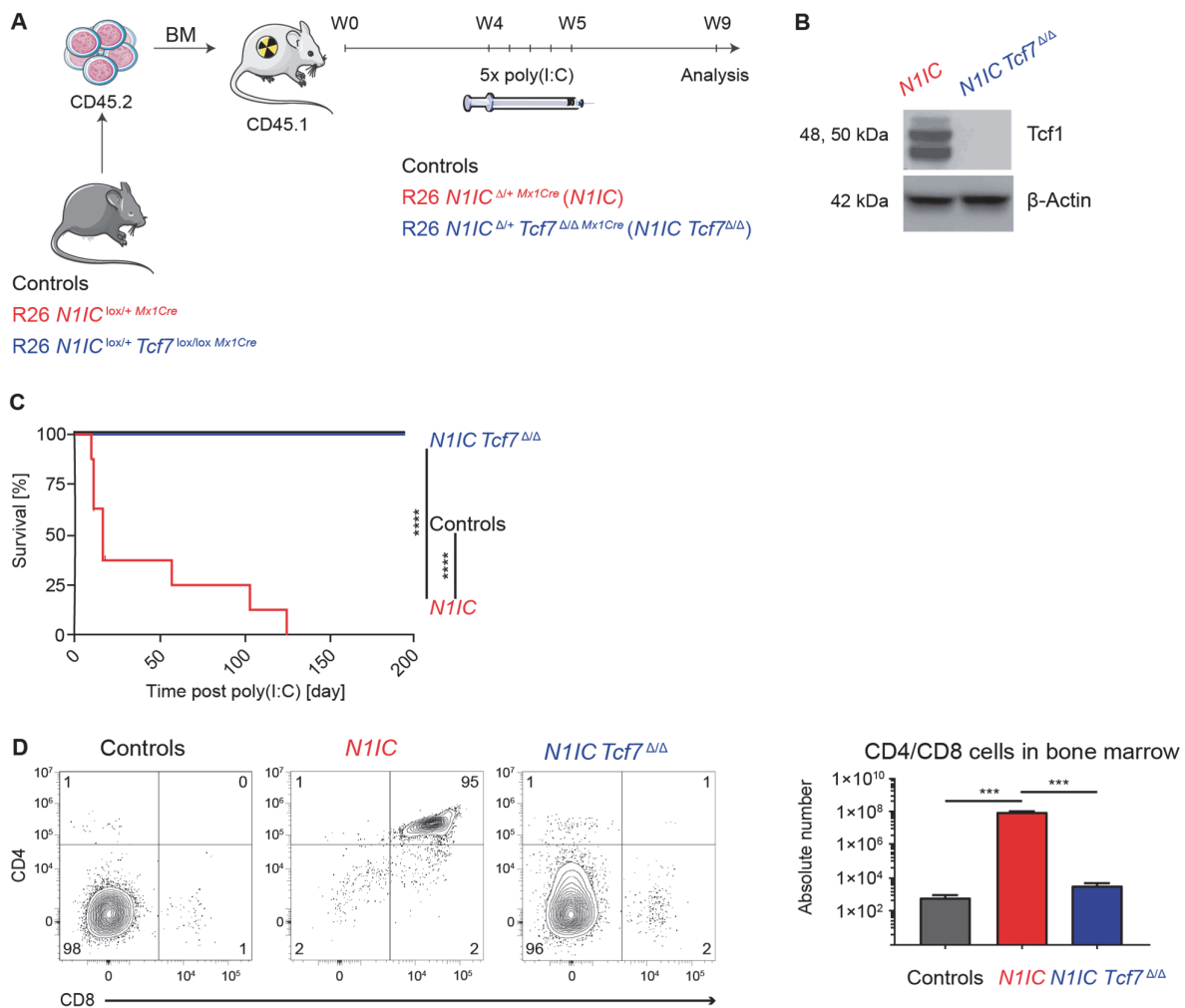


Figure 8 – Initiation of Notch1-driven T-ALL is Tcf7-dependent

A, Schematic representation of bone marrow (BM) chimeras transplanted with the indicated genotypes: *R26 N1IC^{lox/+}* or *R26 N1IC^{lox/+} Tcf7^{lox/lox}* (Controls, black), *R26 N1IC^{lox/+} Mx1Cre* (*N1IC*, red) or *R26 N1IC^{lox/+} Tcf7^{lox/lox} Mx1Cre* (*N1IC Tcf7^{lox/lox}*, blue) and treatment schedule. **B**, Total protein analyses for Tcf1 and β -actin on isolated BM cells of experimental samples: *N1IC*, *N1IC Tcf7 $\Delta\Delta$* . **C**, Kaplan-Meier survival plot of chimeras after last poly(I:C) injection. *N1IC* mice (n=8), *N1IC Tcf7 $\Delta\Delta$* (n=10) and *Controls* (n=7) followed for 199 days. Log-rank (Mantel-Cox) test, ****, p-value<0.0001. **D**, Phenotypic flow cytometric analysis of transplanted (CD45.2⁺) and induced (eGFP⁺ for *N1IC* and *N1IC Tcf7 $\Delta\Delta$*) BM cells. Left panels depict representative plots from *Controls* (n=4), *N1IC* (n=6) and *N1IC Tcf7 $\Delta\Delta$* (n=5), with quantification of absolute numbers on the right. Data are represented as mean \pm SEM. Unpaired t-test, ***, p-value<0.001.

Expression of *N1IC* resulted in T-ALL development with full penetrance (Figure 8C). Flow cytometric analysis of *N1IC* GoF chimeric BM cells revealed an accumulation of CD4⁺ CD8⁺ DP T-ALL leukemic cells (Figure 8D), with concomitant loss of other *N1IC*-expressing hematopoietic lineages including erythroblasts, B lymphocytes and myeloid cells (Figure 9A-C). Surprisingly, none of the *N1IC Tcf7 $\Delta\Delta$* BM chimeras developed disease (Figure 8C). Importantly, the abrogation of T-ALL in *N1IC Tcf7 $\Delta\Delta$* BM chimeras was not a mere consequence of loss of the transplant since donor chimerism (CD45.2⁺ cells detected in periphery) was maintained over time (Figure 9D). However, erythroblasts, myeloid cells, immature B220⁺ IgM⁻ B cells, and to a somewhat lesser extent mature B220⁺ IgM⁺ B cells, were still efficiently suppressed by oncogenic expression of *Notch1* (Figure 9A-C). *N1IC* GoF BM chimeras revealed preferential differentiation of hematopoietic progenitors into T-ALL cells, while *N1IC Tcf7 $\Delta\Delta$* BM chimeras revealed increased numbers of progenitors without a visible changes in their phenotype (data not shown). This observation was not further pursued in the context of this thesis project.

In order to determine an involvement of β -catenin-mediated canonical Wnt signaling in Notch1-driven T-ALL, we performed β -catenin LoF studies in an oncogenic Notch1 GoF background. To this end, *β -catenin^{lox/lox}* mice were crossed with the *R26 N1IC^{lox/lox} Mx1Cre* (*N1IC $\Delta\Delta$*) transgenic mouse model to generate experimental *R26 N1IC^{lox/lox} β -catenin^{lox/lox} Mx1Cre* (*N1IC $\Delta\Delta$ β -catenin $\Delta\Delta$*) compound animals (Figure 10A,B). Phenotypic analysis of BM at the experimental endpoint revealed accumulation of CD4⁺ CD8⁺ DP and CD8⁺ SP T-ALL cells only in *N1IC $\Delta\Delta$ β -catenin $\Delta\Delta$* and *N1IC $\Delta\Delta$* chimeras. Again, no disease was observed in *N1IC $\Delta\Delta$ Tcf7 $\Delta\Delta$* chimeras, whereas all *N1IC $\Delta\Delta$ β -catenin $\Delta\Delta$* BM chimeras succumbed to T-ALL with a modest but significant kinetic delay compared to *N1IC $\Delta\Delta$* chimeras (Figure 10C,D).

These results demonstrate that Tcf1 exerts essential, β -catenin independent, functions in Notch1-driven T-ALL initiation, while the suppression of other hematopoietic lineages imposed by forced Notch signaling appears to be largely Tcf1-independent.

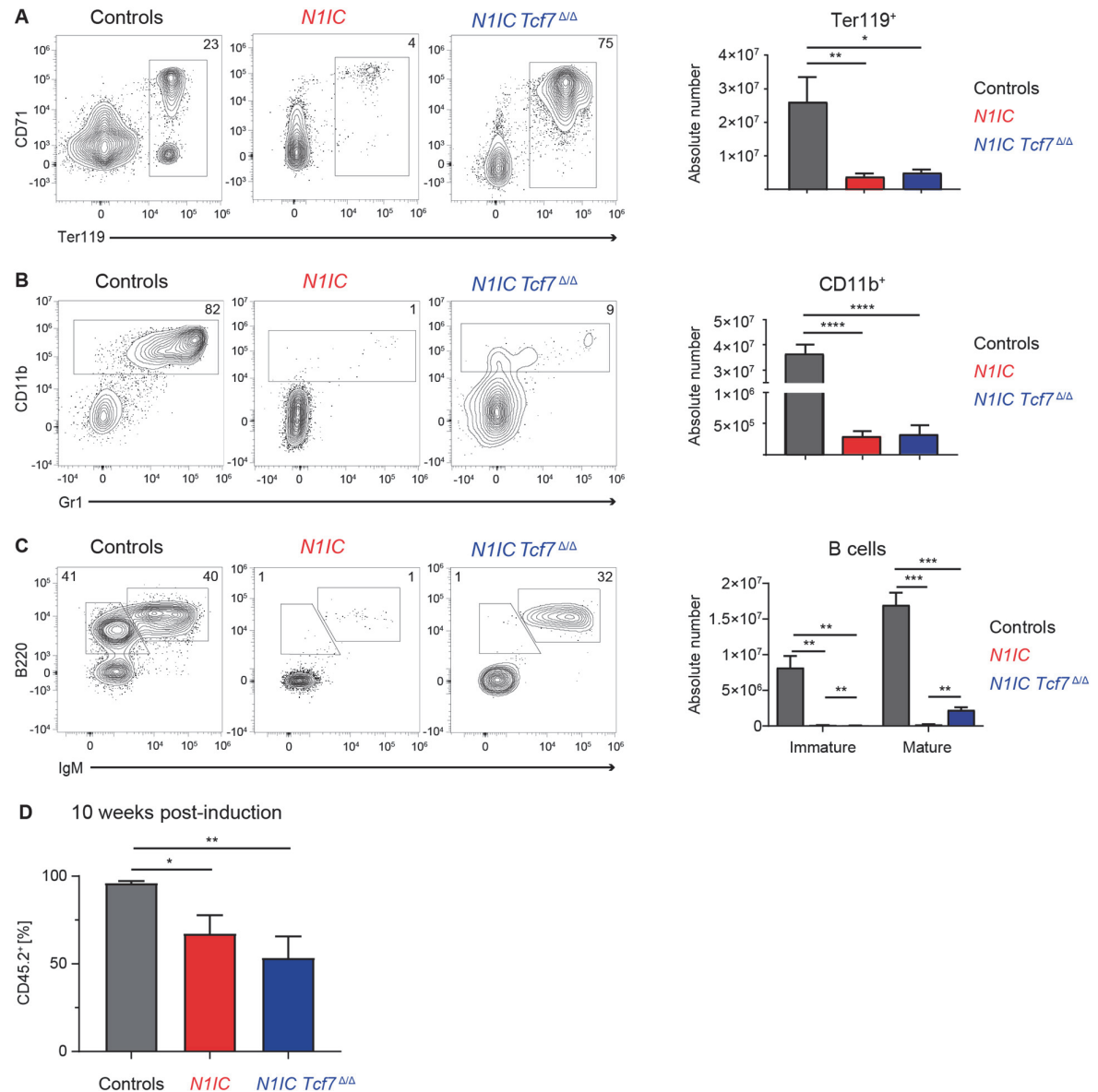


Figure 9 – Suppression of erythroid, myeloid and B lineages is mediated by Notch1

A-C, Phenotypic flow cytometric analysis of transplanted (CD45.2⁺) and induced (eGFP⁺ for *N1IC* and *N1IC Tcf7 Δ/Δ*) BM cells. Left panels depict representative plots from *Controls* (n=4), *N1IC* (n=6) and *N1IC Tcf7 Δ/Δ* (n=5), with quantification of absolute numbers on the right for **(A)** erythroid cells, **(B)** myeloid cells and **(C)** B cells. Data are represented as mean \pm SEM. Unpaired t-test, *, p-value<0.05; **, p-value<0.01; ***, p-value<0.001; ****, p-value<0.0001. **D**, Quantification of phenotypic flow cytometric analysis of CD45.2⁺ transplanted cells in peripheral blood of *Controls*, *N1IC* and *N1IC Tcf7 Δ/Δ* , 10 weeks after induction with poly(I:C). Data are represented as mean \pm SEM. Unpaired t-test, *, p-value<0.05; **, p-value<0.01.

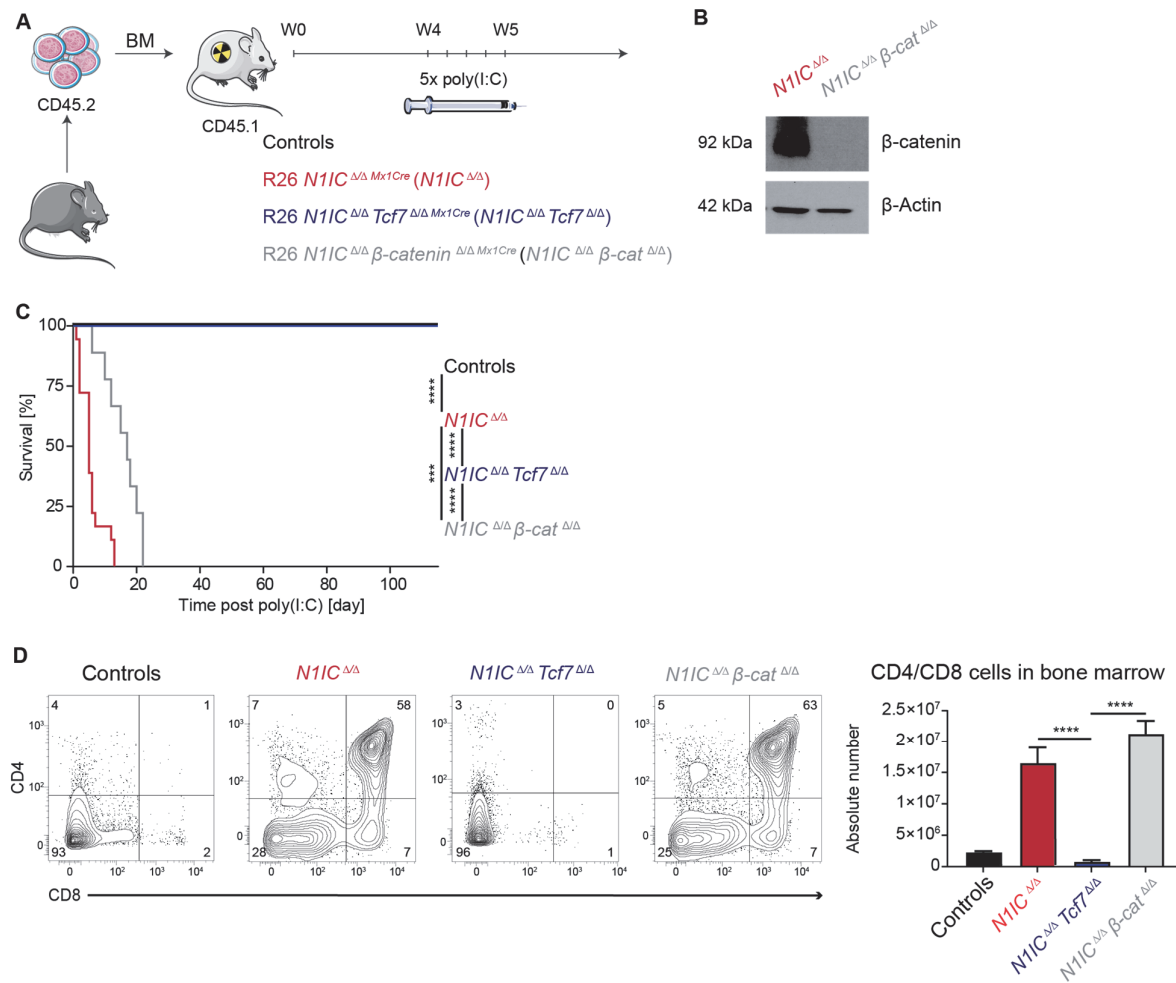


Figure 10 – β-catenin is dispensable in Notch-driven T-ALL

A, Schematic representation of bone marrow (BM) chimeras with *Controls* (black, n=3), $R26 N1IC^{lox/lox} Mx1Cre$ ($N1IC^{\Delta/\Delta}$, red, n=18), $R26 N1IC^{lox/lox} Tcf7^{lox/lox} Mx1Cre$ ($N1IC^{\Delta/\Delta} Tcf7^{\Delta/\Delta}$, blue, n=15) and $R26 N1IC^{lox/lox} \beta\text{-catenin}^{lox/lox} Mx1Cre$ ($N1IC^{\Delta/\Delta} \beta\text{-catenin}^{\Delta/\Delta}$, grey, n=9) mice. **B**, Total protein analyses for β-catenin and β-actin on isolated BM T-ALL cells of experimental samples: $N1IC^{\Delta/\Delta}$, $N1IC^{\Delta/\Delta} \beta\text{-catenin}^{\Delta/\Delta}$. **C**, Kaplan-Meier survival analysis of transplanted mice after last poly(I:C) injection and followed for 115 days. Log-rank (Mantel-Cox) test, ***, p-value<0.001; ****, p-value<0.0001. **D**, Phenotypic flow cytometric analysis of transplanted (CD45.2+) and induced (eGFP+ for $N1IC^{\Delta/\Delta}$, $N1IC^{\Delta/\Delta} Tcf7^{\Delta/\Delta}$ and $N1IC^{\Delta/\Delta} \beta\text{-catenin}^{\Delta/\Delta}$) BM. Panels on the left depict representative plots of CD4 and CD8 T cells with quantification of the absolute numbers on the right. Data are represented as mean ± SEM. Unpaired t-test, ****, p-value<0.0001.

4.3. Oncogenic Notch1 requires Tcf1 to induce a T cell-specific gene expression program in early hematopoietic progenitors

The advantage of BM chimera setting allows for *Mx1Cre*-mediated *N1/C* expression, that occurs in all blood lineages including hematopoietic stem cells (HSCs) and their progenitors within the different chimeric cohorts. As *Tcf7* gene deletion strongly affects *N1/C*-driven T-ALL induction, we aimed to investigate early changes during the onset of T-ALL. Thus, we performed RNA-seq analysis on total RNA isolated from sorted lineage⁻ Sca1⁺ cKit⁺ (LSK) BM progenitor populations from *Controls* (*N1/C*^{*lox/+*} *Tcf7*^{*lox/lox*}) and *Tcf7* ^{Δ/Δ} chimeras or transplanted GFP⁺ LSKs from *N1/C* and *N1/C Tcf7* ^{Δ/Δ} chimeras 72 hours post *Mx1Cre*-mediated recombination (Figure 11A).

Analysis of differential gene expression revealed no major differences between *Controls* and *Tcf7* ^{Δ/Δ} LSKs, indicating that ablation of *Tcf7* alone had no major impact on gene expression in LSKs (Figure 11B,C). In contrast, expression of leukemogenic *N1/C* led to a profound reprogramming of the cellular transcriptome. We identified 414 and 423 genes as significantly down- and upregulated, respectively, in *N1/C*-expressing LSK compared to *Controls* (Figure 11B,C). Among the 423 upregulated genes, 119 were Tcf1-dependent as they were lost in the LSK population of *N1/C Tcf7* ^{Δ/Δ} *Mx1Cre* BM chimeras (Annexed Table 3). Interestingly, analysis of Gene Ontology (GO) biological processes (GOBP) of the most significantly *Tcf7*-dependent upregulated genes in LSKs derived from *N1/C* chimeras, revealed a strong association with lymphocyte differentiation/activation and included T cell activation and differentiation (Figure 11D). Transcriptional regulation by Notch1 and Tcf1 repressed other genetic programs, for instance, TRK, FGFR signaling pathways and processes involved in lung development (Figure 11E). Quantitative analysis of gene expression confirmed upregulation of T cell-specific transcripts including *Tcf7*, *Il2ra*, *Gata3* and *CD3e* in *N1/C*-expressing LSKs (Figure 11F) (34). In contrast, *N1/C* was unable to upregulate T cell-specific genes in the absence of Tcf1 (Figure 12A). Processes associated with TCD were largely lost following deletion of *Tcf7* even though typical Notch target genes such as *Notch1* itself and *Hes1* were significantly upregulated by *N1/C*, independently of Tcf1 (Figure 12B).

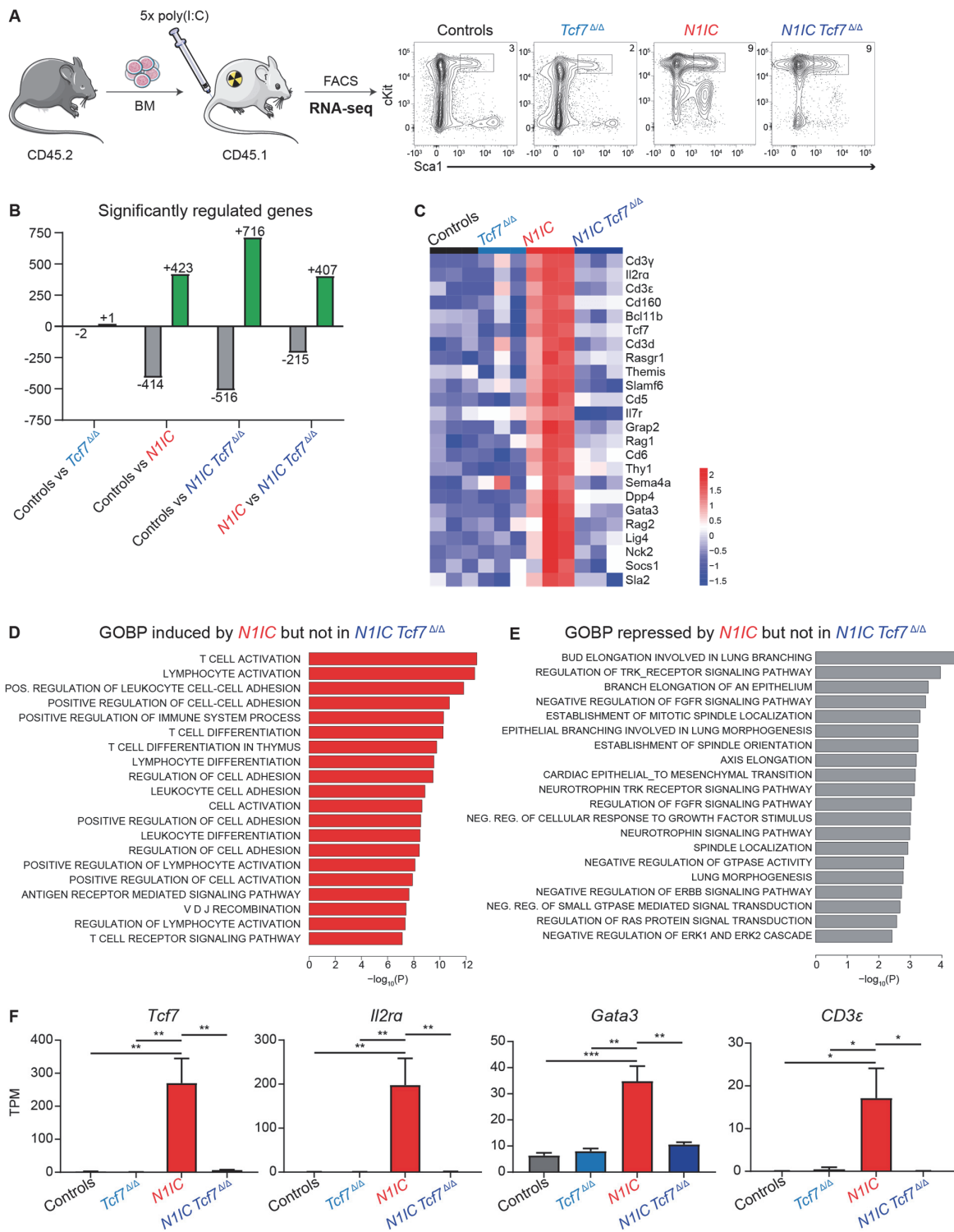


Figure 11 - *Tcf7* regulates expression of genetic T cell signature in bone marrow progenitors in response to oncogenic Notch1

A, Experimental setup: Induced CD45.2⁺ bone marrow (BM) cells from *Controls* (black, n=3), *Tcf7*^{Δ/Δ} (blue, n=3), *N1IC* (red, n=3) or *N1IC Tcf7*^{Δ/Δ} (dark blue, n=3) mice were FACS purified for lineage⁻, cKit⁺ (CD117⁺) and Sca1⁺ BM progenitors (LSK) for RNA-seq analysis. Representative flow cytometric plots are shown. **B**, Quantitative analysis of differentially expressed genes in comparisons between experimental groups: upregulated - green and downregulated - grey (FDR < 0.05, -2 > FC > 2). **C**, Heatmap depicting regulated genes in *N1IC* vs *Controls* (FDR < 0.05, -2 > FC > 2) from Gene Ontology (GO) T cell activation collection, shown for all experimental groups. **D**, Enrichment of biological pathways from Gene ontology biological process (GOBP) collection in genes with induced expression by *N1IC* and *Tcf7* from RNA-seq on LSK cells. Top 20 pathways are shown. P-values were calculated with Fisher's exact test. **E**, Enrichment of biological pathways from GOBP collection in genes with decrease expression by *N1IC* and *Tcf7* from RNA-seq on LSK cells. Top 20 pathways are shown. p-values were calculated with Fisher's exact test. **F**, Expression of investigated genes measured as TPM (Transcripts per kilobase Million) with induced expression by *N1IC* and *Tcf7* from RNA-seq on LSK cells. Barplots from left to right of each graph: *Controls*, *Tcf7*^{Δ/Δ}, *N1IC* and *N1IC Tcf7*^{Δ/Δ} LSK. Data are represented as mean ± SEM. One-way ANOVA, *, p-value<0.05; **, p-value<0.01; ***, p<0.001.

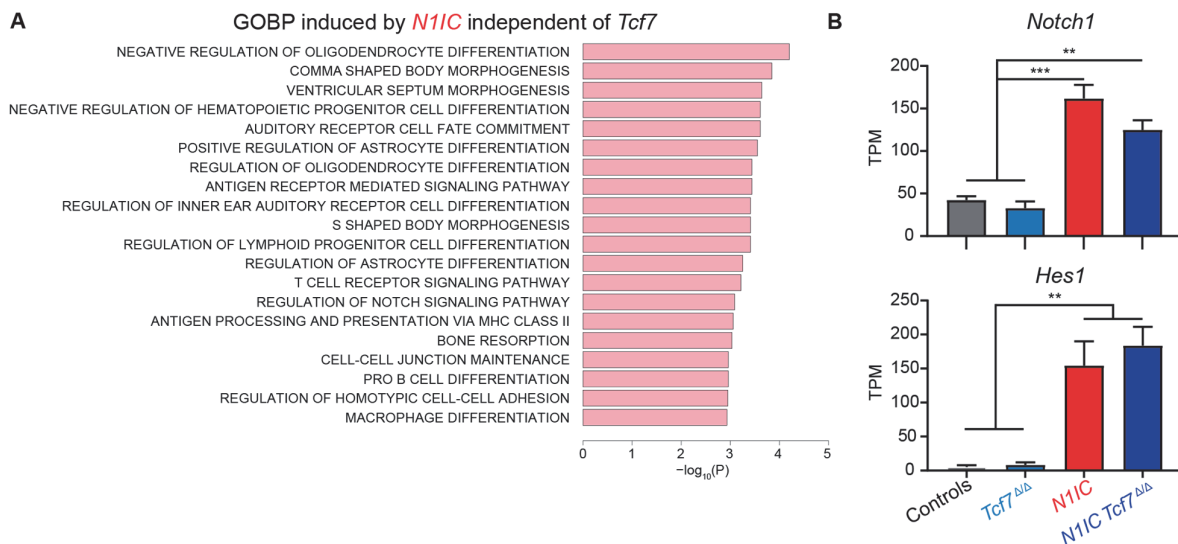


Figure 12 – Notch1 regulates non-T cell developmental process independently of Tcf1

A, Enrichment of biological pathways from Gene ontology biological process (GOBP) collection in genes with induced expression by *N1IC* and independent of *Tcf7* from RNA-seq on LSK cells. Top 20 pathways are shown. P-values were calculated with Fisher's exact test. **B**, Expression of investigated genes measured as TPM with induced expression by *N1IC* and independent of *Tcf7* from RNA-seq on LSK cells. Barplots from left to right of each graph: *Controls*, *Tcf7*^{Δ/Δ}, *N1IC* and *N1IC Tcf7*^{Δ/Δ} LSKs. Data are represented as mean ± SEM. One-way ANOVA, **, p-value<0.01; ***, p-value<0.001.

Next, we tested whether GoF *Tcf7* in Notch1-wild type BM progenitors would be sufficient to induce ectopic TCD and/or T-ALL. Thus, we performed *Tcf1* GoF experiments using chimeras transplanted with *Tcf7 IRES eGFP*-retrovirally transduced BM progenitors (Figure 13A). Analysis of *Tcf7* GoF chimeras 13 weeks post transplantation revealed neither ectopic TCD nor T-ALL induction compared to *eGFP*-expressing *Controls* or retrovirally-driven *N1ICD* BM chimeras analyzed

at disease endpoint (9 weeks post transplantation) (Figure 13B,C). We confirmed efficient retrovirally induced expression of Tcf1 by immunoblotting in *Tcf7*-expressing BM cells as well as expression of Tcf1 downstream of Notch1 in *N1ICD*-expressing BM cells (Figure 13D).

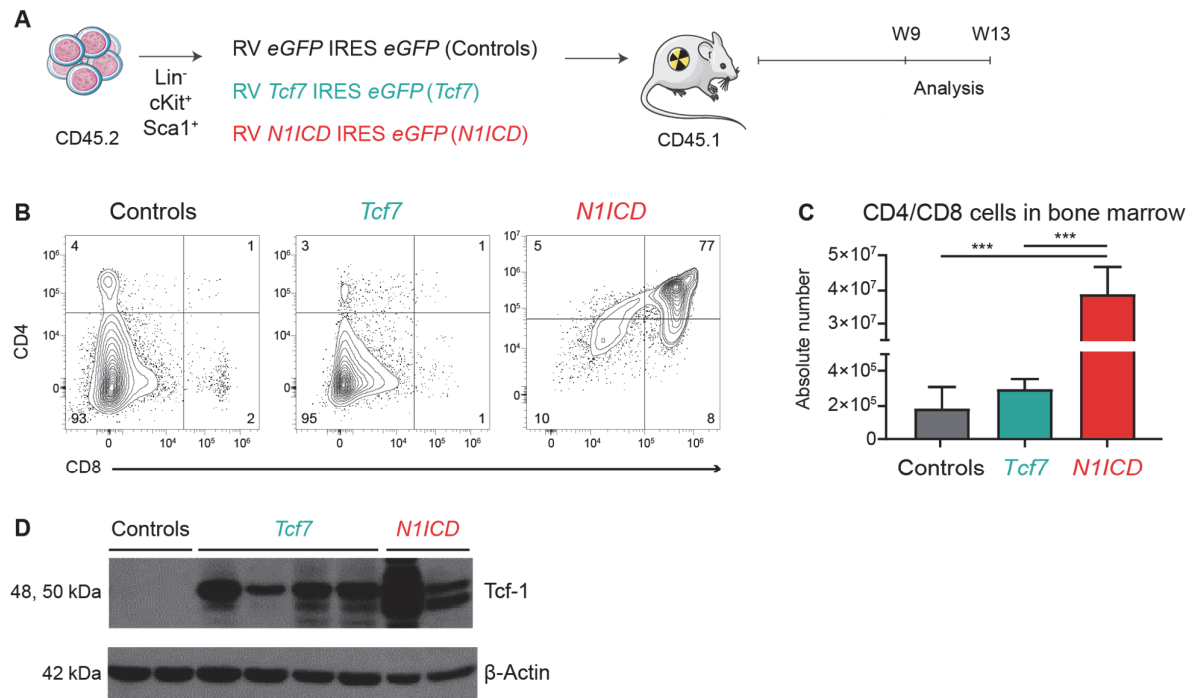


Figure 13 – Ectopic expression of *Tcf7* in Notch1-proficient BM is not sufficient to induce T-ALL

A, Schematic representation of retroviral-based overexpression experiment: BM progenitors infected with MigR1 viruses overexpressing *eGFP* (*Controls*, black, n=4), *Tcf7 eGFP* (*Tcf7*, turquoise, n=5) or *N1ICD eGFP* (*N1ICD*, red, n=3). Depicted timepoints of analysis performed at experimental endpoints. **B**, Phenotypic flow cytometric analysis of *eGFP*⁺ CD4 and CD8 T cells derived from BM at endpoint. **C**, Quantification of absolute number of T cells in BM. Data are represented as mean ± SEM. One-way ANOVA, ***, pvalue<0.001. **D**, Total protein analyses for Tcf1 and β-actin on isolated BM cells of experimental groups: *Controls* (n=2), *Tcf7* (n=4) and *N1ICD* (n=2).

Altogether, this demonstrates that Tcf1 is essential for N1IC to elicit a T cell-specific gene expression program. In the absence of Tcf1, N1IC had lost its oncogenic specificity already in early hematopoietic progenitors. However, Tcf1 alone *in vivo* is not sufficient to induce a T cell program with leukemic self-renewal activity even in a Notch1-proficient background.

4.4. Tcf1 regulates chromatin accessibility in *N1IC*-expressing LSKs

As Tcf1 has previously been associated with the epigenetic regulation of TCD (92,107) we asked whether Tcf1 is necessary to modulate chromatin accessibility, thus enabling forced N1IC to permit a T cell- and leukemia-specific program in early hematopoietic progenitors and HSCs. Since *Tcf7* is not expressed in physiological LSKs no significant differences in gene expression between *Controls* and *Tcf7*^{ΔΔ} BM chimeras were observed, thus ATAC-seq analysis was performed on sorted LSKs derived from *Controls*, *N1IC* and *N1IC Tcf7*^{ΔΔ} BM chimeras 72 hours post *Mx1Cre*-driven recombination (Figure 14A). Differential accessibility analysis showed pronounced modulation of the epigenome in response to N1IC and Tcf1 (Figure 14B,C). Genes in the proximity to N1IC-induced Tcf1-dependent chromatin modulation are predominantly associated with T cell differentiation, proliferation and activation (Figure 14D,E). Indeed, N1IC-driven chromatin accessibility at promoter and putative enhancers of T cell-specific genes (34), including *Ptcrα* and *Cd3ε*, are Tcf1-dependent (Figure 14F).

Lineage determination of early hematopoietic progenitors is governed by specific master TFs and their controlled binding to regulatory chromatin loci. To assess whether such regulation in T-ALL initiation is dependent on N1IC- and Tcf1-mediated chromatin modulation, we performed TF binding and footprint analysis of gained and lost ATAC-seq peaks. Thus, we examined whether N1IC regulates chromatin topology in a Tcf1-dependent manner, coordinating the accessibility of TF binding sites (BSs) of such lineage specific master regulators in early hematopoietic progenitors. The top differentially enriched TFs at the accessible loci were Runx factors, Tcf factors, Lef1 and RBPJ in *N1IC*-expressing versus *Control* and *N1IC* vs *N1IC Tcf7*^{ΔΔ}. These findings confirmed that chromatin loci are open and probably bound by these TFs in a Notch1- and Tcf1-regulated manner. Gain of Gata TFs BSs, sharing similar DNA binding motifs, as a consequence of *Tcf7* deficiency in *N1IC* and *N1IC Tcf7*^{ΔΔ}, indicates that in a N1IC GoF context their repression is *Tcf7* dependent. In contrast, Cebp and Pax5 TFs BSs correlate with negative differential binding scores independent of *Tcf7* but efficiently repressed by Notch1 (Figure 15A-D).

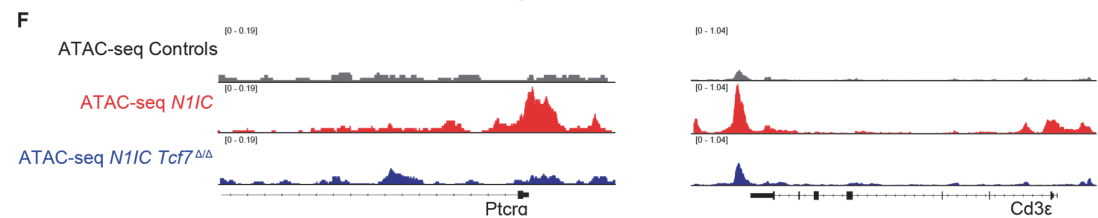
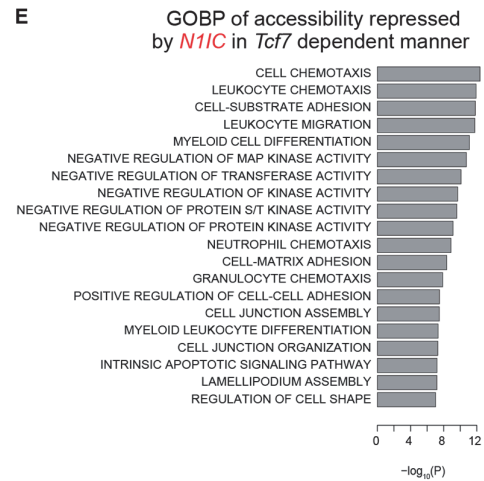
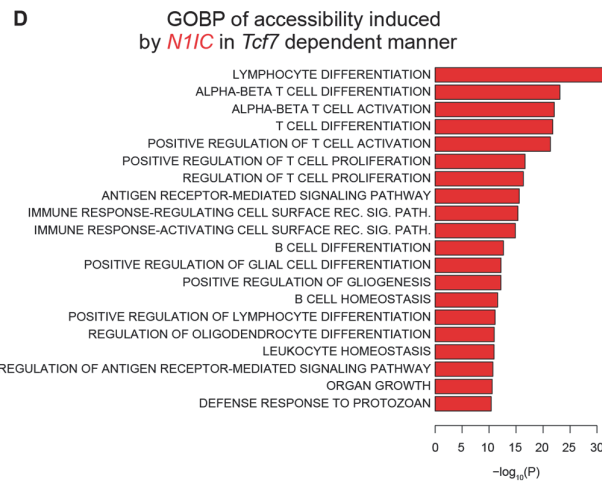
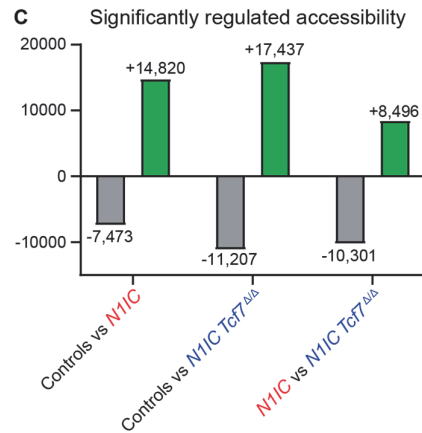
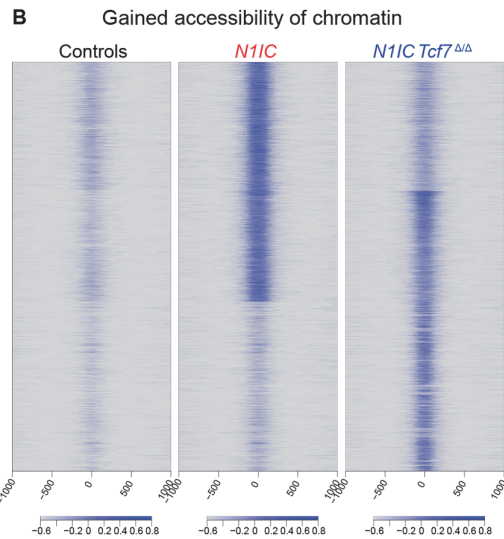
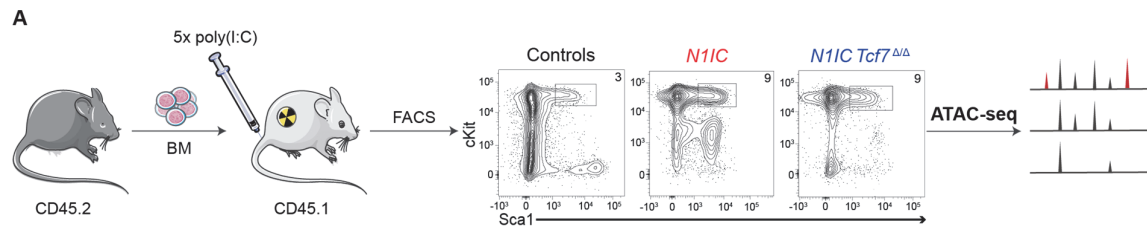
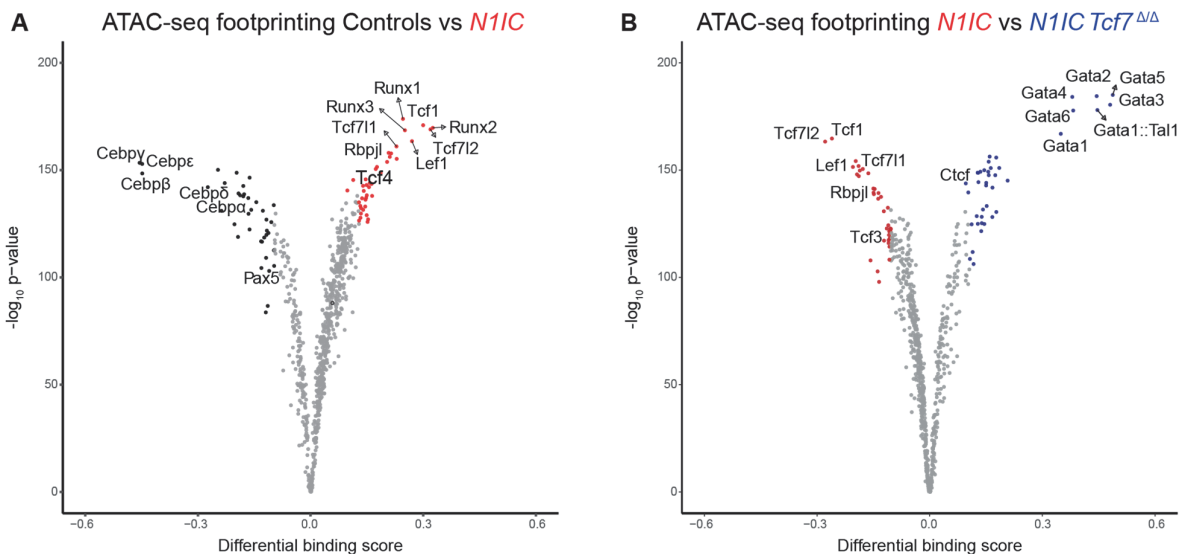


Figure 14 - Notch1 and Tcf1 epigenetically establish T lineage specification in early bone marrow progenitors

A, Induced CD45.2⁺ bone marrow (BM) cells from *Controls* (black, n=3), *N1/C* (red, n=3) or *N1/C Tcf7^{Δ/Δ}* (dark blue, n=3) mice were FACS purified for lineage⁻, cKit⁺ (CD117) and Sca1⁺ BM progenitors (LSK) for ATAC-seq analysis. Characteristic flow cytometric plots are shown. **B**, Heatmap depicting all regulated genomic loci in comparison *N1/C* vs *Controls* (FDR<0.01) for ATAC-seq called peaks, shown for all experimental groups. Color scale is shown below the heatmap. **C**, Quantitative analysis of differentially accessible genetic loci in comparisons between experimental groups: upregulated - green and downregulated - grey (FDR<0.01). **D**, Enrichment of biological pathways from Gene Ontology biological process (GOBP) collection in genes with induced proximal accessibility by *N1/C* and *Tcf7*. Top 20 pathways are shown from ontologies with a fold enrichment >2 and FDR<0.05. P-values were calculated with Fisher's exact test. **E**, Enrichment of biological pathways from GOBP collection regulated as decreased accessibility proximal to genes by *N1/C* and *Tcf7* from ATAC-seq on LSK cells. Top 20 pathways are shown. p-values were calculated with Fisher's exact test. **F**, IGV chromatin accessibility profiles for all experimental groups shown at the promoter of *Ptcrα* and for *Cd3ε*. Tracks were group-scaled, scaling is shown in the top left corner. Schematic representation of genetic loci is depicted below the profiles.

These results suggest that on one hand forced *N1/C* expression in LSKs modulates a chromatin landscape that allows induction of T cell-specific genes and this process is *Tcf1*-dependent at an early hematopoietic progenitor stage. On the other hand, forced *N1/C* expression simultaneously closes chromatin loci that would be permissive for the induction of alternative hematopoietic cell fates such as myeloid, B cell or erythroid cell lineages. These processes appear to be regulated by both *Tcf7*-dependent and -independent mechanisms.



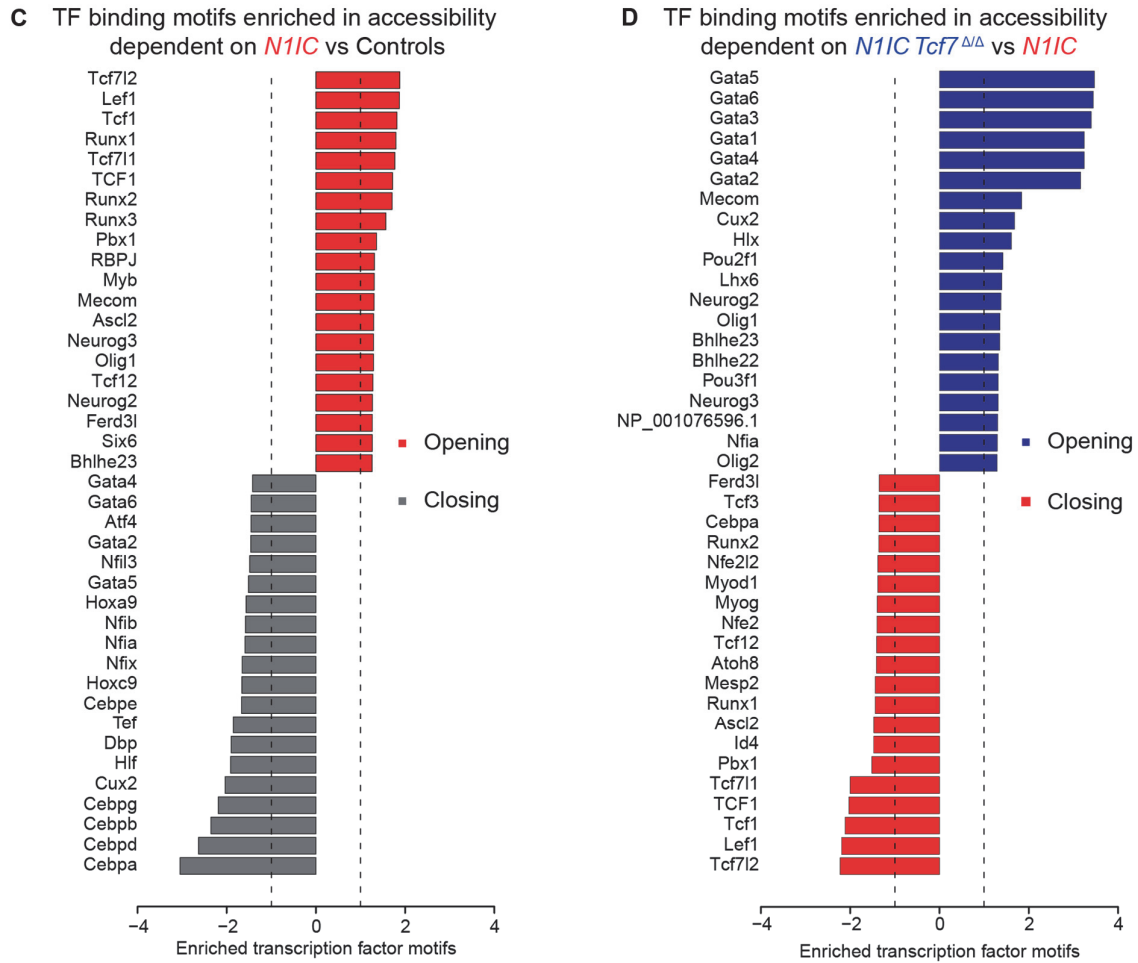


Figure 15 – Lineage specification dependent on Notch1 and Tcf1 in early bone marrow progenitors

A,B, Footprint analysis for transcription factors binding in *Controls* (black, n=3), *N1IC* (red, n=3) or *N1IC Tcf7^{Δ/Δ}* (dark blue, n=3) bone marrow (BM) chimeras. Chimeras were FACS purified for lineage⁺, cKit⁺ (CD117) and Sca1⁺ BM progenitors (LSK) and analysis of ATAC-seq footprint revealed regulation by **(A)** *N1IC* vs *Controls* and **(B)** *N1IC* vs *N1IC Tcf7^{Δ/Δ}* LSK. **C,D**, Analysis of transcription factor binding motifs in CIS-BP at loci with increased (red) or decreased (grey) accessibility in comparison between ATAC-seq on: **C**, *N1IC* vs *Controls* LSKs and **D**, *N1IC Tcf7^{Δ/Δ}* vs *N1IC* LSKs.

4.5. Dynamic large-scale genomic interactions promoting leukemogenesis rely on Notch1 and Tcf1

Using chromatin accessibility analysis, we identified an early involvement of Tcf1 and Notch1 in the events of T-ALL-commitment from hematopoietic BM progenitors. It is not clear whether 3D genome folding is equally affected and thus impacting cell fate decisions in oncogenic processes (6). Therefore, we performed *in situ* Hi-C allowing for the spatial profiling of all genomic loci at once (159). Sorted LSK cells from *N11C*, *N11C Tcf7^{ΔΔ}* and *Control* mice were isolated, and DNA proximity ligation and high-throughput sequencing was performed with the commercially available Arima Hi-C kit (Figure 16A). Paired-end sequencing reads were aligned and chromatin contacts maps were generated using Juicer (206) (Annexed Figure 1A,B). Data resolution of 2.5 kb (Figure 16B,C) and improved quality over recently published *in situ* Hi-C on BM HSCs (207) allowed us to proceed confidently with the analysis of topology (Figure 16D).

Genomic compartment A regions contain open and active chromatin, while B compartments are correlated with heterochromatin (208,209). Oncogenic Notch1 and subsequent inactivation of *Tcf7* did not induce significant differences in global segmentation of the genome into A/B compartments (Annexed Figure 1C). Nonetheless, direct analysis of dynamic A/B compartment switching revealed dependencies on Notch1 and Tcf1, ranging from 0.6-2.4% of the genome, switching from inactive B to active A compartments, while not more than 2.2% of identified compartments lost their activation profile. This shows that global compartment switching is relatively stable over all genetic backgrounds. Interestingly, dynamic compartment switching correlated positively with significantly differentially expressed genes after integration of our RNA-seq data (Figure 16E-G). Amongst the genes whose expression was directly affected by compartment switching in response to LoF *Tcf7* in a Notch1-oncogenic background (*N11C Tcf7^{ΔΔ}* vs *N11C*), we identified *Prss2*, *Gata3* and *Siglece* (involved in TCD and T-ALL) (Figure 16H) (34,216,217).

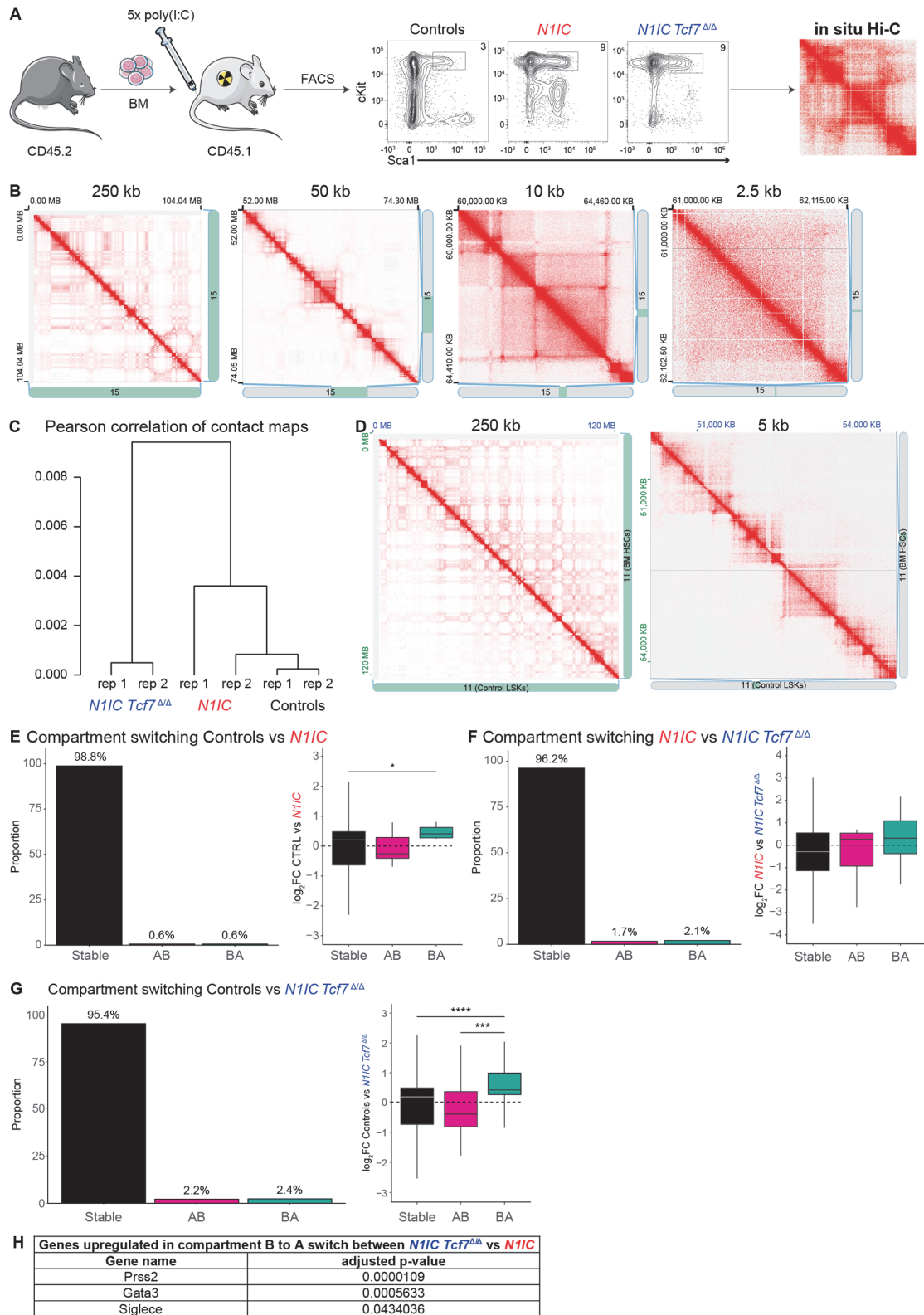


Figure 16 – Genome-wide analysis of dynamic compartments A and B by *in situ* Hi-C

A, Induced CD45.2⁺ bone marrow (BM) cells from *Controls* (black, n=2), *N1IC* (red, n=2) or *N1IC Tcf7^{ΔΔ}* (dark blue, n=2) mice were FACS purified for lineage⁺, cKit⁺ (CD117) and Sca1⁺ BM progenitors (LSK) and processed for *in situ* Hi-C analysis. Characteristic flow cytometric plots are shown. **B**, Juicebox-generated contact matrices depicting chromatin interactions (red) from chromosome 15: whole chromosome, at 250kb resolution (far left); A/B compartments at 50 kb resolution (middle left); chromatin domains at 10 kb resolution (middle right); chromatin loops at highest resolution of 2.5 kb (far right) shown for *Controls*. The 1D regions corresponding to a contact matrix are indicated in the diagrams below and at right. The intensity of each pixel represents the normalized number of contacts between a pair of chromatin loci. Maximum intensity: 1350, 293, 20, 3 (from left to right). **C**, Hierarchical clustering of Pearson correlation analysis on the KR-normalized contact matrices at 1 Mb resolution. **D**, Juicebox-generated contact matrices from chromosome 11: the whole chromosome, at 250 kb resolution (left); chromatin loops at the resolution of 5 kb (right) shown for *Controls* vs BM HSCs (GSE119347). The 1D regions corresponding to a contact matrix are indicated in the diagrams below and at right. The intensity of each pixel represents the normalized number of contacts between a pair of loci. Maximum intensity: 1349, 14 (for left and right). **E-G**, Chromatin compartment A/B switching between (**E**) *Controls* and *N1IC* (**F**) *N1IC* and *N1IC Tcf7^{ΔΔ}*, between (**G**) *Controls* and *N1IC Tcf7^{ΔΔ}* quantified on the left. Association with gene expression differences (adjusted p-values ≤ 0.05) for genes within dynamic compartments is shown on the right. AB – switching from active compartment A to inactive compartment B, BA – from B to A. Unpaired Wilcoxon test, *, p-value < 0.05. **H**, List of differentially expressed genes in an activated compartments (compartment switch B to A) by *Tcf7* in oncogenic *N1IC* background. Values of adjusted p-value are shown in comparison *N1IC* vs *N1IC Tcf7^{ΔΔ}*, which were calculated with Fisher's exact test.

We next identified topologically associating domains (TADs) from contact matrices at 5 kb resolution. Observed TADs ranged in size from 39 kb to about 3 Mb, with a median of 180 kb (Figure 17A). Boundaries of TADs are known to be enriched for CTCF (159,160) therefore we performed CTCF analysis by ChIP-seq on *ex vivo* LSKs from *Controls*, *N1IC* and *N1IC Tcf7^{ΔΔ}*. Enrichment analysis at both TAD anchors identified oriented binding of CTCF at over 86.6% of chromatin domains (Figure 17B,C), thus only these domains were taken into consideration for subsequent analyses. We focused on condition-specific TADs associated with each experimental group and identified 124 TADs that were regulated by Notch1 and Tcf1 (*N1IC*-specific), whereas 341 TADs were regulated in a Notch1-dependent Tcf1-independent fashion (*N1IC Tcf7^{ΔΔ}*-specific) (Figure 17D). Differential expression analysis of genes within *N1IC*-specific TADs showed a trend for correlation between gene transcription and overexpression of *N1IC* (Figure 17E,F). Over-representation analysis (ORA) identified ‘enlarged thymus’ as the most enriched ontology, including several T-ALL-related genes associated with *N1IC* LSKs (Figure 17G). One of these genes, *Id2*, revealed 4- or 2.16-fold increased expression in *N1IC* over *Controls* and in the comparison of *N1IC* and *N1IC Tcf7^{ΔΔ}*, respectively, in association with establishment of specific chromatin domains (Figure 17H and Annexed Table 3) (218).

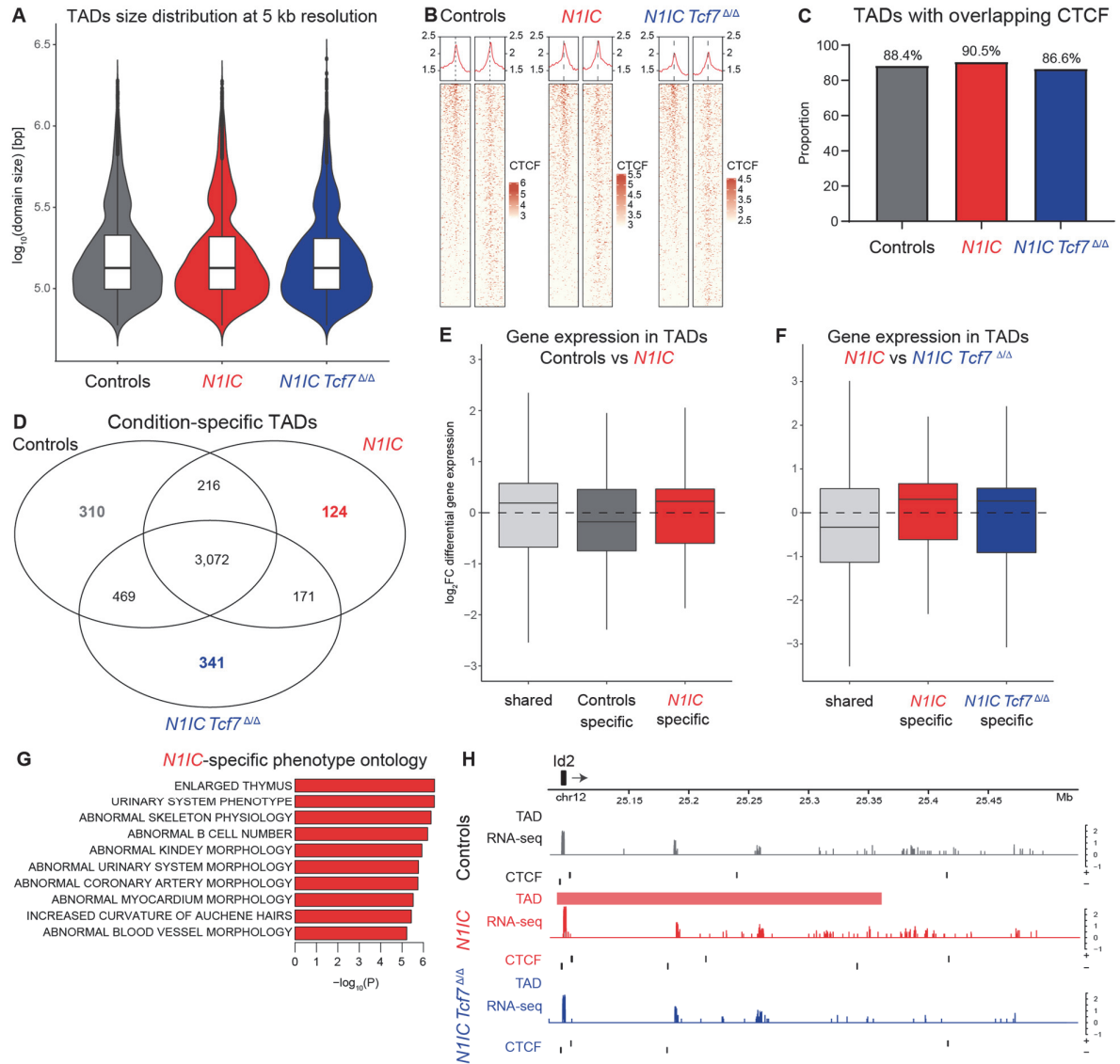


Figure 17 - Notch1 and Tcf1 regulate 3D organization of chromatin domains

A, Size distribution in \log_{10} base pairs for identified TADs at 5 kb chromatin interaction matrix resolution in LSKs from BM chimeras: *Controls*, *N1IC* and *N1IC Tcf7 $\Delta\Delta$* . **B**, CTCF ChIP-seq binding signal at the left and right boundaries of TADs. Shown at 50 kb windows around TAD boundaries, with 1 kb read coverage bins. Enrichment for CTCF is scaled on the right. Data shown from left to right for: *Controls*, *N1IC* and *N1IC Tcf7 $\Delta\Delta$* . **C**, Quantification of the proportion of identified TADs with confirmed CTCF ChIP-seq signal at the boundaries shown for: *Controls*, *N1IC* and *N1IC Tcf7 $\Delta\Delta$* . **D**, Three-way quantitative comparison of identified TADs for condition-specific and shared loops for *Controls*, *N1IC* and *N1IC Tcf7 $\Delta\Delta$* . **E,F**, TADs analysis with Juicer at 5 kb resolution focusing on condition-specific TADs between (**E**) *Controls* and *N1IC* and (**F**) *N1IC* vs *N1IC Tcf7 $\Delta\Delta$* for association with gene expression differences (adjusted p -value ≤ 0.05). **G**, Over representation analysis (ORA) for *N1IC*-specific TAD-associated genes from phenotype catalogue. Top 10 pathways are shown from ontologies with a differential gene expression FDR < 0.05. p -values were calculated with Fisher's exact test. **H**, Schematic depiction of *N1IC*-specific TAD regulating the expression of *Id2* gene. Representation of genetic loci is depicted above the profiles for Arrowhead-identified TADs, RNA-seq and directional CTCF binding identified for *Controls*, *N1IC* and *N1IC Tcf7 $\Delta\Delta$* LSKs. Expression is depicted in \log_{10} -scale shown on the right. Binding for CTCF from ChIP-seq analysis is shown for both DNA strands.

Our analysis revealed fine-tuned coordination by N1IC and Tcf1 of a pathological cell-fate program regulating higher-order genomic folding. Tcf1 not only restricts A/B compartments but also selectively induces appropriate TADs. Such adjustments of the T-ALL chromatin landscape at the level of immature BM progenitors demonstrates the essential role for both TFs during initiation of leukemogenesis.

4.6. Establishment of enhancer-promoter interactions in T-ALL initiation partly depends on *Tcf7*

After assessing the effects of Notch1 and Tcf1 on high-order genome organization, we focused on 3D chromatin loop interactions established in *N1IC* and *N1IC Tcf7^{Δ/Δ}*. Local interactions within the genome are of particular importance when connecting regulatory regions, such as promoters with distal enhancers, leading to modulated gene expression (219). Thus, we took advantage of the identified chromatin loops confirmed within at least three resolutions (between 2.5 kb and 25 kb at 1 kb increment). These interactions were identified in condition-specific comparison as well as shared between experimental groups. Fewer chromatin loops were regulated by both Notch1 and Tcf1 in *N1IC in vivo* LSKs (Figure 18A).

Since not all of the identified chromatin loops connect genes with potential regulatory regions, we focused on those with confirmed proximity to genes at one of the loop anchors. Investigation of chromatin loops connecting genes with differential expression dependent on both Notch1 and Tcf1 revealed genes from leukemic ontology associated with T-ALL, such as *Pdgfrb* (220) (Figure 18B,C). Although investigation of Notch1-dependent but Tcf1-independent chromatin loops in *N1IC Tcf7^{Δ/Δ}* also identified leukemic ontology as being highly enriched, the affected genes cannot be considered T-ALL-related, as they were reported in the context of myeloid malignancies (Figure 18D,E) (220). Moreover, analysis of transcriptomic data for genome-wide correlation within dynamic condition-specific chromatin loops revealed no differences (Figure 18F), thus validating the computational approach restricted to analysis of functional, expression-promoting chromatin interactions.

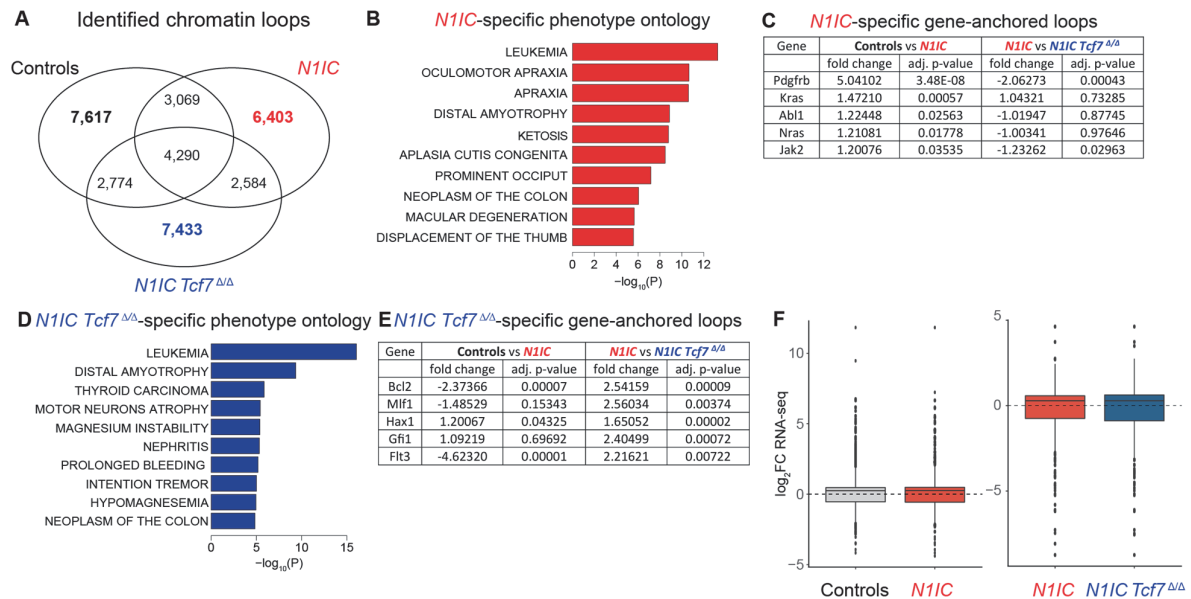


Figure 18 - Analysis of chromatin loops regarding regulation by Notch1 and Tcf1

A, Three-way quantitative comparison of identified chromatin loops for condition-specific and shared loops for *Controls*, *N1IC* and *N1IC Tcf7* Δ/Δ . **B**, ORA for *N1IC*-specific loop-associated genes for phenotype catalogue. Top 10 pathways are shown. p-values were calculated with Fisher's exact test. **C**, List of differentially expressed genes in a *N1IC*-specific chromatin loops anchored in proximity to the genes. Values of adjusted p-value were calculated with Fisher's exact test. **D**, Gene enrichment analysis for *N1IC Tcf7* Δ/Δ -specific gene-associated loops from human phenotype catalogue. Top 10 pathways are shown from ontologies with a differential gene expression FDR<0.05. P-values were calculated with Fisher's exact test. **E**, List of differentially expressed genes in a *N1IC Tcf7* Δ/Δ -specific chromatin loops anchored in proximity to the genes. Values of adjusted p-value were calculated with Fisher's exact test. **F**, Association of gene expression differences (adjusted p-value≤0.05) for genes within dynamic condition-specific loops (from panel). Left and middle panel show log₂ fold-change for condition-specific loop-associated genes from RNA-seq analysis.

Regulation of gene expression in T-ALL by NOTCH1 has been linked to distal enhancers, where NOTCH1 occupancy correlates with increased levels of H3K27ac (170,221). Thus, LSKs from *Controls*, *N1IC* and *N1IC Tcf7* Δ/Δ BM chimeras were FACS-isolated for genome-wide ChIP-seq analysis of histone marks associated with promoters (H3K4me3), enhancers (H3K4me1) and their activation status (activation: H3K27ac and repression: H3K27me3) (Figure 19A,B). We first investigated whether identified chromatin loops were connecting active regulatory regions in Notch1- or Tcf1-dependency, by profiling H3K27ac at the loop anchors distal to genes. Interestingly, the highest genome-wide acetylation levels of connected chromatin loci were detected in *N1IC*-specific loops, highlighting the importance of Tcf1 in distal activation of regulatory elements downstream of Notch1-signaling (Figure 19C). Subsequently, all genes transcriptionally controlled by both, Notch1 and Tcf1 were examined for possible involvement of distal regulatory elements.

Indeed, distal looping of potential enhancer sites (presence of H3K4me1 and H3K27ac peaks) to the proximity of a gene in *N1/C* LSKs resulted in increased expression of the canonical T cell gene *Cd5* (Figure 19D,E).

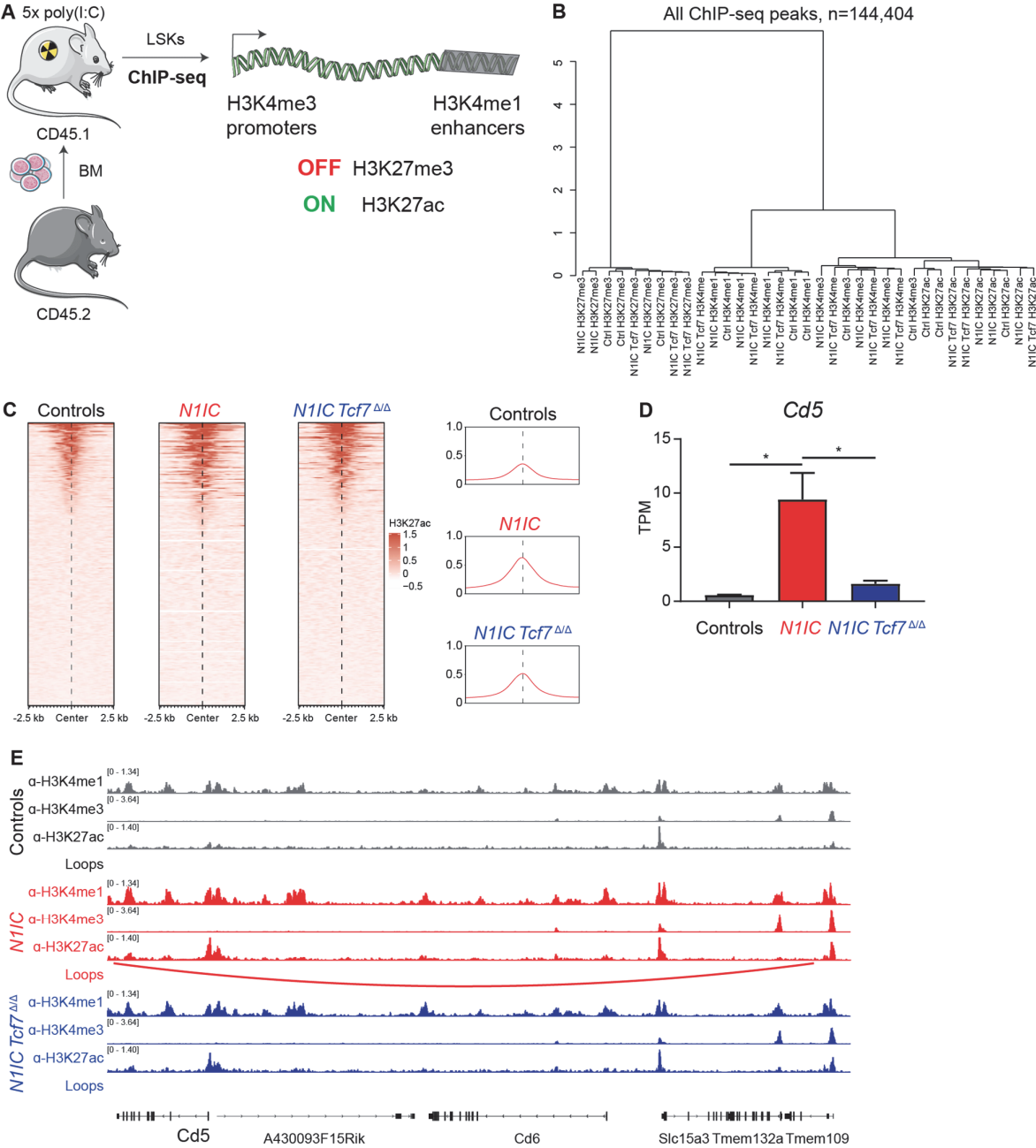


Figure 19 – Activation of chromatin loops is mediated by Notch1 and Tcf1

A, Induced CD45.2⁺ bone marrow (BM) cells from *Controls* (black, n=3), *N1IC* (red, n=3) or *N1IC Tcf7^{ΔΔ}* (dark blue, n=3) mice were FACS purified for lineage⁻, cKit⁺ (CD117) and Sca1⁺ BM progenitors (LSK) for histone mark ChIP-seq analysis with depicted antibodies. Characteristic flow cytometric plots are shown. **B**, Hierarchical clustering of Spearman correlation analysis on all ChIP-seq peaks for histone marks in *Controls*, *N1IC* and *N1IC Tcf7^{ΔΔ}* LSKs. **C**, H3K27ac ChIP-seq signal at the anchors distal to genes. Shown at 5kb windows around center of a peak or loop anchor. Enrichment for H3K27ac is scaled. Quantification of the global signal for non-gene loop anchors is depicted on the right. Data shown from left to right for: *Controls*, *N1IC* and *N1IC Tcf7^{ΔΔ}*. **D**, Expression of *Cd5* measured as Transcript Per Kilobase Million (TPM) from RNA-seq on LSK cells. Barplots from left to right of each graph: *Controls*, *N1IC* and *N1IC Tcf7^{ΔΔ}*. Data are represented as mean ±SEM. One-way ANOVA, *, p-value<0.05. **E**, IGV profiles for *Controls*, *N1IC* and *N1IC Tcf7^{ΔΔ}* from Hi-C-identified loops and ChIP-seq for histone marks. Tracks were group-scaled, scaling is shown in the top left corner. Schematic representation of genetic loci is depicted below the profiles.

Next, we performed unbiased genome-wide analysis for *N1IC*-specific enhancer-gene (E-G) interactions correlated with differential expression of genes. We characterized putative enhancer regions as H3K4me1⁺ and H3K4me3⁻ loci with *N1IC*-specific increase in H3K27ac signals, which were then annotated to the anchor distal to genes of condition-specific loops. This approach allowed us to identify 3,595 *N1IC*-specific E-G interactions, slightly fewer than amongst *Controls*- and *N1IC Tcf7^{ΔΔ}*-specific loops (Figure 20A). Nevertheless, unbiased integration of transcriptomic data, interactome and ChIP-seq for activation of regulatory elements determined a subset of genes regulated by Notch1 and Tcf1 (Figure 20B,C). Moreover, genes such as *Cdh23*, *Tspan2* and *Snx20* were significantly upregulated due to *N1IC*-specific activation of E-G loops (Figure 20D-F). Importantly, amongst identified genes, a subset was reported to be differentially expressed or affected by epigenetic regulation during TCD or in T-ALL (170,222).

Taken together, three-dimensional interactions of chromatin in T-ALL-prone LSKs is regulated by Tcf1 in order to calibrate the transcriptional output of genes during Notch1-mediated transformation processes.

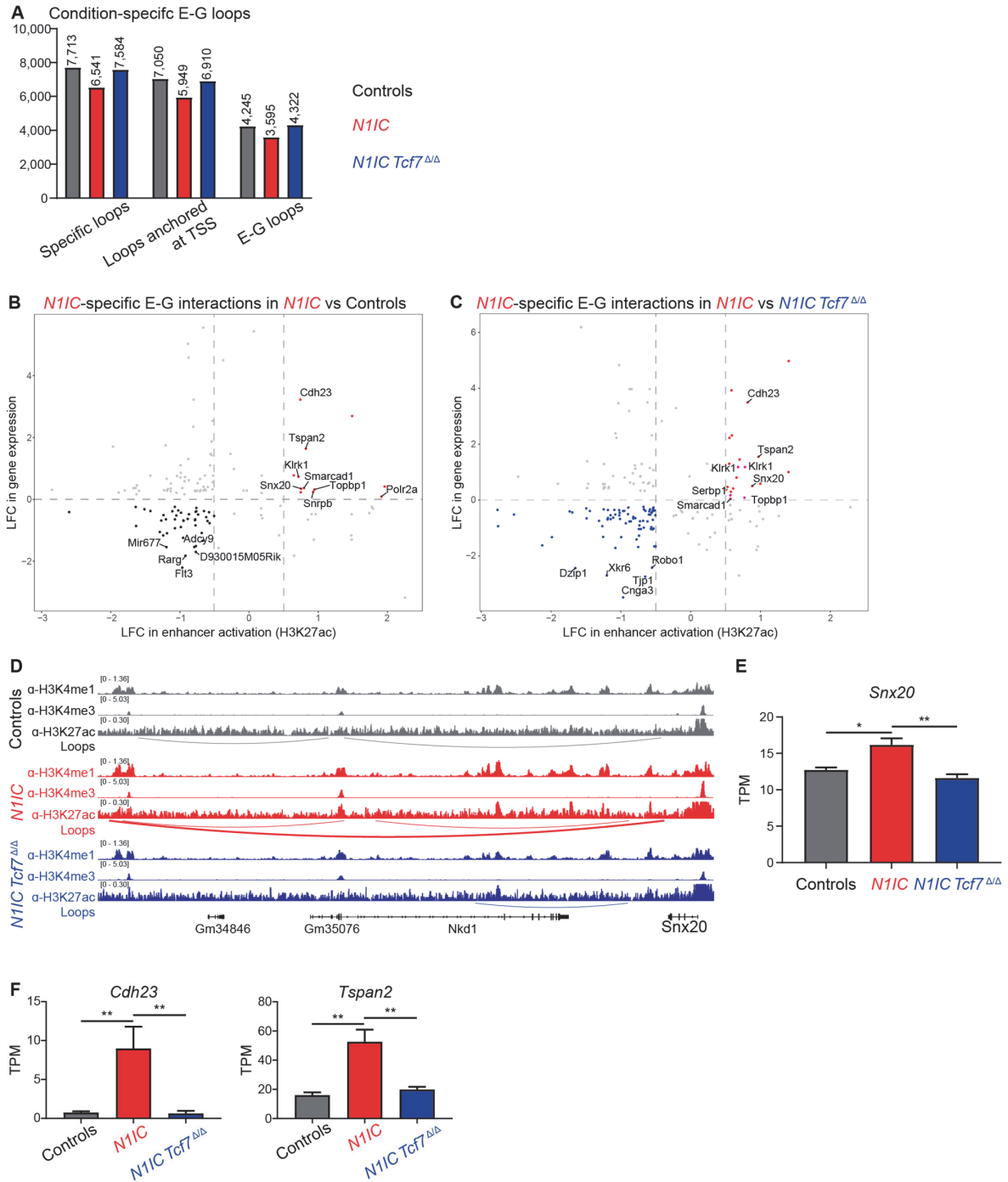


Figure 20 – Notch1 and Tcf1 regulation involving distal elements

A, Quantification of identified chromatin loops specific for: *Controls* (grey), *N1IC* (red) and *N1IC Tcf7^{ΔΔ}* (blue). **B,C**, Scatterplots for associate changes in gene expression (LFC on y-axis) with changes in H3K27ac signal (x-axis) for *N1IC*-specific E-G interactions between: **(B)** *N1IC* vs *Controls* and **(C)** *N1IC* vs *N1IC Tcf7^{ΔΔ}*. Dots for genes with differential expression of p-value < 0.05 are shown in darker color. **D**, IGV profiles for *Controls*, *N1IC* and *N1IC Tcf7^{ΔΔ}* from Hi-C identified loops and ChIP-seq for histone marks. Tracks were group-scaled, scaling is shown in the top left corner. Schematic representation of genetic loci is depicted below the profiles. **E**, Expression of *Snx20* measured as Transcript Per Kilobase Million (TPM) from RNA-seq on LSK cells. Barplots from left to right of each graph: *Controls*, *N1IC* and *N1IC Tcf7^{ΔΔ}*. Data are represented as mean ± SEM. One-way ANOVA, *, p-value < 0.05; **, p-value < 0.01. **F**, Expression of *Cdh23* and *Tspan2* measured as TPM from RNA-seq on LSK cells. Barplots from left to right of each graph: *Controls*, *N1IC* and *N1IC Tcf7^{ΔΔ}*. Data are represented as mean ± SEM. One-way ANOVA, **, p-value < 0.01

4.7. A novel Tcf1-regulated *Myc*-enhancer region is essential for Notch1-driven T-ALL progression

Unbiased analysis of the epigenome revealed fine-tuning of the subset of genes. However, activation of the regulatory elements in hematopoietic progenitors might not result in an immediate 3D looping without affecting phenotype of cells. Therefore, we have investigated in depth a conserved *Notch1-MYC enhancer (NMe)* located downstream of the *MYC* promoter. *NMe* is localized in a broad superenhancer region regulating TCD and T-ALL (141,142). Genetic deletion of *NMe* abrogates chromatin looping and expression of *MYC* (142). We investigated whether the *NMe* and the *Myc* promoter are regulated in a *Tcf7*-dependent manner during the early initiation phase of T-ALL in *N1/C*-expressing LSKs. While chromatin accessibility at the *Myc* promoter was not significantly different, H3K27ac was moderately increased in *N1/C* compared to *Controls* and reduced in *N1/C Tcf7^{ΔΔ}* (Figure 21A). Interestingly, gain of the accessibility and activation at the *NMe* enhancer site 1.3 Mb downstream of *Myc* were strictly dependent on Tcf1, demonstrating the essential *Tcf7* pioneering role to open this regulatory element (Figure 21A). However, in *N1/C*-expressing LSKs, gene expression and chromatin looping of *Myc* itself were not differentially regulated at this early stage of hematopoietic progenitors (Figure 21B,C).

Unexpectedly, analysis of chromatin accessibility and enhancer-related H3K27ac revealed a prominent regulatory site 14 kb downstream of the *NMe*, regulated by Notch1 via Tcf1. We named this newly discovered region *TMe* for *Tcf1-regulated Myc enhancer* (Figure 21A). Attributing a functional relevance to the *TMe*, we hypothesized that cis-acting elements within this regulatory region would be conserved between species, as has previously been shown for the *NMe* (149). Phylogenetic footprint analysis of the *TMe* across vertebrates revealed multiple highly conserved regulatory elements (Figure 21D). The high conservation of this cluster of TF BSs in placental mammals is indicative of a functional role for the *TMe* region.

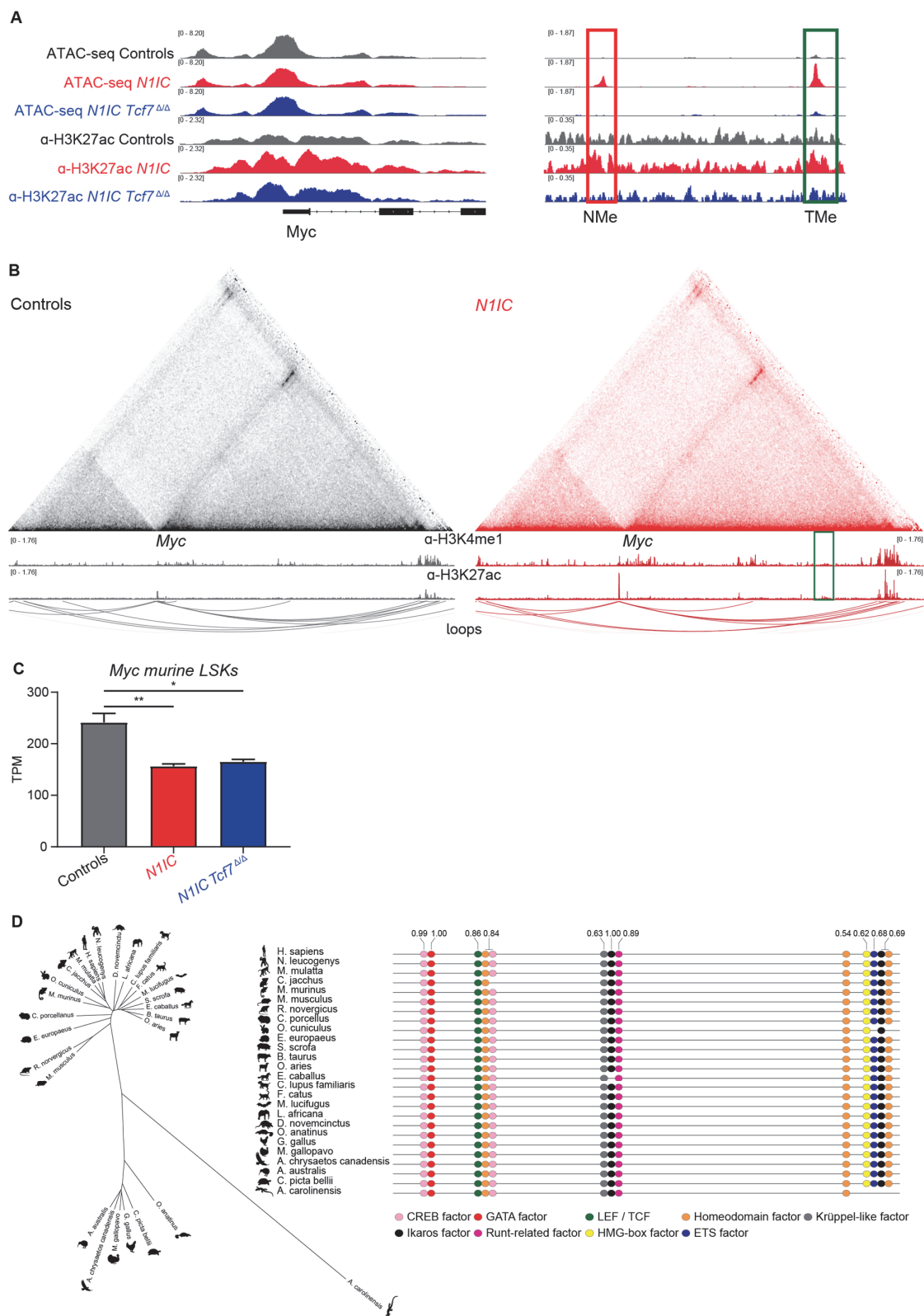


Figure 21 – Tcf1 exerts a crucial regulation within distal *Myc* enhancers

A, IGV profiles for *Controls*, *N11C* and *N11C Tcf7^{ΔΔ}* from ATAC-seq and ChIP-seq for H3K27ac performed on sorted murine LSKs for *Myc* promoter (left panel), *NMe* (red) and *TMe* (green) (right panel). Tracks were group-scaled, scaling is shown in the top left corner. Schematic genetic loci below the profiles. **B**, Contact matrices at 10 kb resolution depicting chromatin interactions of *Myc* promoter for *Controls* and *N11C*. ChIP-seq for α -H3K4me1 and α -H3K27ac with identified chromatin loops IGV profiles shown below. Tracks were group-scaled, scaling is shown in the top corners. **C**, Expression of *Myc* measured as TPM with induced expression by *N11C* and *Tcf7* from RNA-seq on murine LSK cells. Barplots from the left: *Controls*, *N11C*, *N11C Tcf7^{ΔΔ}*. Unpaired t-test, *, p-value<0.05; **, p-value<0.01. **D**, *TMe* evolutionary conservation tree (left panel) and predicted ultraconserved transcription factor binding motifs in the *TMe* sequence (right panel). PhastCons conservation scores are indicated above the sites (score >0.5).

To further support the hypothesis of cross-species conservation we assessed the ability of forced *NOTCH1* expression to establishing an oncogenic chromatin landscape in human hematopoietic progenitor cells. We used a previously reported system that models *NOTCH1*-mediated T-ALL *in vitro* through lentiviral transduction of human cord blood cells (133). Specifically oncogenic *NOTCH1* was expressed in CD34⁺ cells, cultured on OP9-DLL1 stroma cells for 8 days, and then the most immature cells (CD38⁺ CD34⁻ CD7⁺ CD5⁻) overexpressing *NOTCH1* were analyzed for chromatin accessibility. ATAC-seq profiles of *NOTCH1*-expressing CD34⁺ cells were compared with chromatin accessibility of wild type CD34⁺ cells (GSM4743251 and GSM4743252) for identification of NOTCH1-specific modulations of chromatin accessibility (Figure 22A). Annotation of gained accessibility peaks to the nearest genes, and subsequent ORA revealed that NOTCH1-regulated chromatin modulation is predominantly associated with immune response-activating cell surface receptor signaling, TCR signaling, leukocyte activation and others (Figure 22B). Taking advantage of footprint analysis, we identified TCF1 as a regulator of ontologies such as TCR signaling and pathways in cancer. Moreover, forced *NOTCH1* expression induced chromatin accessibility and TCF1 binding in T cell genes, such as *IL2RA*, as well as within the *TMe* region (Figure 22C,D). This indicates that not only DNA sequences are conserved between mammalian species, but that Notch-mediated chromatin accessibility gain is also conserved between mice and human. Furthermore, protein-centered analysis by ChIP-qPCR with α TCF1 antibody on murine T-ALL cells and human DND-41 T-ALL cell line identified binding of the protein in both, *NMe* and *TMe* (Figure 23A,B). Next, DNA locus-centered proteomic analysis, as assessed by reverse ChIP assay with biotinylated DNA bait, confirmed that TCF1 binds to *TMe* in human T-ALL cell line DND-41 (Figure 23C). Among identified co-factors of TCF1 we detected a known regulator of *NMe* - GATA3 (149), but also RUNX1 and BCL11B

indicating a potential existence of a dynamic co-regulation between a multitude of TCD-related proteins (84).

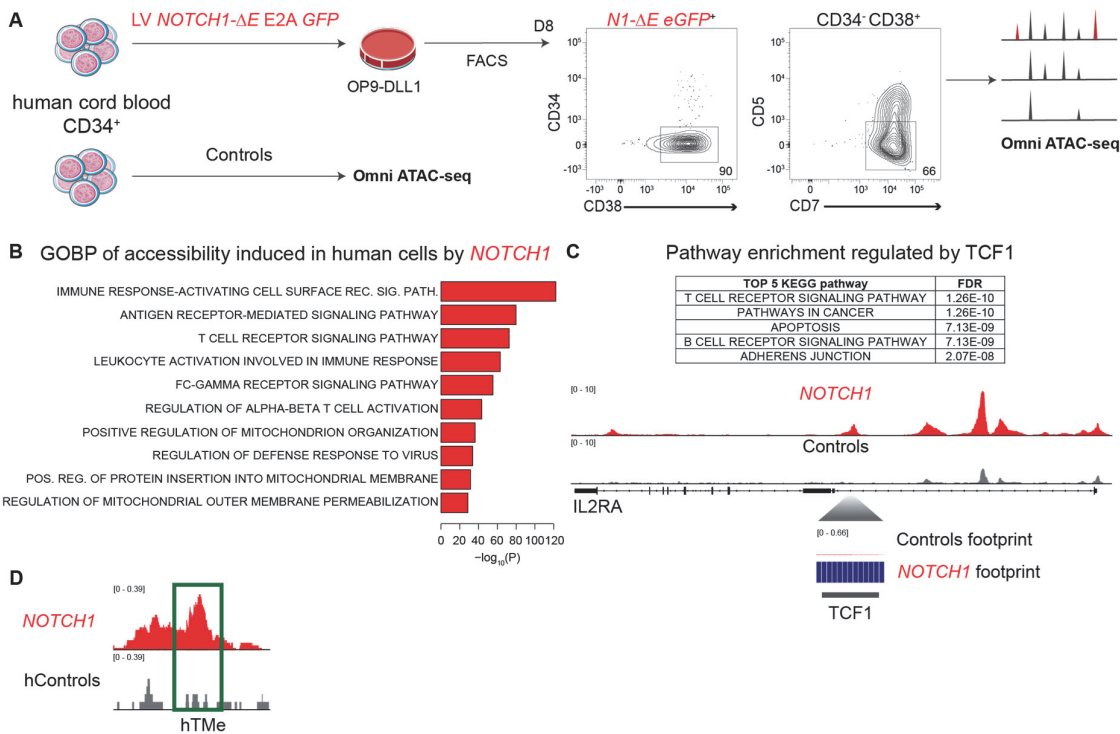


Figure 22 – TCF1 with NOTCH1 initiates genetic T cell signature and activates TMe
A, Schematic representation of lentiviral (LV) overexpression experiment using CD34⁺ human cord blood cells transduced with LV overexpressing NOTCH1 (red, n=2). Cells were used for ATAC-seq analysis. ATAC-seq (GSM4743251 and GSM4743252) data sets from CD34⁺ human cord blood cells were used as a Controls. **B**, Enrichment of biological pathways from Gene Ontology biological process collection in genes with induced proximal accessibility by human NOTCH1 and Controls CD34⁺ human cord blood cells. Top 10 pathways are shown from ontologies with an FDR≤0.01. p-values were calculated with Fisher's exact test. **C**, TOBIAS footprint analysis NOTCH1 vs Controls. Pathway enrichment analysis from KEGG pathway catalogue regulated by TCF1-confirmed footprint. Top 5 pathways are shown with corresponding FDR. Panel below represents IGV chromatin accessibility profiles for both experimental groups shown for IL2RA. Tracks were group-scaled, scaling is shown in the top left corner. Schematic representation of genetic loci is depicted below the profiles together with footprint analysis at TCF1-binding motif. **D**, IGV chromatin accessibility profiles for TMe in human NOTCH1 and Controls CD34⁺ human cord blood cells. Tracks were group-scaled, scaling is shown in the top left corner.

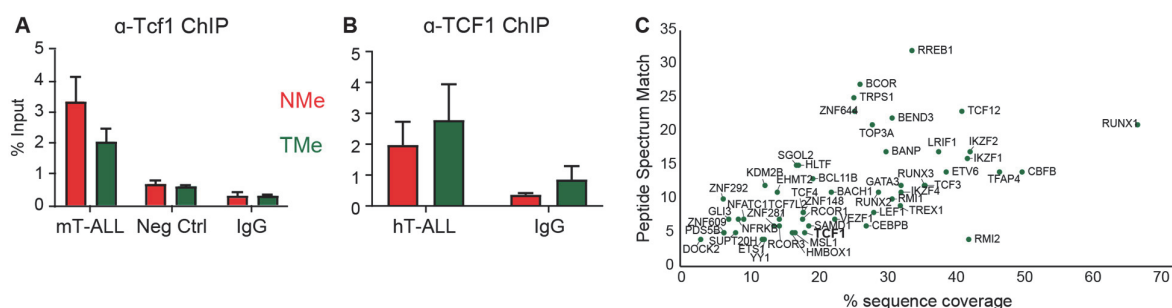


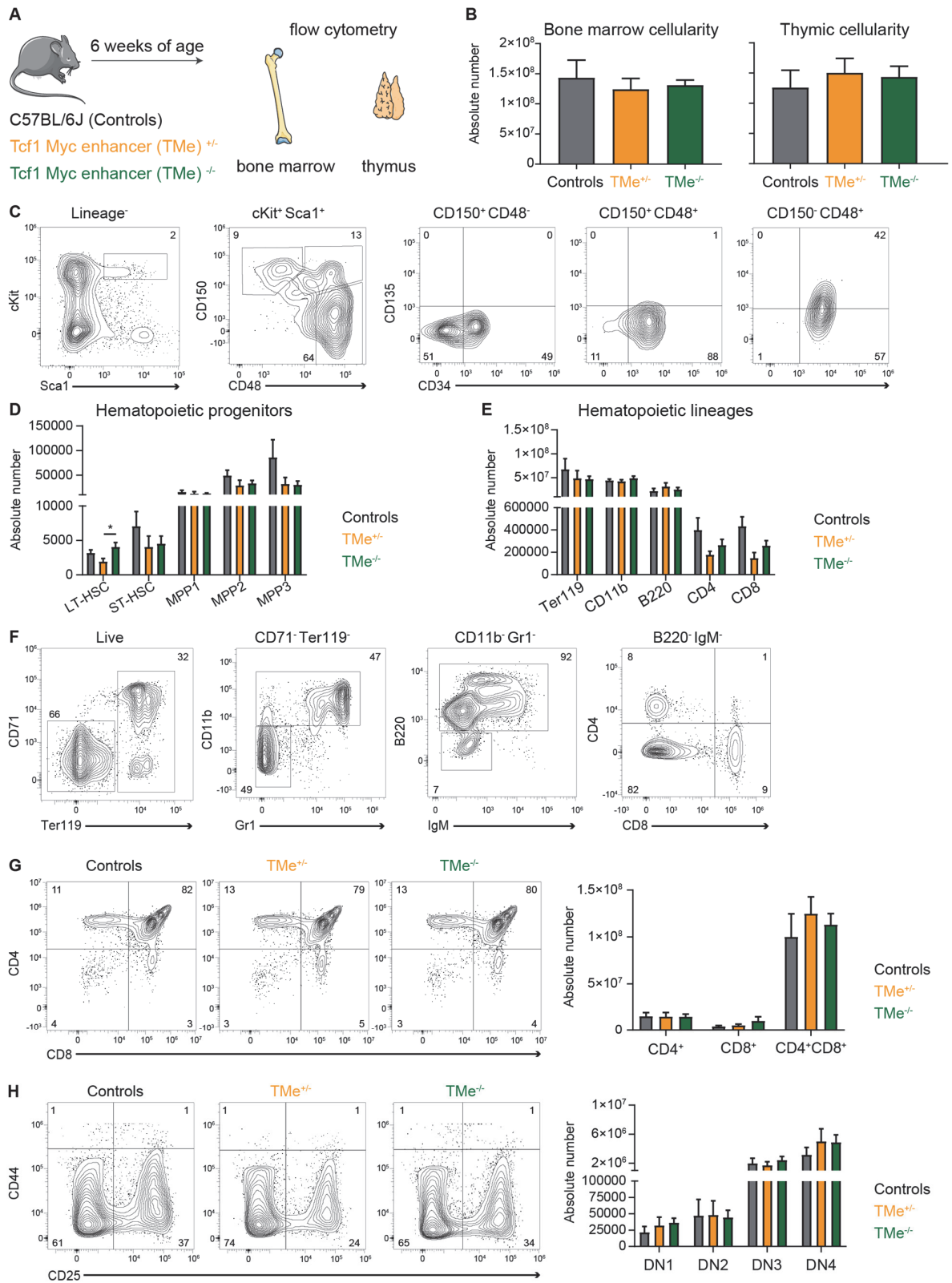
Figure 23 – Tcf1 directly regulates *NMe* and *TMe* regulatory elements in T-ALL cells
A, ChIP-qPCR analysis for Tcf1 binding in murine T-ALL (mT-ALL, n=3), wild type LSKs (Neg Ctrl, n=3) and IgG Controls (n=2) at *NMe* (each left bar, red) and *TMe* (each right bar, green). Data are represented as mean \pm SEM. **B**, ChIP-qPCR analysis for TCF1 binding in human T-ALL (hT-ALL, n=3) and IgG Controls (n=2) at *NMe* (each left bar, red) and *TMe* (each right bar, green). Data are represented as mean \pm SEM. **C**, Reverse ChIP identification of potential *TMe*-binding factors. An *TMe* DNA bait was incubated in the presence of nuclear extracts from DND-41 cells and recovered peptides were analyzed by mass spectrometry.

We thus hypothesized that Tcf1 orchestrates Notch1-induced chromatin organization in the distal *Myc*-enhancer through binding to *NMe* and/or *TMe*. To test the putative function of the *TMe* region in the context of Notch1-driven T-ALL, we generated CRISPR-targeted mice with two sgRNAs targeting broad *TMe* region and established *R26 N1IC lox/+ TMe +/- Mx1Cre* and *R26 N1IC lox/+ TMe -/- Mx1Cre* compound lines (Figure 24 and 25A). *TMe -/-* mice are fertile, viable and exhibit normal hematopoietic development (Figure 24). The consequences of *TMe* deletion in the context of Notch-driven T-ALL were assessed in chimeras using BM cells from the different compound animals. The effect of *TMe* genomic deletion on epigenetic features was addressed by ATAC-seq on LSKs of *N1IC* and *N1IC TMe -/-* mice. As expected, chromatin accessibility was easily detectable for both the *NMe* and *TMe* regions in *N1IC* derived LSKs, while the *NMe* region retained chromatin accessibility in *N1IC TMe -/-* derived chimeras (Figure 25B). Strikingly, analysis of T cell leukemogenesis revealed that none of the *N1IC TMe -/-* chimeras developed T-ALL and only 40% of *N1IC TMe +/-* succumbed to disease, while chimerism was stable over time on all genetic backgrounds (Figure 25C). Flow cytometric analysis of BM cells at mid-stage disease of *N1IC* and at endpoint of *N1IC TMe +/-* and *N1IC TMe -/-* chimeras revealed similar proportions of CD4⁺ CD8⁺ DP pre-leukemic cells in all compound chimeras (Figure 25D). However, deletion of the *TMe* inhibited progression of the T-ALL. Generally, initiation of T-ALL in BM progenitors leads to development of thymic-independent DP pre-leukemic cells and then progressing to lethal CD8⁺ SP T-ALL

blasts (223). While pre-leukemic cells in *N1/C* BM chimeras progressed from a *Myc* negative CD4⁺ CD8⁺ DP stage to *Myc*-expressing CD8⁺ SP leukemic cells, efficient progression to aggressive leukemia is impaired in the majority of *N1/C TMe*^{+/-} and all *N1/C TMe*^{-/-} (Figure 25E,F). This indicates that *TMe* is of crucial importance for the T-ALL disease progression.

Figure 24 - Physiological analysis of hematopoietic lineages in mice with genomic deletion of Tcf1-regulated *Myc* enhancer (*TMe*) (following page)

A, Schematic representation of the phenotypic analysis of bone marrow (BM) and thymi, using CRISPR-edited transgenic mouse models: *Controls* (black, n=3), *Tcf1-regulated Myc enhancer*^{+/-} (*TMe*^{+/-}, orange, n=4) or *Tcf1-regulated Myc enhancer*^{-/-} (*TMe*^{-/-}, green, n=7) mice. **B**, Quantification of the absolute cellularity in BM (left panel) and thymi (right panel) of all experimental groups. **C**, Phenotypic flow cytometric analysis of BM progenitors. Panels depict representative plots of gating strategy applied for all experimental groups, shown for *Controls*. Parental populations are shown above the plots. **D**, Absolute numbers of the BM progenitors from flow-cytometric-based analysis in panel **C**. Data are represented as mean ± SEM. Unpaired t-test, *, p-value<0.05. **E**, Absolute numbers of hematopoietic lineages in BM from flow cytometric-based analysis in panel **F**. Data are represented as mean ± SEM. **F**, Phenotypic flow cytometric analysis of hematopoietic lineages in BM. Panels depict representative plots of gating strategy applied to all experimental groups, shown for *Controls*. Parental populations are shown above the plots. **G,H**, Phenotypic flow cytometric analysis of thymocytes. Left panels depict representative plots of gating strategy for all experimental groups, shown for *Controls*, with absolute numbers in the right panels for **G**, CD4 and CD8 T cells and **H**, immature T cells gated from hematopoietic lineage- population. Data are represented as mean ± SEM.



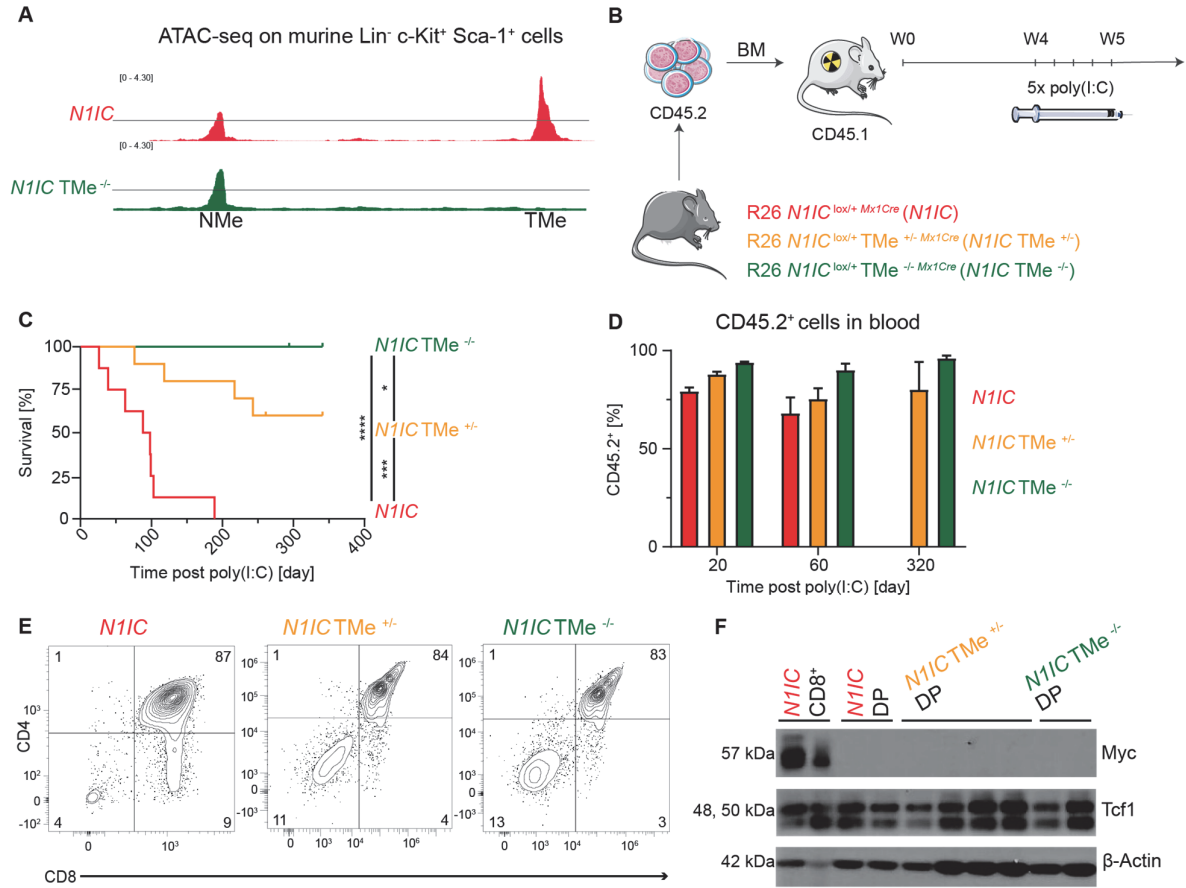


Figure 25 – Loss of *TMe* inhibits overexpression of *Myc* during T-ALL progression

A, IGV profiles for *N1IC* (top, red, n=3) and *N1IC TMe^{-/-}* (bottom, green, n=3) showing chromatin accessibility from ATAC-seq analysis on sorted LSKs. Tracks were group-scaled, scaling is shown in the top left corner. **B**, Schematic representation of bone marrow (BM) chimeras *R26 N1IC^{lox/+} Mx1Cre (N1IC)*, *R26 N1IC^{lox/+} TMe^{+/-} Mx1Cre (N1IC TMe^{+/-})* and *R26 N1IC^{lox/+} TMe^{-/-} Mx1Cre (N1IC TMe^{-/-})* mice. **C**, Kaplan-Meier survival analysis of transplanted mice after last poly(I:C) injection. *N1IC* mice (red, n=8), *N1IC TMe^{+/-}* (orange, n=10) and *N1IC TMe^{-/-}* (green, n=11) were followed for 341 days post poly(I:C) injection. Log-rank (Mantel-Cox) test, *, p-value<0.05; ***, p-value<0.001; ****, p-value<0.0001. **D**, Relative percentages of CD45.2⁺ transplanted cells in peripheral blood of *N1IC* mice (red, n=12), *N1IC TMe^{+/-}* (orange, n=11) and *N1IC TMe^{-/-}* (green, n=12), post poly(I:C) injection. Timepoints are indicated below the graph. Data are represented as mean \pm SEM. **E**, Flow cytometric-based phenotypic analysis of transplanted (CD45.2⁺) and induced (eGFP⁺) BM cells. Plots depict representative profiles from *N1IC* mouse T-ALL mid-stage progression (red), *N1IC TMe^{+/-}* at the endpoint (orange) and *N1IC TMe^{-/-}* at the endpoint (green). **F**, Total protein analysis by Western blot for Myc, Tcf1 and β -actin on FACS purified T cells from BM of experimental groups: *N1IC* CD8⁺ (n=2), *N1IC* DP (CD4⁺ CD8⁺, n=2), *N1IC TMe^{+/-}* DP (CD4⁺ CD8⁺, n=4) and *N1IC TMe^{-/-}* DP (CD4⁺ CD8⁺, n=2) as indicated.

5. Conclusion and discussion

T-ALL is a pediatric neoplasm of developing thymocytes. Signaling through the Notch1 receptor is essential for physiological development of T cells, while constitutive activation of the Notch1 signaling pathway initiates T-ALL leukemogenesis. Together with Notch1, a plethora of other transcription factors is involved in the regulation of TCD, including the high mobility group box (HMG-box) T cell factor 1 - Tcf1. However, a potential involvement of Tcf1 during the initiation of leukemogenesis has not been addressed. We identified Tcf1 to be essential for the initiation of Notch1-driven T-ALL in the BM. Simultaneous overexpression of oncogenic Notch1 and deletion of *Tcf7* inhibited the induction of the Notch1-driven T cell leukemogenesis *in vivo* in BM chimeras. Importantly, this process was β -catenin independent. Moreover, we also confirmed that leukemogenesis was inhibited not due to oncogenic activity of Tcf1, as its overexpression in Notch1-proficient hematopoietic progenitors did not induce transformation of T cells. Therefore, Tcf1 is essential for initiation of Notch1-driven

T-ALL but not sufficient for the development of the disease. We found that Tcf1 regulates genes commonly attributed to the T lymphocyte lineage, these are genes expressed in developing thymocytes. Oncogenic Notch1 drives the expression of Tcf1, thus promoting expression of T cell genes through increased chromatin accessibility and activated promoters of target genes. However, we have also identified fine-tuned modulation of 3D chromatin looping. A subset of T-ALL-related genes was expressed due to enhancer-gene interactions established in Tcf1- and Notch1-dependency. Modulation of the chromatin accessibility status, activation of regulatory elements, dynamic chromatin looping constitute *bona fide* epigenetic features. We verified that the primary mechanism leading to Notch1-driven and Tcf1-dependent T cell leukemogenesis is of epigenetic nature. Molecular analysis presented herein focuses on early hematopoietic progenitors to determine the primary mechanisms leading to leukemogenesis. Our results establish that events leading to the initiation of the T-ALL occur very early, in LSKs, even before the cells adopt T cell-like phenotype.

Amongst well-established drivers of T-ALL leukemogenesis, the *Myc* oncogene is essential for the proliferation of cells (140). In Notch1-driven T-ALL *Myc* is regulated by Notch1 binding to its distal enhancer (141,142). Thus, we analyzed how the distal

T-ALL-specific superenhancer of *Myc* is epigenetically regulated in response to oncogenic Notch1 and Tcf1. We found that the previously identified *Notch1-Myc enhancer (NMe)* can be activated only in presence of Tcf1. Our data, in agreement with previously reported reverse ChIP analysis, suggests that the protein complex at the *NMe* enhancer region involves Tcf1 and Notch1, amongst others (149). Moreover, for the first time, we have identified a novel regulatory element downstream of *NMe*, termed *Tcf1-regulated Myc enhancer (TMe)*. Epigenetic analysis revealed that *TMe* shows even stronger than *NMe* increase of chromatin accessibility in response to oncogenic *N1/C*-expression in dependency of Tcf1. Importantly, CRISPR-mediated deletion of the *TMe* was sufficient to block the *Myc*-dependent progression of the disease from pre-T-ALL CD4⁺ CD8⁺ DP cells to the lethal CD8⁺ SP T-ALL. The *TMe* enhancer site is highly conserved across species and is not accessible in wild type BM progenitors. Activation of the T-ALL-specific *Myc* enhancers is established already in leukemia-prone hematopoietic progenitors. Thus, distal regulatory elements, vital for T-ALL, are accessible already in LSKs and potentially bound by pioneering protein complexes. This will then initiate looping of the chromatin and consequently drive disease progression.

In conclusion, we have identified novel epigenetic mechanisms essential for T-ALL. They are induced by Tcf1 downstream of hyperactivated Notch1 and are activated during the first stages of T-ALL leukemogenesis in early hematopoietic progenitors. Developing leukemic cells overexpressing Notch1 and its downstream targets adopt a genetic T cell signature already in those hematopoietic progenitors. Subsequently, during disease progression they overexpress *Myc* via distal regulation of the *NMe* and *TMe* enhancers to progress from pre-leukemic to lethal T-ALL cells (Figure 26).

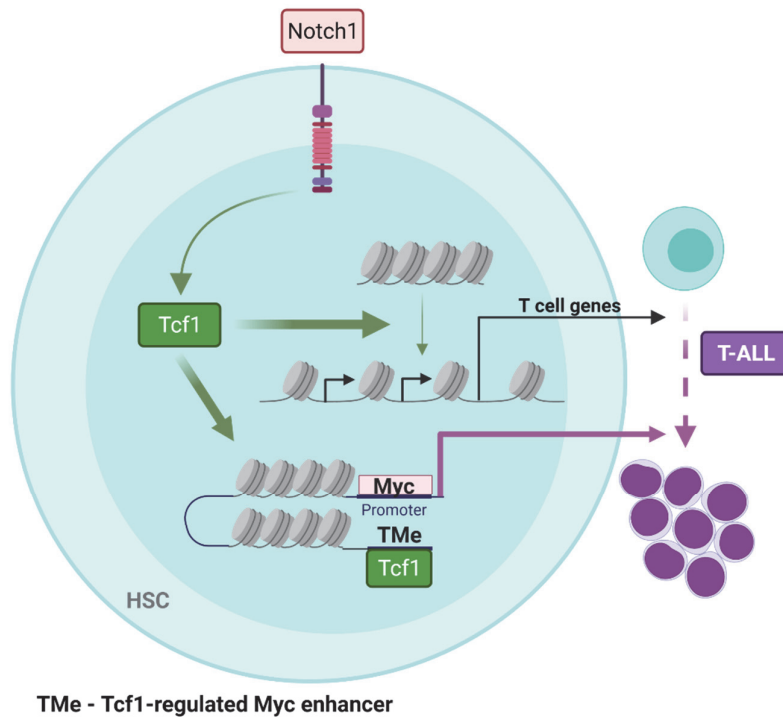


Figure 26 - Model of Tcf1-dependent regulation of chromatin accessibility and topology in Notch1-driven T-ALL

Oncogenic Notch1 directly induces expression of Tcf1 in early hematopoietic progenitors. Notch1 and Tcf1 increase the accessibility of chromatin in proximity to the promoters of canonical T cell genes, thus driving their expression. Moreover, Tcf1 binds to the Tcf1-regulated Myc enhancer (*TMe*) downstream from the *Myc* oncogene. This binding is essential for expression of *Myc* in promoting the progression of pre-leukemic cells to leukemic T-ALL blasts.

5.1. β -catenin is dispensable for Tcf1-dependent Notch1-driven T-ALL

Tcf and Lef protein family members are well established β -catenin binding partners in the canonical Wnt signaling pathway. Manipulations of *Apc* levels or *VavCre*-mediated deletion of β -catenin (*Ctnnb1*) led to alteration of physiological hematopoiesis or to impaired T-ALL initiation, respectively (46,224). On the other hand, stabilization of β -catenin in developing thymocytes increases their susceptibility to lymphopoiesis (225). Therefore, it has been speculated for a long time that canonical Wnt signaling plays an essential role in T cell leukemogenesis (226). However, an elegant investigation of concomitant loss of β -catenin and γ -catenin established hematopoiesis and lymphopoiesis to be Wnt signaling independent (48,49).

The role of Tcf1 in physiological TCD was shown to be Notch1-dependent (99,102), besides its established role as a Wnt (β -catenin) responsive transcription factor. Our data addressing the function of Tcf1 for the initiation of Notch1-driven T-ALL agrees with a β -catenin independent role (Figure 8 and 10). However, we have also addressed possible redundancy between supraphysiological levels of *Tcf7* and physiological levels of *Notch1* expression for the initiation of T-ALL *in vivo*. Forced retroviral expression of *Tcf7* in Notch1-proficient BM chimeras was not sufficient to induce leukemogenesis (Figure 13). In summary, this demonstrates that oncogenic levels of Notch1 need to drive downstream expression of *Tcf7* for T-ALL initiation.

A previous study using retrovirally-driven NOTCH1-induced T-ALL and inducible deletion of *β -catenin*, found that loss of β -catenin led to a reduction in the frequency of leukemia-initiating cells which results in a modest delay of disease onset (50). Therefore, we confirmed that genetic overexpression of *N1IC* and simultaneous deletion of *β -catenin* in BM chimeras initiated a process of leukemogenesis from early hematopoietic progenitors with full penetrance. Similarly to the reported study, the kinetics of disease initiation and progression was significantly, but modestly, delayed compared to *N1IC β -catenin*-proficient BM chimeras (Figure 10).

5.2. Conditional *Tcf7*-deficiency impedes T cell development without inducing lymphomagenesis

Tcf1, encoded by the *Tcf7* gene, plays a crucial role in the early stages of physiological thymic T cell development. The conventional *Tcf7*^{-/-} line, being deficient for exon 7 encoding the DNA binding domain, revealed that deficiency of *Tcf7* leads to a strong decrease in overall thymocytes numbers due to a developmental block in early T cells (103). However, we aimed for temporal control over deletion of *Tcf7* thus we generated the conditional *Tcf7*^{lox/lox} mouse line targeting exon 3 of *Tcf7*, which encodes the β -catenin binding domain. To this end, we obtained targeted embryos from International Knockout Mouse Consortium, similarly to the approach described in Steinke et al., 2014, and crossed them with the *Mx1Cre* transgenic line (227). *Mx1Cre*-driven deletion of exon 3 leads to loss of Tcf1 protein, blocks physiological

T cell development at DN1 immature thymocytes and diminishes total thymocytes number (Figure 7). Thus, the extent of TCD inhibition is vastly similar between reported *Tcf7*^{-/-} and our generated *Tcf7*^{Δ/Δ Mx1Cre} mouse models.

Multiple reports have described the development of lymphomas in *Tcf7*^{-/-} mice or in mice with *VavCre*-mediated deletion of *Tcf7*. Lymphomas are developing with age in animals over 15 weeks old (105,228). Genetic analysis of these tumors revealed an accumulation of secondary mutations, including infrequent mutations affecting *Notch1*. However, the analysis of *Tcf7*^{Δ/Δ CD4Cre} mice in the Steinke et al. study, did not mention the development of lymphomas 10 weeks post BM transplantation (227). Similarly, loss of *Tcf7* in a supraphysiological *Notch1* background in *N1IC Tcf7*^{Δ/Δ} BM chimeras monitored for 28 weeks for leukemia development did not reveal the development of lymphomas or thymomas. A potential discrepancy between these mouse models in the age-related development of tumors might be explained by the overexpression of *Lef1* only in thymocytes of *Tcf7*^{-/-} and *Tcf7*^{Δ/Δ VavCre} mice (105,228), but not in *Tcf7*^{lox/lox CD4Cre} or *Tcf7*^{lox/lox Mx1Cre} mouse lines (Annexed Table 3) (227). Moreover, induction of *Tcf7* deletion in adult animals addresses the role of *Tcf1* post-embryonic life, in contrast to *Tcf7*^{-/-} and *Tcf7*^{Δ/Δ VavCre} approaches (229,230).

5.3. Investigation of early T-ALL initiation events in hematopoietic progenitors

Notch1 signaling is essential for the development of T cells, but it is expressed only until the β -selection checkpoint (81). Induction of *Notch1* expression relies on the interaction between *Notch1*-expressing ETPs and *Dll4*-expressing thymic epithelial cells (231). Expression of *Notch1* is subsequently sustained by *Notch1* itself, via positive feedback regulation, and by *E2A*. At the β -selection checkpoint pre-TCR signaling indirectly represses the expression of *Notch1* via *Id3*-mediated inhibition of *E2A* (97). Such regulation of *Notch1* signaling is vital for the physiological development of thymic T cells, while dysregulation of *Notch1* inhibition at β -selection leads to transformation of immature thymocytes (232,233). Expression of constitutively active form of *Notch1* receptor - *N1ICD*, initiated in thymic DN2/DN3 T cells with

the stage-specific *lck* promoter induces a transformation of developing T cells, leading to deprivation of CD4⁺ T cells and accumulation of immature CD8⁺ SP T-ALL cells in the thymus (234). Therefore, T-ALL indeed originates from developing thymic T cells constitutively expressing *Notch1* past β -selection checkpoint.

Despite aforementioned studies that established thymus to be a murine T-ALL-originating organ, investigation of leukemogenesis is frequently performed in murine models overexpressing *Notch1* in BM. It has been shown that retrovirally-driven expression of diverse *NOTCH1* GoF mutations also in hematopoietic progenitors, not exclusively in immature thymocytes, is sufficient to induce T-ALL leukemogenesis and ectopic TCD (235,236). Therefore, the expression of active forms of the *Notch1* receptor in hematopoietic cells became a well-established experimental approach for the investigation of murine Notch1-driven T-ALL (236). However, retroviral-based models do not allow for temporospatial control over initiation of expression. Therefore, in order to synchronize the expression of *N1/C* and simultaneously induce deletion of *Tcf7*, we took advantage of genetically engineered mouse models with inducible *Mx1Cre* (Figure 8). After BM transplantation and reconstitution of recipients, poly(I:C)-mediated induction of the *Mx1* promoter allows for efficient Cre-mediated recombination only in hematopoietic lineages (Figure 8 and 9). Importantly, overexpression of Notch1 leads to T-ALL initiation in the earliest populations of hematopoietic progenitors (237) (Figure 8 and 11). Understanding of mechanisms establishing the initiation of T-ALL is interesting in the scope of fundamental biology, but also from a clinical and therapeutical perspective. Case reports discussing the occurrence of the same Notch1 mutations in siblings, accumulation of T-ALL-associated mutations in hematopoietic progenitors, and separation of ETP-ALL as an independent subtype of T-ALL, implicates HSCs as potential disease initiating cells of origin (39,121,127,217). Unfortunately, in our experimental model we cannot decipher which population of immature hematopoietic cells is the cell of origin for Tcf1-dependent Notch1-induced T-ALL.

Taking advantage of our experimental approach allowing for *Rosa26*-driven expression of *N1/C* and simultaneous deletion of *Tcf7* in LSKs, we were able to show, for the very first time, the pronounced involvement of epigenetic regulation in Notch1-driven T-ALL as one of the primary events leading to leukemogenesis

(Figure 14). Moreover, this regulation is Tcf1-dependent and initiated in LSKs before their phenotypic differentiation into T cells progenitors or their progenies (Figure 11 and 14).

5.4. Epigenetic role of Tcf1 in Notch1-driven T-ALL

The role of Tcf1 in physiological T cell development has been widely described, including the essential involvement of Notch1 signaling regulating the expression of the *Tcf7* gene (99,103). The important role of *Tcf7* in TCD has been linked to the epigenetic modulation. An intrinsic domain of Tcf1 has histone deacetylase activity regulating maturation of immature thymocytes during the CD4 and CD8 T cell bifurcation, while binding of Tcf1 across the genome has been associated with increased chromatin accessibility in proximity to T cell genes (106,107). Lastly, ectopic expression of Tcf7 induced the accessibility of T cell genes in fibroblasts *in vitro* (107). However, no reports have so far addressed the involvement of Tcf1 in Notch1-driven T-ALL. Here we show, to the best of our knowledge for the first time, that Tcf1 establishes a leukemia-prone chromatin structure in hematopoietic progenitors downstream of oncogenic Notch1 (Figure 11 and 14). Thus, in a pathological setting Tcf1 exerts its function downstream of leukemogenic Notch1 already in LSKs that are not yet committed to the T cell lineage, while in physiological cells *Tcf7* is expressed predominantly in T cells. Identification of the new *Myc* regulatory element *TMe* located within the *Myc* superenhancer, accessible only in developing leukemia-prone LSKs, highlights another main novelty of the study (Figure 21 and 25). In addition, our data is in agreement with the role of Tcf1 in shaping the epigenetic landscape targeting the proximity of T cell-specific genes (Figure 14), as is discussed in previous reports (92,106,107).

Notch1 directly regulates *Tcf7* in thymic TCD and deletion of *Tcf7* strongly attenuates the thymic output (99,103). On top of that, *Notch1* is the most frequently mutated gene in pediatric T-ALL (112). Consequently, the focus of this study addresses the role of Tcf1 in Notch1-driven murine T-ALL initiation. However, data from scRNA-seq analysis of human T-ALL samples describes mutations affecting NOTCH1 to be occurring with disease progression, but not as tumor-initiating

mutations (127). Therefore, it would be overly interesting to address the role of TCF1 in pediatric T-ALL induced by tumor-initiating mutations as described in scRNA-seq study, i.e.: *MED12*, *STAT5B*, *CDKN2A*, or in combination with other initiating mutations. On top of that, Tcf1 and Lef1 have shown redundancy in CD4⁺ CD8⁺ DP stages of murine TCD. Loss of *Tcf7* can be rescued by overexpression of *Lef1* to efficiently drive the maturation of thymocytes through later stages of TCD (105). Therefore, the continuation of the study addressing the initiation of T-ALL at a different stage of TCD would require the assessment of the involvement of Lef1 itself and in coordinate function with Tcf1 (105).

The most robust clinical applicability of biological studies originates from the identification of the molecular mechanisms promoting growth and survival of already established cancerous cells, while recent developments demonstrate the unmet medical need for targeted therapeutic approaches (238–241). Moreover, patients are diagnosed with neoplastic tissue when tumor cells are abundant, usually not when disease development is only initiated. Therefore, the continuation of the study should address the involvement of TCF1 in the survival and progression of T-ALL cells. Progression of human disease initiated by oncogenic NOTCH1 from human hematopoietic CD34⁺ progenitors is dependent only with the concomitant mutations in *HOXB* genes (133). Moreover, mutations of other known T-ALL oncogenes such as *LMO2*, *TAL1*, *KRAS* are frequently identified among patients but were not included in the presented analysis focusing on NOTCH1- and TCF1-dependency (132). In conclusion, investigation of mechanisms dependent on TCF1 during progression of T-ALL should take into account also mutations detected in progressing human T-ALL, other than NOTCH1.

5.5. Analysis of 3D chromatin topology in LSKs

Pronounced regulation of epigenetic features dependent on Tcf1 downstream of oncogenic Notch1, such as chromatin accessibility and activation of regulatory elements, prompted us to investigate the genome interactome in hematopoietic progenitors in a series of genetically modified animals (Figure 16). Such analysis allowed us to identify interactions dependent on Notch1 and Tcf1 in early stages of

T-ALL initiation. These interactions would then subsequently affect the fate of T-ALL-prone LSKs. Therefore, LSKs have been FACS-isolated from BM chimeras overexpressing *N1/C*, overexpressing *N1/C* and deficient for *Tcf7*, and *Controls*. *In situ* Hi-C analysis was performed and sequenced according to established guidelines allowing for identification of chromatin topology at a resolution ranging between ten and twenty kilobase pairs (Figure 16).

Analysis of 3D chromatin organization identified only a minor subset of differentially expressed genes to be regulated by chromatin looping between enhancers and promoters. Moreover, re-organization of TADs and chromatin compartments showed fine-tuned effects on gene expression (Figure 16-18). Indeed, amongst the plethora of T cell-specific genes, transcriptionally dependent on Notch1 and Tcf1, a set of them is regulated directly at the promoter via increased chromatin accessibility (Figure 14). Thus, regulation of their expression through dynamic changes in chromatin topology is not essential for the initiation of transcription. Interestingly, overexpression of oncogenic *Notch1* and *Tcf7* downstream of Notch1 showed rather a restriction of global chromatin interactions (Figure 20), suggesting that Tcf1 is important for the specification of chromatin topology towards transcription of a subset of genes. Among genes with increased expression dependent on chromatin looping regulated by Notch1 and Tcf1 we identified genes detected in clinical T-ALL samples (Figure 20). However, the identified dependencies are far less impressive than major disturbances of 3D looping when T-ALL cells are compared with physiological T cells, or with analysis of the role of interactome in the development of tissues (170,242).

It has been suggested that induction of gene expression requires a series of temporally isolated events. First, initiating events start with the activation of regulatory elements via modulation of chromatin accessibility. Then, changes in chromatin interactions are established to subsequently induce gene expression (158). Therefore, the analysis of chromatin topology could be potentially revised by the addition of other cellular states or phenotypes, rather than focusing only on the population of LSKs in different genetically engineered animals. Improvement of our experimental approach would be possible with the analysis of cells at the initiation of T-ALL from hematopoietic progenitors (i.e. performing analysis on LSKs) combined with the interactome analysis

of *N1/C*-driven early (DP T-ALL cells) and established CD8⁺ SP T-ALL cells. This would allow to identify interactions that are not yet functional in LSKs but that do affect the expression of target genes over disease development. The limitations of snapshot analysis might be also possible to overcome by integration of quantitative analysis of looping strength, rather than the herein applied qualitative approach (213). Chromatin interactions are dynamic, thus analysis of looping strength might identify differential dynamic 3D topology directly affecting gene expression at higher sensitivity.

Moreover, a recent report has identified cohesin as an important regulator for distal enhancer-promoter induction of gene expression (161). However, because of the previously published data demonstrating CTCF-mediated organization of TADs, our analysis is centered only on genome-wide binding of CTCF (Figure 17) (160). Therefore, the addition of cohesin binding data (through ChIP-seq analysis) in LSKs might accelerate the identification of important interactions that are established before the induction of gene expression.

5.6. Tcf1 and Notch1 activate the novel identified *TMe* region in leukemia-prone LSKs

Oncogenic Notch1 directly and positively regulates expression of *Myc* in T-ALL. Notch1 binds to the region proximal to *Myc* promoter and to distal T-ALL-specific enhancer of *Myc* – *NMe*, located in mice approximately 1.3 Mb downstream from the promoter (141,142,243,244). Oncogenic *Myc* regulates a set of genes driving the growth and survival of leukemic T cells and can substitute growth-promoting Notch1 signaling when Notch is pharmacologically inhibited (17,81,140,245).

Here we have identified previously not reported *Tcf1*-regulated *Myc* enhancer site (*TMe*) localized in a T-ALL-specific superenhancer region (Figure 21). *TMe* is localized approximately 14 kb downstream from the previously identified *NMe*, but still 0.4 Mb upstream from the previously identified blood enhancer cluster (*BENC*) region regulating *Myc* expression in normal HSCs and in murine acute myeloid leukemia cells (145). *TMe* is essential for *Myc*-dependent progression of pre-leukemic to leukemic cells in Notch1-driven T-ALL (Figure 25). Without overexpression of *Myc* pre-leukemic CD4⁺ CD8⁺ DP T-ALL cells, not yet expressing *Myc*, cannot progress to lethal CD8⁺

SP T-ALL cells expressing high levels of oncogenic *Myc* (Figure 25). Phylogenetic analysis of genomic sequences revealed *TMe* to reside in a highly conserved region (Figure 21D). Conservation of *TMe* resembles the conservation of binding loci recognized by NOTCH1 and GATA3 in *NMe*. These binding sites have been demonstrated to be of functional importance in both, human and murine cells (141,142,149). Indeed, TCF1 binds to *TMe* also in human DND-41 T-ALL cells (Figure 23). Such conservation of *Myc*-regulating enhancers regions within the T-ALL-specific superenhancer region resembles previously identified ultraconserved regulatory elements (246). To determine a functional importance of *TMe* in human disease it would be necessary to inhibit or delete this genomic region in human T-ALL cells. Therefore, in a continuation of the project, we will aim to perform a CRISPR-mediated deletion of the genomic region encompassing *TMe* in established human leukemic cells. We envision, based on the results reported for *NMe*, that deletion of *TMe* would lead to a decrease in *MYC* expression levels and subsequent induction of apoptosis (142,149).

Importantly, the *TMe* demonstrates an astounding specificity for activation only in T-ALL cells. While *NMe* and *BENC* are regulating physiological lymphopoiesis and hematopoiesis, respectively, *TMe* is not accessible and thus not involved in the regulation of *Myc* expression during physiological hematopoiesis or lymphopoiesis (Figure 21 and 24) (142,145,149). Therefore, it seems feasible to develop therapeutic options targeting regulators of *TMe* that would show efficacy only in T-ALL but not altering physiological processes of TCD or hematopoiesis.

5.7. Identification of potential therapeutic targets regulating *TMe*

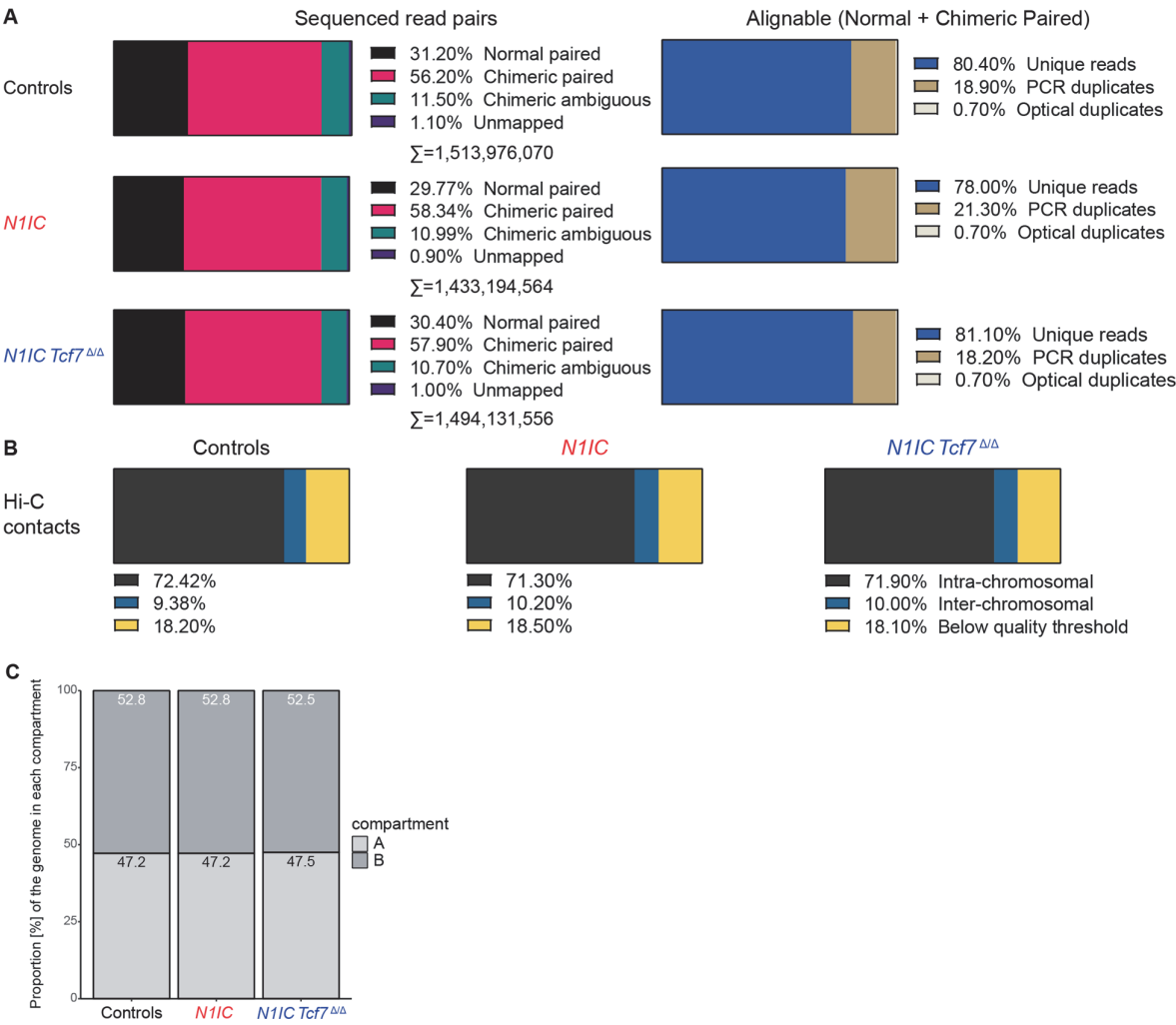
As the *TMe* region demonstrates increased chromatin accessibility only in T-ALL-prone LSKs and then has functional importance in progression of T-ALL to lethal disease, it can be considered a valuable target for development of therapeutic options. A potential therapeutic strategy would aim at inhibition of epigenetic activators bound to *TMe* in established T-ALL. However, Tcf1 binds to both, *TMe* and *NMe*, thus other complex-forming proteins might exhibit similar involvement in broad activation of enhancers. It is therefore crucial to differentiate between protein complexes bound to

NMe and focus on those specific to *TMe*, as deletion of *NMe* inhibits T-ALL initiation but also impairs physiological TCD (142,149).

In vitro analysis of protein complexes formed on *TMe*-biotinylated DNA bait by reverse ChIP paired with mass spectrometry revealed a plethora of factors bound in DND-41 human T-ALL cells (Figure 23). Despite the identification of known regulators of TCD and T-ALL, including BCL11B, GATA3, and RUNX1, it is of therapeutic importance to characterize epigenetic activators that would increase the accessibility of this enhancer site. Taking advantage of publicly available databases of epigenetic regulators, we have identified IKZF1 as an enhancer-activating factor bound at the *TMe* (247). Unfortunately, it has also been reported to bind to *NMe* in human T-ALL cells, thus targeting IKZF1 might lead to a block of physiological TCD at the DN3 stage, similarly to the deletion of *NMe* (149). However, selective IKZF inhibition by treatment with lenalidomide in human T-ALL cells would be required to validate IKZF1-mediated activation of *Myc* enhancers (248).

The analysis of biotinylated DNA by reverse ChIP, similarly to previously published results for *NMe*, does not allow for the identification of NOTCH1 or RBPJ amongst detected peptides bound to *TMe* (149). Therefore, generated data should be analyzed with caution and functionally validated. Generation of higher quality data would be required before the development of *TMe*-targeting therapeutic strategies can be undertaken. Moreover, reverse ChIP allows for the identification of peptides potentially regulating enhancers, but this method is not feasible for the analysis of enhancer-associated RNAs that might be of potential functional importance (249). Locus-specific *in vivo* analysis of protein complexes and RNAs at different enhancer sites would determine a composition of regulatory machinery with high confidence. The analysis of proteins, RNA and DNA molecules associated with the regulatory elements is possible with deactivated and biotinylated Cas9 in CAPTURE (CRISPR affinity purification *in situ* of regulatory elements) method as it was reported by Liu X et al., 2017 (250). Therefore, it would be interesting to perform CAPTURE analysis on *NMe* and *TMe* in murine and human T-ALL cells to identify regulatory complexes.

6. Annex



Annexed Figure 1 – Quality of data generated by *in situ* Hi-C on *ex vivo* LSKs
A,B, Quality control analysis by Juicer depicting distribution of sequenced reads, alignable reads and generated Hi-C contacts for *Controls*, *N1IC* and *N1IC Tcf7^{ΔΔ}* LSKs. **C**, Proportion of the genome that corresponds to each compartment type in the different biological samples with division to type A and type B. Calculated on the KR-normalized contact matrices at 1 Mb resolution.

Annexed Table 1 – Genotyping primers

204_N1 5' lox FW	CTGAGGCCTAGAGCCTTGAA
205_N1 3' lox RV	TGTGGGACCCAGAAGTTAGG
219_Mx1-Cre	GGCAGGGCTCCTCAGTGATTC
220_Cre2L21	CTGGCGATCCCTGAACATGTC
336_FW1 TMe_BS	ACTGCCTGACTTGACTCCCTAGC
337_Rev1 TMe_BS_Del	GAAGTGGGAGTGGGTTGGTTG
338_Rev2 TMe_BS_WT	TGAGTCAGCGGGTTTCTCTT
3251_Ef(3251) Tcf7 lox sense	GGAAGCTGACCCCTGTTGTAG
3253_Er(3253) Tcf7 lox as	CTGGTTTCCTTAGCACTGCAAG
3249_L3r2 Tcf7 Del as	TAGCCTAGAAGAACCTGACCTG
155_Rosa26 WT sense	AAAGTCGCTCTGAGTTGTTAT
156_Rosa26 Neo as	GCGAAGAGTTTGTCTCAACC
157_Rosa26 WT as	GGAGCGGGAGAAATGGATATG
005_b-cat lox sense RM41	AAGGTAGAGTGATGAAAGTTGTT
006_b-cat lox as RM42	CACCATGTCCTCTGTCTATCC

Annexed Table 2 - Antibodies

Antibodies	Source	ID
anti-Biotin, Streptavidin PE Texas Red - Flow Cytometry	Invitrogen Molecular Probes	Cat# SA1017
anti-mouse B220, PE Texas Red - Flow Cytometry	Thermo Fisher Scientific	Cat# RM2617; RRID:AB_10372805
anti-mouse B220, AlexaFluor 700 - Flow Cytometry	Thermo Fisher Scientific	Cat# 56-0452-82; RRID:AB_891458
anti-mouse B220, Pacific Blue, clone RA3-6B2 - Flow Cytometry	EPFL UPRAD	N/A
anti-mouse B220, FITC, clone RA3-6B2 - Flow Cytometry	EPFL UPRAD	N/A
anti-mouse CD117, APC - Flow Cytometry	Thermo Fisher Scientific	Cat# 17-1171-81; RRID:AB_469429
anti-mouse CD117, APCeF780 - Flow Cytometry	Thermo Fisher Scientific	Cat# 47-1171-80; RRID:AB_1272213
anti-mouse CD11b, PE-Cy7 - Flow Cytometry	Thermo Fisher Scientific	Cat# 25-0112-81; RRID:AB_469587
anti-mouse CD11b, AlexaFluor 700 - Flow Cytometry	Thermo Fisher Scientific	Cat# 56-0112-82; RRID:AB_657585
anti-mouse CD11b, FITC, clone M1/70 - Flow Cytometry	EPFL UPRAD	N/A
anti-mouse CD135, PE - Flow Cytometry	Thermo Fisher Scientific	Cat# 12-1351-83; RRID:AB_465860
anti-mouse CD150, PE-Cy5 - Flow Cytometry	BioLegend	Cat# 115912; RRID:AB_493598
anti-mouse CD19, AlexaFluor 700 - Flow Cytometry	Thermo Fisher Scientific	Cat# 56-0193-80; RRID:AB_837082
anti-mouse CD25, APCeF780 - Flow Cytometry	Thermo Fisher Scientific	Cat# 47-0251-82; RRID:AB_1272179
anti-mouse CD34, eF660 - Flow Cytometry	Thermo Fisher Scientific	Cat# 50-0341-80; RRID:AB_10609352
anti-mouse CD4, PE-Cy7 - Flow Cytometry	Thermo Fisher Scientific	Cat# 25-0041-82; RRID:AB_469576

anti-mouse CD4, AlexaFluor 700 - Flow Cytometry	Thermo Fisher Scientific	Cat# 56-0041-80; RRID:AB_494001
anti-mouse CD4, FITC, clone YTS191.1 - Flow Cytometry	EPFL UPRAD	N/A
anti-mouse CD44, PE - Flow Cytometry	Thermo Fisher Scientific	Cat# 12-0441-82; RRID:AB_465664
anti-mouse CD44, PE-Cy7 - Flow Cytometry	Thermo Fisher Scientific	Cat# 12-0441-82; RRID:AB_465664
anti-mouse CD45.1, Pacific Blue - Flow Cytometry	BioLegend	Cat# 110722; RRID:AB_492866
anti-mouse CD45.1, AlexaFluor 700 - Flow Cytometry	BioLegend	Cat# 110724; RRID:AB_493733
anti-mouse CD45.2, PerCpCy5.5 - Flow Cytometry	BioLegend	Cat# 109828; RRID:AB_893350
anti-mouse CD45.2, Pacific Blue - Flow Cytometry	BioLegend	Cat# 109820; RRID:AB_492872
anti-mouse CD48, Biotin - Flow Cytometry	Thermo Fisher Scientific	Cat# 13-0481-82; RRID:AB_466470
anti-mouse CD71, PE - Flow Cytometry	Thermo Fisher Scientific	Cat# 12-0711-81; RRID:AB_465739
anti-mouse CD8, AlexaFluor 700 - Flow Cytometry	Thermo Fisher Scientific	Cat# 56-0081-80; RRID:AB_494006
anti-mouse CD8, Alexa647, clone YTS169.4 - Flow Cytometry	EPFL UPRAD	N/A
anti-mouse CD8, FITC, clone YTS169.4 - Flow Cytometry	EPFL UPRAD	N/A
anti-mouse Gr1, AlexaFluor 700 - Flow Cytometry	Thermo Fisher Scientific	Cat# 56-5931-82; RRID:AB_494007
anti-mouse Gr1, PerCpCy5.5 - Flow Cytometry	Thermo Fisher Scientific	Cat# 45-5931-80; RRID:AB_906247
anti-mouse Gr1, FITC, clone RB6-8C5 - Flow Cytometry	EPFL UPRAD	N/A
anti-mouse IgM, eF660 - Flow Cytometry	Thermo Fisher Scientific	Cat# 50-5790-80; RRID:AB_2574245
anti-mouse IgM, FITC - Flow Cytometry	Thermo Fisher Scientific	Cat# 11-5790-81; RRID:AB_465244

anti-mouse Sca1, PE-Cy7 - Flow Cytometry	Thermo Fisher Scientific	Cat# 25-5981-81; RRID:AB_469668
anti-mouse Sca1, Pacific Blue - Flow Cytometry	BioLegend	Cat# 108120; RRID:AB_493273
anti-mouse Ter119, APCeF780 - Flow Cytometry	Thermo Fisher Scientific	Cat# 47-5921-80; RRID:AB_1548794
anti-mouse Ter119, FITC, clone Ter119 - Flow Cytometry	EPFL UPRAD	N/A
anti-mouse NK1.1, clone PK136 - in vivo NK cell depletion	EPFL UPRAD	N/A
anti-Tcf1 (human, mouse), clone C63D9 – Western and ChIP	Cell Signaling Technology	Cat# 2203; RRID:AB_2199302
anti-beta-catenin (dog, chicken, human, mouse, rat) - Western	BD Biosciences	Cat# 610153; RRID:AB_397554
anti-actin (mouse, rat, human) - Western	Abcam	Cat# ab8226; RRID:AB_306371
anti c-Myc (mouse, rat, human), clone Y69 - Western	Abcam	Cat# ab32072; RRID:AB_731658
anti-mouse IgG HRP conjugate - Western	GE Healthcare	Cat# NXA931; RRID:AB_772209
anti-human CD5, BV421 - Flow Cytometry	BD Biosciences	Cat# 562646; RRID:AB_2737700
anti-human CD7, PE-CF594 - Flow Cytometry	BD Biosciences	Cat# 562541; RRID:AB_2737642
anti-human CD34, APC - Flow Cytometry	BioLegend	Cat# 343510; RRID:AB_187715
anti-human CD38, PerCp Cy5.5 - Flow Cytometry	BioLegend	Cat# 356614; RRID:AB_2562183
anti-human CD45, AlexaFluor 700 - Flow Cytometry	BioLegend	Cat# 304024; RRID:AB_493761
anti-IgG - ChIP-seq	Diagenode	Cat# C15400001-100; RRID:AB_2722553
anti-H3K4me1 – ChIP-seq	Diagenode	Cat# C15410194; RRID:AB_2637078
anti-H3K4me3 – ChIP-seq	Diagenode	Cat# C15410003-50; RRID:AB_2616052

anti-H3K27ac – ChIP-seq	Diagenode	Cat# C15410196; RRID:AB_2637079
anti-H3K27me3 – ChIP-seq	Diagenode	Cat# C15410195; RRID:AB_2753161
anti-CTCF – ChIP-seq	Diagenode	Cat# C15410210; RRID:AB_2753160

Annexed Table 3 - TPM (Transcripts Per kilobase Million) expression values for selected genes

Gene symbol	<i>N1IC Tcf7</i> Δ/Δ			Controls			<i>N1IC</i>			<i>Tcf7</i> Δ/Δ		
<i>Tcf7</i>	6.5	5.1	8.7	2.3	2.1	2.9	134.4	392.5	283.6	0.4	1.2	0.1
<i>Ctnnb1</i>	271.4	279.8	255.4	249.9	221.9	191.0	226.9	214.7	217.8	184.5	166.1	220.3
<i>Cdh23</i>	1.3	0.4	0.2	0.9	0.4	1.0	2.3	6.2	11.8	0.6	0.2	0.5
<i>Pax5</i>	0.2	0.1	0.1	0.2	0.1	0.6	0.0	0.0	0.1	0.1	1.3	0.8
<i>Gata2</i>	121.5	119.0	121.2	80.4	80.2	72.0	65.1	20.2	43.6	59.5	57.9	72.6
<i>Gata3</i>	12.3	9.4	10.1	4.5	7.4	7.3	25.9	45.6	32.9	10.1	6.9	7.1
<i>Gata5</i>	0.4	0.3	0.4	0.2	0.3	0.1	0.1	0.3	0.4	0.2	0.2	0.2
<i>Rbpjl</i>	0.4	0.5	0.5	0.4	0.5	0.4	0.3	0.5	0.3	0.4	0.3	0.3
<i>Id2</i>	11.0	7.0	15.3	6.0	5.2	5.3	8.8	41.9	28.6	9.5	15.5	8.4
<i>Gata4</i>	0.1	0.0	0.1	0.0	0.2	0.0	0.0	0.0	0.0	0.1	0.3	0.0
<i>Myc</i>	163.9	158.3	173.2	211.4	240.0	272.4	154.8	164.9	149.3	215.8	183.7	216.0
<i>Hes1</i>	169.0	237.4	144.5	9.4	5.5	1.3	223.5	105.5	133.6	12.6	11.7	1.3
<i>Runx1</i>	42.3	43.8	41.6	22.1	27.2	29.1	34.1	41.5	43.6	29.5	25.9	29.0
<i>Pdgfrb</i>	181.8	211.2	173.1	16.5	20.2	16.4	99.9	77.5	85.9	11.5	8.8	18.3
<i>Cd5</i>	2.2	1.4	1.3	0.6	0.6	0.6	5.8	14.1	8.3	0.4	0.2	0.7
<i>Jak2</i>	39.7	40.5	43.7	28.0	26.6	26.2	31.9	31.3	33.2	30.0	33.8	30.9
<i>Tcf7l2</i>	5.8	7.7	5.8	6.5	5.1	4.3	6.3	4.2	5.3	5.8	3.7	7.4
<i>Il2ra</i>	0.8	0.9	1.5	0.4	0.6	0.5	97.2	306.2	190.2	0.4	0.8	0.4
<i>Gfi1b</i>	89.8	91.4	113.9	51.5	49.5	52.4	52.4	36.2	52.0	54.2	83.9	41.7
<i>Abl1</i>	73.9	88.7	83.3	61.5	61.5	52.9	76.6	64.6	70.6	47.1	42.0	59.4
<i>Notch1</i>	115.2	147.1	112.6	47.5	45.8	33.7	131.4	167.4	186.3	31.1	19.9	47.4
<i>Nras</i>	49.2	53.4	52.6	42.3	40.8	40.1	43.0	51.1	49.4	42.0	36.4	42.5
<i>Tspan2</i>	18.7	23.6	17.1	17.6	18.3	12.2	37.2	66.4	54.1	15.8	11.3	16.7
<i>Hax1</i>	14.8	14.8	15.3	16.1	14.7	15.2	14.8	20.2	16.1	15.3	13.0	15.0
<i>Lef1</i>	0.3	0.2	0.3	0.5	0.4	0.5	0.3	1.5	3.2	0.3	0.8	0.3
<i>Gfi1</i>	11.4	14.8	8.7	27.4	25.0	25.0	19.5	29.6	30.1	28.4	26.3	27.4
<i>Kras</i>	53.1	62.0	61.1	45.4	45.0	38.0	58.1	68.6	58.9	43.1	44.7	43.2

<i>Siglece</i>	0.4	0.6	0.6	0.7	0.9	0.7	0.7	1.3	2.5	1.6	4.6	1.2
<i>Gata1</i>	44.2	10.8	59.3	14.2	17.5	27.6	11.8	8.2	13.5	23.2	49.3	14.7
<i>Snx20</i>	11.8	12.4	10.7	12.2	12.6	13.4	14.9	15.8	17.8	11.0	11.4	16.4
<i>Cd3e</i>	0.0	0.0	0.2	0.1	0.0	0.0	3.4	21.8	26.3	0.0	1.4	0.0
<i>Mycbp2</i>	61.9	70.5	56.7	56.5	56.0	52.8	57.8	62.4	61.5	51.6	44.4	62.3
<i>Cebpa</i>	0.1	0.0	0.0	12.4	17.6	34.6	0.8	1.0	2.8	29.7	32.0	15.6
<i>Ptcra</i>	0.0	0.1	0.0	0.0	0.0	0.0	4.3	21.7	37.3	0.0	0.0	0.0
<i>Rbpj</i>	35.7	37.6	34.0	29.5	29.3	28.2	32.4	35.1	35.1	30.4	26.8	29.3
<i>Prss23</i>	0.0	0.1	0.0	0.1	0.0	0.1	0.0	0.0	0.1	0.1	0.1	0.0
<i>Flt3</i>	15.1	23.5	12.9	171.1	164.9	146.6	37.1	28.5	39.1	115.7	76.8	199.6
<i>Mlf1</i>	0.6	0.5	0.4	3.1	2.0	1.4	1.5	1.1	1.2	1.5	1.4	1.5
<i>Cebpe</i>	0.2	0.4	0.2	0.4	0.9	6.8	0.8	1.3	2.7	11.6	15.6	2.1
<i>Tcf4</i>	31.3	41.0	31.5	42.0	43.0	40.4	34.9	27.9	33.2	31.9	26.1	44.8
<i>Tcf7l1</i>	0.3	0.2	0.7	2.0	1.3	0.8	0.6	0.2	0.5	0.9	0.5	1.5
<i>Cebpb</i>	0.7	1.6	1.0	3.3	2.5	2.1	2.7	2.3	2.1	6.4	7.2	2.9
<i>Prss2</i>	2.2	2.5	1.4	0.1	0.0	0.0	29.5	94.2	72.9	0.0	0.0	0.0
<i>Bcl2</i>	5.3	3.5	4.7	24.0	25.8	28.1	9.0	12.4	11.2	26.3	19.6	22.7
<i>Cebpd</i>	0.1	0.6	0.2	1.0	2.0	3.7	0.7	0.5	1.5	5.5	6.6	2.4

7. Bibliography

1. Graf T, Enver T. Forcing cells to change lineages [Internet]. Vol. 462, Nature. Nature Publishing Group; 2009 [cited 2021 Jun 22]. p. 587–94. Available from: <https://www.nature.com/articles/nature08533>
2. Siebel C, Lendahl U. Notch signaling in development, tissue homeostasis, and disease. *Physiol Rev.* 2017;97(4):1235–94.
3. Bale AE. Hedgehog signaling and human disease [Internet]. Vol. 3, Annual Review of Genomics and Human Genetics. Annual Reviews 4139 El Camino Way, P.O. Box 10139, Palo Alto, CA 94303-0139, USA ; 2002 [cited 2021 Jun 9]. p. 47–65. Available from: www.annualreviews.org
4. Klaus A, Birchmeier W. Wnt signalling and its impact on development and cancer. *Nat Rev Cancer.* 2008;8(5):387–98.
5. Furlong EEM, Levine M. Developmental enhancers and chromosome topology. *Science* (80-). 2018;361(6409):1341–5.
6. Stadhouders R, Filion GJ, Graf T. Transcription factors and 3D genome conformation in cell-fate decisions [Internet]. Vol. 569, Nature. Nature Publishing Group; 2019 [cited 2021 Jun 17]. p. 345–54. Available from: <https://doi.org/10.1038/s41586-019-1182-7>
7. Takahashi K, Yamanaka S. Induction of Pluripotent Stem Cells from Mouse Embryonic and Adult Fibroblast Cultures by Defined Factors. *Cell* [Internet]. 2006 Aug 25 [cited 2021 Jun 22];126(4):663–76. Available from: <http://www.cell.com/article/S0092867406009767/fulltext>
8. Loughran SJ, Haas S, Wilkinson AC, Klein AM, Brand M. Lineage commitment of hematopoietic stem cells and progenitors: insights from recent single cell and lineage tracing technologies. *Exp Hematol* [Internet]. 2020;88:1–6. Available from: <https://doi.org/10.1016/j.exphem.2020.07.002>
9. Bradner JE, Hnisz D, Young RA. Transcriptional Addiction in Cancer. *Cell* [Internet]. 2017;168(4):629–43. Available from: <http://dx.doi.org/10.1016/j.cell.2016.12.013>
10. Guruharsha KG, Kankel MW, Artavanis-Tsakonas S. The Notch signalling system: recent insights into the complexity of a conserved pathway. *Nat Rev Genet* [Internet]. 2012 Sep 7;13(9):654–66. Available from: <http://www.nature.com/articles/nrg3272>
11. Ellisen LW, Bird J, West DC, Soreng AL, Reynolds TC, Smith SD, et al. TAN-1, the human homolog of the Drosophila Notch gene, is broken by chromosomal translocations in T lymphoblastic neoplasms. *Cell.* 1991;66(4):649–61.
12. Vijayaraghavan J, Osborne BA. Noncanonical Notch Signaling. In: Miele L, Artavanis-Tsakonas S, editors. Targeting Notch in Cancer: From the Fruit Fly to the Clinic [Internet]. New York, NY: Springer New York; 2018. p. 35–53. Available from: https://doi.org/10.1007/978-1-4939-8859-4_2
13. Sprinzak D, Lakhanpal A, Lebon L, Santat LA, Fontes ME, Anderson GA, et al. Cis-interactions between Notch and Delta generate mutually exclusive signalling

- states. *Nature*. 2010;465(7294):86–90.
14. Kovall RA, Gebelein B, Sprinzak D, Kopan R. The Canonical Notch Signaling Pathway: Structural and Biochemical Insights into Shape, Sugar, and Force. *Dev Cell* [Internet]. 2017;41(3):228–41. Available from: <http://linkinghub.elsevier.com/retrieve/pii/S1534580717302940>
 15. Bray SJ. Notch signalling in context. *Nat Rev Mol Cell Biol*. 2016;17(11):722–35.
 16. Kovall RA, Hendrickson WA. Crystal structure of the nuclear effector of Notch signaling, CSL, bound to DNA. *EMBO J* [Internet]. 2004;23(17):3441–51. Available from: <http://emboj.embopress.org/cgi/doi/10.1038/sj.emboj.7600349>
 17. Lehal R, Zaric J, Vigolo M, Urech C, Frismantas V, Zangger N, et al. Pharmacological disruption of the Notch transcription factor complex. *Proc Natl Acad Sci U S A*. 2020;117(28):16292–301.
 18. Gupta-Rossi N, Six E, LeBail O, Logeat F, Chastagner P, Olry A, et al. Monoubiquitination and endocytosis direct γ -secretase cleavage of activated Notch receptor. *J Cell Biol*. 2004;166(1):73–83.
 19. Kobia FM, Preusse K, Dai Q, Weaver N, Hass MR, Chaturvedi P, et al. Notch dimerization and gene dosage are important for normal heart development, intestinal stem cell maintenance, and splenic marginal zone B-cell homeostasis during mite infestation [Internet]. Vol. 18, *PLoS Biology*. 2020. 1–33 p. Available from: <http://dx.doi.org/10.1371/journal.pbio.3000850>
 20. Kakuda S, Haltiwanger RS. Deciphering the Fringe-Mediated Notch Code: Identification of Activating and Inhibiting Sites Allowing Discrimination between Ligands. *Dev Cell*. 2017;40(2):193–201.
 21. Kopan R, Ilagan MXG. The Canonical Notch Signaling Pathway: Unfolding the Activation Mechanism. *Cell*. 2009;137(2):216–33.
 22. Severson E, Arnett KL, Wang H, Zang C, Taing L, Liu H, et al. Genome-wide identification and characterization of Notch transcription complex-binding sequence-paired sites in leukemia cells. *Sci Signal* [Internet]. 2017;10(477):eaag1598. Available from: <http://stke.sciencemag.org/lookup/doi/10.1126/scisignal.aag1598>
 23. Hori K, Sen A, Artavanis-Tsakonas S. Notch signaling at a glance. *J Cell Sci* [Internet]. 2013;126(10):2135–40. Available from: <http://jcs.biologists.org/cgi/doi/10.1242/jcs.127308>
 24. Carmeliet P, Jain RK. Molecular mechanisms and clinical applications of angiogenesis. *Nature* [Internet]. 2011;473(7347):298–307. Available from: <http://www.nature.com/doi/doi/10.1038/nature10144>
 25. Lomelí H, Castillo-Castellanos F. Notch signaling and the emergence of hematopoietic stem cells. *Dev Dyn*. 2020;249(11):1302–17.
 26. Bigas A, Espinosa L. Hematopoietic stem cells: To be or Notch to be. *Blood*. 2012;119(14):3226–35.
 27. Radtke F, editor. *Notch Regulation of the Immune System* [Internet]. Berlin,

- Heidelberg: Springer Berlin Heidelberg; 2012. (Current Topics in Microbiology and Immunology; vol. 360). Available from: <http://link.springer.com/10.1007/978-3-642-24294-6>
28. Lampreia FP, Carmelo JG, Anjos-Afonso F. Notch Signaling in the Regulation of Hematopoietic Stem Cell. *Curr Stem Cell Reports*. 2017;3(3):202–9.
 29. Maillard I, Koch U, Dumortier A, Shestova O, Xu L, Sai H, et al. Canonical Notch Signaling Is Dispensable for the Maintenance of Adult Hematopoietic Stem Cells. *Cell Stem Cell*. 2008 Apr 10;2(4):356–66.
 30. Lechner M, Engleitner T, Babushku T, Schmidt-Supprian M, Rad R, Strobl LJ, et al. Notch2-mediated plasticity between marginal zone and follicular B cells. *Nat Commun* [Internet]. 2021;12(1):1–13. Available from: <http://dx.doi.org/10.1038/s41467-021-21359-1>
 31. Saito T, Chiba S, Ichikawa M, Kunisato A, Asai T, Shimizu K, et al. Notch2 is preferentially expressed in mature B cells and indispensable for marginal zone B lineage development. *Immunity*. 2003 May 1;18(5):675–85.
 32. Radtke F, MacDonald HR, Tacchini-Cottier F. Regulation of innate and adaptive immunity by Notch. *Nat Rev Immunol* [Internet]. 2013;13(6):427–37. Available from: <http://www.ncbi.nlm.nih.gov/pubmed/23665520>
 33. Radtke F, Wilson A, Stark G, Bauer M, Meerwijk J Van, MacDonald HR, et al. Deficient T cell fate specification in mice with an induced inactivation of Notch1. *Immunity*. 1999;10(5):547–58.
 34. Hosokawa H, Rothenberg E V. How transcription factors drive choice of the T cell fate. *Nat Rev Immunol* [Internet]. 2021;21(3):162–76. Available from: <http://dx.doi.org/10.1038/s41577-020-00426-6>
 35. Wang J, Sullenger BA, Rich JN. Notch Signaling in Cancer Stem Cells. In 2012. p. 174–85. Available from: http://link.springer.com/10.1007/978-1-4614-0899-4_13
 36. Nicolas M, Wolfer A, Raj K, Kummer JA, Mill P, Van Noort M, et al. Notch1 functions as a tumor suppressor in mouse skin. *Nat Genet* [Internet]. 2003 Mar 1 [cited 2021 Jun 13];33(3):416–21. Available from: <http://www.nature.com/naturegenetics>
 37. Nowell CS, Radtke F. Notch as a tumour suppressor. *Nat Rev Cancer*. 2017;17(3):145–59.
 38. Tardivon D, Antoszewski M, Zangger N, Nkosi M, Sordet-Dessimoz J, Hendriks R, et al. Notch signaling promotes disease initiation and progression in murine chronic lymphocytic leukemia. *Blood* [Internet]. 2021 Jun 3;137(22):3079–92. Available from: <https://ashpublications.org/blood/article/doi/10.1182/blood.2020006701/474750/Notch-Signaling-Promotes-Disease-Initiation-and>
 39. Knoechel B, Bhatt A, Pan L, Pedamallu CS, Severson E, Gutierrez A, et al. Complete hematologic response of early T-cell progenitor acute lymphoblastic leukemia to the γ -secretase inhibitor BMS-906024: genetic and epigenetic findings in an outlier case. *Mol Case Stud* [Internet]. 2015 Oct 24;1(1):a000539.

- Available from:
<http://molecularcasestudies.cshlp.org/lookup/doi/10.1101/mcs.a000539>
40. Petrovic J, Zhou Y, Fasolino M, Goldman N, Schwartz GW, Mumbach MR, et al. Oncogenic Notch Promotes Long-Range Regulatory Interactions within Hyperconnected 3D Cliques. *Mol Cell* [Internet]. 2019;73(6):1174-1190.e12. Available from: <https://linkinghub.elsevier.com/retrieve/pii/S1097276519300061>
 41. Steinhart Z, Angers S. Wnt signaling in development and tissue homeostasis. *Development*. 2018;145(11):1–8.
 42. Bugter JM, Fenderico N, Maurice MM. Mutations and mechanisms of WNT pathway tumour suppressors in cancer. *Nat Rev Cancer* [Internet]. 2021;21(1):5–21. Available from: <http://dx.doi.org/10.1038/s41568-020-00307-z>
 43. Duncan AW, Rattis FM, DiMascio LN, Congdon KL, Pazianos G, Zhao C, et al. Integration of Notch and Wnt signaling in hematopoietic stem cell maintenance. *Nat Immunol*. 2005;6(3):314–22.
 44. Olson OC, Kang YA, Passequé E. Normal hematopoiesis is a balancing act of self-renewal and regeneration. *Cold Spring Harb Perspect Med*. 2020;10(12):1–23.
 45. Ioannidis V, Beermann F, Clevers H, Held W. The β -catenin–TCF-1 pathway ensures CD4⁺ CD8⁺ thymocyte survival. *Nat Immunol* [Internet]. 2001 Aug 1;2(8):691–7. Available from: <http://www.nature.com/doi/10.1038/90623>
 46. Luis TC, Naber BAE, Roozen PPC, Brugman MH, De Haas EFE, Ghazvini M, et al. Canonical wnt signaling regulates hematopoiesis in a dosage-dependent fashion. *Cell Stem Cell*. 2011;9(4):345–56.
 47. Cobas M, Wilson A, Ernst B, Mancini SJC, MacDonald HR, Kemler R, et al. β -Catenin Is Dispensable for Hematopoiesis and Lymphopoiesis. *J Exp Med* [Internet]. 2004;199(2):221–9. Available from: <http://www.jem.org/lookup/doi/10.1084/jem.20031615>
 48. Koch U, Wilson A, Cobas M, Kemler R, MacDonald HR, Radtke F. Simultaneous loss of β - and γ -catenin does not perturb hematopoiesis or lymphopoiesis. *Blood*. 2008;111(1):160–4.
 49. Jeannet G, Scheller M, Scarpellino L, Duboux S, Gardiol N, Back J, et al. Long-term, multilineage hematopoiesis occurs in the combined absence of β -catenin and γ -catenin. *Blood*. 2008 Jan 1;111(1):142–9.
 50. Giambra V, Jenkins CE, Lam SH, Hoofd C, Belmonte M, Wang X, et al. Leukemia stem cells in T-ALL require active Hif1 α and Wnt signaling. *Blood*. 2015;125(25):3917–27.
 51. Ramalho-Santos M, Willenbring H. On the Origin of the Term “Stem Cell.” *Cell Stem Cell*. 2007;1(1):35–8.
 52. Till JE, McCulloch EA. A Direct Measurement of the Radiation Sensitivity of Normal Mouse Bone Marrow Cells. *Radiat Res* [Internet]. 1961 Feb;14(2):213. Available from: <https://www.jstor.org/stable/3570892?origin=crossref>
 53. Morrison SJ, Shah NM, Anderson DJ. Regulatory mechanisms in stem cell

- biology. *Cell* [Internet]. 1997 Feb;88(3):287–98. Available from: <https://linkinghub.elsevier.com/retrieve/pii/S009286740081867X>
54. Laurenti E, Göttgens B. From haematopoietic stem cells to complex differentiation landscapes. *Nature* [Internet]. 2018;553(7689):418–26. Available from: <http://dx.doi.org/10.1038/nature25022>
 55. Weissman IL. Stem cells: Units of development, units of regeneration, and units in evolution. *Cell*. 2000;100(1):157–68.
 56. Wilson A, Laurenti E, Oser G, van der Wath RC, Blanco-Bose W, Jaworski M, et al. Hematopoietic Stem Cells Reversibly Switch from Dormancy to Self-Renewal during Homeostasis and Repair. *Cell*. 2008;135(6):1118–29.
 57. Liggett LA, Sankaran VG. Unraveling Hematopoiesis through the Lens of Genomics. *Cell* [Internet]. 2020;182(6):1384–400. Available from: <https://doi.org/10.1016/j.cell.2020.08.030>
 58. Iwasaki H, Akashi K. Hematopoietic developmental pathways: On cellular basis. *Oncogene*. 2007;26(47):6687–96.
 59. Kondo M, Weissman IL, Akashi K. Identification of Clonogenic Common Lymphoid Progenitors in Mouse Bone Marrow. *Cell* [Internet]. 1997 Nov;91(5):661–72. Available from: <http://linkinghub.elsevier.com/retrieve/pii/S0092867400804535>
 60. Adolfsson J, Månsson R, Buza-Vidas N, Hultquist A, Liuba K, Jensen CT, et al. Identification of Flt3+ lympho-myeloid stem cells lacking erythro-megakaryocytic potential: A revised road map for adult blood lineage commitment. *Cell*. 2005;121(2):295–306.
 61. Majeti R, Park CY, Weissman IL. Identification of a Hierarchy of Multipotent Hematopoietic Progenitors in Human Cord Blood. *Cell Stem Cell*. 2007;1(6):635–45.
 62. Sommarin MNE, Dhapola P, Safi F, Warfvinge R, Ulfsson LG, Erlandsson E, et al. Single-Cell Multiomics Reveals Distinct Cell States at the Top of the Human Hematopoietic Hierarchy. *bioRxiv* [Internet]. 2021 Jan 1;2021.04.01.437998. Available from: <http://biorxiv.org/content/early/2021/04/02/2021.04.01.437998.1.abstract>
 63. Karamitros D, Stoilova B, Aboukhalil Z, Hamey F, Reinisch A, Samitsch M, et al. Single-cell analysis reveals the continuum of human lympho-myeloid progenitor cells. *Nat Immunol* [Internet]. 2018 Jan 21 [cited 2021 Sep 15];19(1):85–97. Available from: <https://www.nature.com/articles/s41590-017-0001-2>
 64. Notta F, Doulatov S, Laurenti E, Poeppl A, Jurisica I, Dick JE. Isolation of single human hematopoietic stem cells capable of long-term multilineage engraftment. *Science* (80-). 2011 Jul 8;333(6039):218–21.
 65. Haas S, Trumpp A, Milsom MD. Causes and Consequences of Hematopoietic Stem Cell Heterogeneity. *Cell Stem Cell* [Internet]. 2018;22(5):627–38. Available from: <https://doi.org/10.1016/j.stem.2018.04.003>
 66. Rodriguez-Fraticelli AE, Wolock SL, Weinreb CS, Panero R, Patel SH, Jankovic M, et al. Clonal analysis of lineage fate in native haematopoiesis. *Nature*.

2018;553(7687):212–6.

67. Hérault L, Poplineau M, Mazuel A, Platet N, Remy É, Duprez E. Single-cell RNA-seq reveals a concomitant delay in differentiation and cell cycle of aged hematopoietic stem cells. *BMC Biol* [Internet]. 2021 Dec 1 [cited 2021 Jun 9];19(1):1–20. Available from: <https://doi.org/10.1186/s12915-021-00955-z>
68. Sawai CM, Babovic S, Upadhaya S, Knapp DJHF, Lavin Y, Lau CM, et al. Hematopoietic Stem Cells Are the Major Source of Multilineage Hematopoiesis in Adult Animals. *Immunity* [Internet]. 2016 Sep 20 [cited 2021 Jun 9];45(3):597–609. Available from: <http://dx.doi.org/10.1016/j.immuni.2016.08.007>
69. Säwen P, Eldeeb M, Erlandsson E, Kristiansen TA, Laterza C, Kokaia Z, et al. Murine HSCs contribute actively to native hematopoiesis but with reduced differentiation capacity upon aging. *Elife*. 2018 Dec 1;7.
70. Giladi A, Paul F, Herzog Y, Lubling Y, Weiner A, Yofe I, et al. Single-cell characterization of haematopoietic progenitors and their trajectories in homeostasis and perturbed haematopoiesis. *Nat Cell Biol* [Internet]. 2018 Jul 18;20(7):836–46. Available from: <http://dx.doi.org/10.1038/s41556-018-0121-4>
71. Buenrostro JD, Corces MR, Lareau CA, Wu B, Schep AN, Aryee MJ, et al. Integrated Single-Cell Analysis Maps the Continuous Regulatory Landscape of Human Hematopoietic Differentiation. *Cell* [Internet]. 2018;173(6):1535–1548.e16. Available from: <https://doi.org/10.1016/j.cell.2018.03.074>
72. Orkin SH, Zon LI. Hematopoiesis: An Evolving Paradigm for Stem Cell Biology. *Cell*. 2008;132(4):631–44.
73. Acar M, Kocherlakota KS, Murphy MM, Peyer JG, Oguro H, Inra CN, et al. Deep imaging of bone marrow shows non-dividing stem cells are mainly perisinusoidal. *Nature* [Internet]. 2015 Oct 23;526(7571):126–30. Available from: <http://www.nature.com/articles/nature15250>
74. Schwartzman O, Tanay A. Single-cell epigenomics: techniques and emerging applications. *Nat Rev Genet* [Internet]. 2015 Dec;16(12):716–26. Available from: <http://dx.doi.org/10.1038/nrg3980>
75. Lara-Astiaso D, Weiner A, Lorenzo-Vivas E, Zaretzky I, Jaitin DA, David E, et al. Chromatin state dynamics during blood formation. *Science* (80-) [Internet]. 2014 Aug 22;345(6199):943–9. Available from: <http://www.sciencemag.org/cgi/doi/10.1126/science.1256271>
76. Laurenti E, Doulatov S, Zandi S, Plumb I, Chen J, April C, et al. The transcriptional architecture of early human hematopoiesis identifies multilevel control of lymphoid commitment. *Nat Immunol* [Internet]. 2013 Jul 26;14(7):756–63. Available from: <http://www.nature.com/articles/ni.2615>
77. Novershtern N, Subramanian A, Lawton LN, Mak RH, Haining WN, McConkey ME, et al. Densely interconnected transcriptional circuits control cell states in human hematopoiesis. *Cell* [Internet]. 2011;144(2):296–309. Available from: <http://dx.doi.org/10.1016/j.cell.2011.01.004>
78. Paul WE. *Fundamental immunology*. 7th ed. Paul WE, editor. Philadelphia: LIPPINCOTT WILLIAMS & WILKINS; 2013. 325–354 p.

79. Somasundaram R, Prasad MAJ, Ungerback J, Sigvardsson M. Transcription factor networks in B-cell differentiation link development to acute lymphoid leukemia. *Blood*. 2015;126(2):144–52.
80. Taghon T, Yui MA, Pant R, Diamond RA, Rothenberg E V. Developmental and Molecular Characterization of Emerging β - and $\gamma\delta$ -Selected Pre-T Cells in the Adult Mouse Thymus. *Immunity* [Internet]. 2006 Jan;24(1):53–64. Available from: <http://linkinghub.elsevier.com/retrieve/pii/S1074761305004073>
81. Koch U, Radtke F. Mechanisms of T cell Development and Transformation. *Annu Rev Cell Dev Biol* [Internet]. 2011;27:539–62. Available from: <http://www.ncbi.nlm.nih.gov/pubmed/21740230>
82. Schlenner SM, Rodewald HR. Early T cell development and the pitfalls of potential. *Trends Immunol*. 2010;31(8):303–10.
83. Zlotoff DA, Sambandam A, Logan TD, Bell JJ, Schwarz BA, Bhandoola A. CCR7 and CCR9 together recruit hematopoietic progenitors to the adult thymus. *Blood*. 2010;115(10):1897–905.
84. Yui MA, Rothenberg E V. Developmental gene networks: a triathlon on the course to T cell identity. *Nat Rev Immunol* [Internet]. 2014 Jul 25;14(8):529–45. Available from: <http://www.nature.com/doi/10.1038/nri3702>
85. Longabaugh WJR, Zeng W, Zhang JA, Hosokawa H, Jansen CS, Li L, et al. Bcl11b and combinatorial resolution of cell fate in the T-cell gene regulatory network. *Proc Natl Acad Sci* [Internet]. 2017;114(23):5800–7. Available from: <http://www.pnas.org/lookup/doi/10.1073/pnas.1610617114>
86. Parker ME, Ciofani M. Regulation of $\gamma\delta$ T Cell Effector Diversification in the Thymus. *Front Immunol*. 2020;11(January):1–11.
87. Michie AM, Zúñiga-Pflücker JC. Regulation of thymocyte differentiation: pre-TCR signals and β -selection. *Semin Immunol* [Internet]. 2002 Oct;14(5):311–23. Available from: <https://linkinghub.elsevier.com/retrieve/pii/S1044532302000647>
88. Wolfer A, Bakker T, Wilson A, Nicolas M, Ioannidis V, Littman DR, et al. Inactivation of Notch 1 in immature thymocytes does not perturb CD4 or CD8T cell development. *Nat Immunol* [Internet]. 2001 Mar 1;2(3):235–41. Available from: http://www.nature.com/nj/journal/v2/n3/abs/ni0301_235.html%5Cnhttp://www.ncbi.nlm.nih.gov/pubmed/11224523
89. Wolfer A, Wilson A, Nemir M, MacDonald HR, Radtke F. Inactivation of Notch1 impairs VDJbeta rearrangement and allows pre-TCR- independent survival of early alpha beta Lineage Thymocytes. *Immunity* [Internet]. 2002;16(6):869–79. Available from: <http://www.ncbi.nlm.nih.gov/htbin-post/Entrez/query?db=m&form=6&dopt=r&uid=12121668>
90. Shan Q, Zeng Z, Xing S, Li F, Hartwig SM, Gullicksrud JA, et al. The transcription factor Runx3 guards cytotoxic CD8+ effector T cells against deviation towards follicular helper T cell lineage. *Nat Immunol* [Internet]. 2017;(June). Available from: <http://www.nature.com/doi/10.1038/ni.3773>
91. Taniuchi I. CD4 Helper and CD8 Cytotoxic T Cell Differentiation. *Annu Rev*

Immunol. 2018;36:579–601.

92. Xing S, Li F, Zeng Z, Zhao Y, Yu S, Shan Q, et al. Tcf1 and Lef1 transcription factors establish CD8⁺ T cell identity through intrinsic HDAC activity. *Nat Immunol* [Internet]. 2016;17(6):695–703. Available from: <http://www.nature.com/doi/10.1038/ni.3456>
93. Lee W, Lee GR. Transcriptional regulation and development of regulatory T cells. *Exp Mol Med* [Internet]. 2018;50(3):e456–10. Available from: <http://dx.doi.org/10.1038/emm.2017.313>
94. Ribot JC, Lopes N, Silva-Santos B. $\gamma\delta$ T cells in tissue physiology and surveillance. *Nat Rev Immunol* [Internet]. 2021;21(4):221–32. Available from: <http://dx.doi.org/10.1038/s41577-020-00452-4>
95. Koch U, Fiorini E, Benedito R, Besseyrias V, Schuster-Gossler K, Pierres M, et al. Delta-like 4 is the essential, nonredundant ligand for Notch1 during thymic T cell lineage commitment. *J Exp Med*. 2008;205(11):2515–23.
96. Fiorini E, Merck E, Wilson A, Ferrero I, Jiang W, Koch U, et al. Dynamic Regulation of Notch 1 and Notch 2 Surface Expression during T Cell Development and Activation Revealed by Novel Monoclonal Antibodies. *J Immunol* [Internet]. 2009 Dec 1 [cited 2021 Jun 13];183(11):7212–22. Available from: <http://www.jimmunol.org/content/183/11/7212><http://www.jimmunol.org/content/183/11/7212.full#ref-list-1>
97. Yashiro-Ohtani Y, He Y, Ohtani T, Jones ME, Shestova O, Xu L, et al. Pre-TCR signaling inactivates Notch1 transcription by antagonizing E2A. [cited 2021 Jul 13]; Available from: <http://www.genesdev.org>.
98. Huang G, Zhang P, Hirai H, Elf S, Yan X, Chen Z, et al. PU.1 is a major downstream target of AML1 (RUNX1) in adult mouse hematopoiesis. *Nat Genet* [Internet]. 2008;40(1):51–60. Available from: <http://www.nature.com/doi/10.1038/ng.2007.7>
99. Weber BN, Chi AW, Chavez A, Yashiro-Ohtani Y, Yang Q, Shestova O, et al. A critical role for TCF-1 in T-lineage specification and differentiation. *Nature* [Internet]. 2011 Aug 3;476(7358):63–8. Available from: <http://dx.doi.org/10.1038/nature10279>
100. Del Real MM, Rothenberg E V. Architecture of a lymphomyeloid developmental switch controlled by PU.1, Notch and Gata3. *Development* [Internet]. 2013 Mar;140(6):1207–19. Available from: <http://www.ncbi.nlm.nih.gov/pubmed/23444353>
101. Staal FJT, Clevers HC. Wnt signaling in the thymus. *Curr Opin Immunol* [Internet]. 2003 Apr;15(2):204–8. Available from: <http://www.ncbi.nlm.nih.gov/pubmed/12633671>
102. Germar K, Dose M, Konstantinou T, Zhang J, Wang H, Lobry C, et al. T-cell factor 1 is a gatekeeper for T-cell specification in response to Notch signaling. *Proc Natl Acad Sci U S A* [Internet]. 2011 Dec 13;108(50):20060–5. Available from: <http://www.ncbi.nlm.nih.gov/pubmed/22109558>

103. Verbeek S, Izon D, Hofhuis F, Robanus-Maandag E, te Riele H, van de Wetering M, et al. An HMG-box-containing T-cell factor required for thymocyte differentiation. *Nature* [Internet]. 1995 Mar 2 [cited 2021 Jun 13];374(6517):70–4. Available from: <http://www.ncbi.nlm.nih.gov/pubmed/7870176>
104. Staal FJ, Meeldijk J, Moerer P, Jay P, van de Weerd BC, Vainio S, et al. Wnt signaling is required for thymocyte development and activates Tcf-1 mediated transcription. *Eur J Immunol* [Internet]. 2001 Jan;31(1):285–93. Available from: <http://www.ncbi.nlm.nih.gov/pubmed/11265645>
105. Yu S, Zhou X, Steinke FC, Liu C, Chen SC, Zagorodna O, et al. The TCF-1 and LEF-1 Transcription Factors Have Cooperative and Opposing Roles in T Cell Development and Malignancy. *Immunity*. 2012;37(5):813–26.
106. Emmanuel AO, Arnovitz S, Haghi L, Mathur PS, Mondal S, Quandt J, et al. TCF-1 and HEB cooperate to establish the epigenetic and transcription profiles of CD4+CD8+ thymocytes. *Nat Immunol* [Internet]. 2018;19(December). Available from: <http://dx.doi.org/10.1038/s41590-018-0254-4>
107. Johnson JL, Georgakilas G, Petrovic J, Bhandoola A, Wherry EJ, Johnson JL, et al. Lineage-Determining Transcription Factor TCF-1 Initiates the Epigenetic Identity of T Cells Article Lineage-Determining Transcription Factor TCF-1 Initiates the Epigenetic Identity of T Cells. *Immunity* [Internet]. 2018;48(2):243–257.e10. Available from: <https://doi.org/10.1016/j.immuni.2018.01.012>
108. Bosticardo M, Pala F, Calzoni E, Delmonte OM, Dobbs K, Gardner CL, et al. Artificial thymic organoids represent a reliable tool to study T-cell differentiation in patients with severe T-cell lymphopenia. *Blood Adv*. 2020;4(12):2611–6.
109. Mancebo E, Clemente J, Sanchez J, Ruiz-Contreras J, De Pablos P, Cortezon S, et al. Longitudinal analysis of immune function in the first 3 years of life in thymectomized neonates during cardiac surgery. *Clin Exp Immunol* [Internet]. 2008 Dec 1 [cited 2021 Jun 13];154(3):375–83. Available from: <https://onlinelibrary.wiley.com/doi/full/10.1111/j.1365-2249.2008.03771.x>
110. Van Den Broek T, Delemarre EM, Janssen WJM, Nievelstein RAJ, Broen JC, Tesselaar K, et al. Neonatal thymectomy reveals differentiation and plasticity within human naive T cells. *J Clin Invest*. 2016 Mar 1;126(3):1126–36.
111. Kumar B V., Connors TJ, Farber DL. Human T Cell Development, Localization, and Function throughout Life. *Immunity*. 2018;48(2):202–13.
112. Weng AP, Ferrando AA, Lee W, Morris JP, Silverman LB, Sanchez-Irizarry C, et al. Activating mutations of NOTCH1 in human T cell acute lymphoblastic leukemia. *Science* [Internet]. 2004;306(5694):269–71. Available from: <http://www.sciencemag.org/cgi/doi/10.1126/science.1102160><http://www.ncbi.nlm.nih.gov/pubmed/15472075>
113. Cancer Research UK [Internet]. Acute lymphoblastic leukaemia (ALL) statistics. Available from: <https://www.cancerresearchuk.org/health-professional/cancer-statistics/statistics-by-cancer-type/leukaemia-all/incidence#heading=Two>
114. NIH. Cancer Stat Facts: Leukemia — Acute Lymphocytic Leukemia (ALL) [Internet]. Available from: <https://seer.cancer.gov/statfacts/html/aly1.html>

115. Hoelzer D, Bassan R, Dombret H, Fielding A, Ribera JM, Buske C, et al. Acute lymphoblastic leukaemia in adult patients: ESMO clinical practice guidelines for diagnosis, treatment and follow-up. *Ann Oncol*. 2016;27(February):v69–82.
116. Hoffbrand V, Moss P. *Essential Haematology*. 6th ed. Wiley-Blackwell; 2011.
117. Kumar V, Abbas AK, Aster JC, Cotran RS, Robbins SL (Stanley L. Robbins & Cotran pathologic basis of disease. 10th ed. Elsevier; 2020.
118. Chiaretti S, Zini G, Bassan R. Diagnosis and subclassification of acute lymphoblastic leukemia. *Mediterr J Hematol Infect Dis*. 2014;6(1).
119. Raetz EA, Teachey DT. T-cell acute lymphoblastic leukemia. *Hematology*. 2016;2016(1):580–8.
120. Castaneda Puglianini O, Papadantonakis N. Early precursor T-cell acute lymphoblastic leukemia: current paradigms and evolving concepts. *Ther Adv Hematol*. 2020;11:204062072092947.
121. Zhang J, Ding L, Holmfeldt L, Wu G, Heatley SL, Payne-Turner D, et al. The genetic basis of early T-cell precursor acute lymphoblastic leukaemia. *Nature* [Internet]. 2012;481(7380):157–63. Available from: <http://www.nature.com/doi/10.1038/nature10725>
122. Jain N, Lamb A V., O'Brien S, Ravandi F, Konopleva M, Jabbour E, et al. Early T-cell precursor acute lymphoblastic leukemia/lymphoma (ETP-ALL/LBL) in adolescents and adults: A high-risk subtype. *Blood*. 2016;127(15):1863–9.
123. Kumar A, Drusbosky LM, Meacham A, Turcotte M, Bhargav P, Vasista S, et al. Computational modeling of early T-cell precursor acute lymphoblastic leukemia (ETP-ALL) to identify personalized therapy using genomics. *Leuk Res*. 2019;78(November 2018):3–11.
124. Pui C-H, Robison LL, Look AT. Acute lymphoblastic leukaemia. *Lancet* [Internet]. 2008 Mar;371(9617):1030–43. Available from: <http://linkinghub.elsevier.com/retrieve/pii/S0140673608604572>
125. Chiang MY, Radojcic V, Maillard I. Oncogenic Notch signaling in T-cell and B-cell lymphoproliferative disorders. *Curr Opin Hematol* [Internet]. 2016;23(4):1. Available from: <http://content.wkhealth.com/linkback/openurl?sid=WKPTLP:landingpage&an=00062752-9000000000-99473>
126. Gallo Llorente L, Luther H, Schneppenheim R, Zimmermann M, Felice M, Horstmann MA. Identification of novel NOTCH1 mutations: Increasing our knowledge of the NOTCH signaling pathway. *Pediatr Blood Cancer* [Internet]. 2014 May;61(5):788–96. Available from: <http://doi.wiley.com/10.1002/pbc.24852>
127. De Bie J, Demeyer S, Alberti-Servera L, Geerdens E, Segers H, Broux M, et al. Single-cell sequencing reveals the origin and the order of mutation acquisition in T-cell acute lymphoblastic leukemia. *Leukemia*. 2018;32(6):1358–69.
128. Belver L, Ferrando A. The genetics and mechanisms of T cell acute lymphoblastic leukaemia. *Nat Publ Gr* [Internet]. 2016;16(8):494–507. Available from: <http://dx.doi.org/10.1038/nrc.2016.63>

129. Pinello L, Xu J, Orkin SH, Yuan G-C. Analysis of chromatin-state plasticity identifies cell-type-specific regulators of H3K27me3 patterns. *Proc Natl Acad Sci* [Internet]. 2014 Jan 21;111(3):E344–53. Available from: <http://www.pnas.org/content/early/2014/01/03/1322570111%5Cnhttp://www.ncbi.nlm.nih.gov/pubmed/24395799>
130. Choi Ah, Illendula A, Pulikkan JA, Roderick JE, Tesell J, Yu J, et al. RUNX1 is required for oncogenic Myb and Myc enhancer activity in T-cell acute lymphoblastic leukemia. *Blood* [Internet]. 2017 Oct 12;130(15):1722–33. Available from: <http://www.bloodjournal.org/lookup/doi/10.1182/blood-2017-03-775536>
131. Dadi S, Le Noir S, Payet-Bornet D, Lhermitte L, Zacarias-Cabeza J, Bergeron J, et al. TLX Homeodomain Oncogenes Mediate T Cell Maturation Arrest in T-ALL via Interaction with ETS1 and Suppression of TCR α Gene Expression. *Cancer Cell*. 2012;21(4):563–76.
132. Cordo' V, van der Zwet JCG, Canté-Barrett K, Pieters R, Meijerink JPP. T-cell Acute Lymphoblastic Leukemia: A Roadmap to Targeted Therapies. *Blood Cancer Discov*. 2021;2(1):19–31.
133. Kusakabe M, Sun AC, Tyshchenko K, Wong R, Nanda A, Shanna C, et al. Synthetic modeling reveals HOXB genes are critical for the initiation and maintenance of human leukemia. *Nat Commun* [Internet]. 2019;10(1):1–15. Available from: <http://dx.doi.org/10.1038/s41467-019-10510-8>
134. Liu Y, Easton J, Shao Y, Maciaszek J, Wang Z, Wilkinson MR, et al. The genomic landscape of pediatric and young adult T-lineage acute lymphoblastic leukemia. *Nat Genet* [Internet]. 2017 Jul 3;49(8):1211–8. Available from: <http://www.nature.com/doi/10.1038/ng.3909>
135. Ma X, Liu, Yu Yanling Y, Alexandrov LB, Edmonson MN, Gawad C, Zhou X, et al. Pan-cancer genome and transcriptome analyses of 1,699 paediatric leukaemias and solid tumours. *Nature* [Internet]. 2018 Mar 15;555(7696):371–6. Available from: <http://dx.doi.org/10.1038/nature25795>
136. Jenkins CE, Gusscott S, Wong RJ, Shevchuk OO, Rana G, Giambra V, et al. RUNX1 promotes cell growth in human T-cell acute lymphoblastic leukemia by transcriptional regulation of key target genes. *Exp Hematol* [Internet]. 2018;64(Lic):84–96. Available from: <https://doi.org/10.1016/j.exphem.2018.04.008>
137. Chang JE, Medlin SC, Kahl BS, Longo WL, Williams EC, Lionberger J, et al. Augmented and standard Berlin–Frankfurt–Münster chemotherapy for treatment of adult acute lymphoblastic leukemia. *Leuk Lymphoma* [Internet]. 2008 Jan;49(12):2298–307. Available from: <http://www.tandfonline.com/doi/full/10.1080/10428190802517732>
138. Ferrarotto R, Mitani Y, Diao L, Gujjarro I, Wang J, Zweidler-McKay P, et al. Activating NOTCH1 mutations define a distinct subgroup of patients with adenoid cystic carcinoma who have poor prognosis, propensity to bone and liver metastasis, and potential responsiveness to Notch1 inhibitors. *J Clin Oncol*. 2017;35(3):352–60.

139. Couch JA, Zhang G, Beyer JC, Zuch De Zafra CL, Gupta P, Kamath A V., et al. Balancing Efficacy and Safety of an Anti-DLL4 Antibody through Pharmacokinetic Modulation. *Clin Cancer Res.* 2016;22(6):1469–79.
140. Weng AP, Millholland JM, Yashiro-Ohtani Y, Arcangeli ML, Lau A, Wai C, et al. c-Myc is an important direct target of Notch1 in T-cell acute lymphoblastic leukemia/lymphoma. *Genes Dev.* 2006;20(15):2096–109.
141. Yashiro-Ohtani Y, Wang H, Zang C, Arnett KL, Bailis W, Ho Y, et al. Long-range enhancer activity determines Myc sensitivity to Notch inhibitors in T cell leukemia. *Proc Natl Acad Sci [Internet].* 2014 Nov 18;111(46):E4946–53. Available from: <http://www.ncbi.nlm.nih.gov/pubmed/25369933>
142. Herranz D, Ambesi-Impiombato A, Palomero T, Schnell S a, Belver L, Wendorff AA, et al. A NOTCH1-driven MYC enhancer promotes T cell development, transformation and acute lymphoblastic leukemia. *Nat Med [Internet].* 2014;20(10):1130–7. Available from: <http://www.ncbi.nlm.nih.gov/pubmed/25194570> <http://www.pubmedcentral.nih.gov/articlerender.fcgi?artid=4192073&tool=pmcentrez&rendertype=abstract>
143. Kalkat M, Melo J De, Hickman KA, Lourenco C, Redel C, Resetca D, et al. MYC Deregulation in Primary Human Cancers. *Genes (Basel) [Internet].* 2017 Jun 1 [cited 2021 Jul 25];8(6):2–30. Available from: <https://pmc/articles/PMC5485515/>
144. Jia Y, Chng W-J, Zhou J. Super-enhancers: critical roles and therapeutic targets in hematologic malignancies. *J Hematol Oncol [Internet].* 2019 Dec 16 [cited 2021 Jun 13];12(1):77. Available from: <https://doi.org/10.1186/s13045-019-0757-y>
145. Bahr C, Paleske L von, Uslu V V., Remeseiro S, Takayama N, Ng SW, et al. A Myc enhancer cluster regulates normal and leukaemic haematopoietic stem cell hierarchies. 2018 Jan [cited 2021 Jun 13];553(7689):515–20. Available from: <https://www.nature.com/articles/nature25193>
146. Zhou H, Schmidt SCS, Jiang S, Willox B, Bernhardt K, Liang J, et al. Epstein-barr virus oncoprotein super-enhancers control B cell growth. *Cell Host Microbe.* 2015 Feb 11;17(2):205–16.
147. Sanchez-Martin M, Ferrando A. The NOTCH1-MYC highway toward T-cell acute lymphoblastic leukemia. *Blood [Internet].* 2017 Mar 2;129(9):1124–33. Available from: <http://www.ncbi.nlm.nih.gov/pubmed/28115368>
148. Chan SM, Weng AP, Tibshirani R, Aster JC, Utz PJ. Notch signals positively regulate activity of the mTOR pathway in T-cell acute lymphoblastic leukemia. *Blood [Internet].* 2007 Jul 1 [cited 2021 Jun 13];110(1):278–86. Available from: <http://www-stat.stanford.edu/>
149. Belver L, Yang AY, Alberio R, Herranz D, Brundu FG, Quinn SA, et al. GATA3-controlled nucleosome eviction drives MYC enhancer activity in T-cell development and leukemia. *Cancer Discov.* 2019;9(12):1774–91.
150. Kramer AC, Kothari A, Wilson WC, Celik H, Nikitas J, Mallaney C, et al. Dnmt3a regulates T-cell development and suppresses T-ALL transformation. *Leukemia [Internet].* 2017;31(11):2479–90. Available from:

<http://dx.doi.org/10.1038/leu.2017.89>

151. Ntziachristos P, Tsirigos A, Vlierberghe P Van, Nedjic J, Trimarchi T, Flaherty MS, et al. Genetic inactivation of the polycomb repressive complex 2 in T cell acute lymphoblastic leukemia. *Nat Med* [Internet]. 2012;18(2):298–303. Available from: <http://www.nature.com/doi/10.1038/nm.2651>
152. Greally JM. A user's guide to the ambiguous word "epigenetics." *Nat Rev Mol Cell Biol* [Internet]. 2018;19(4):207–8. Available from: <http://dx.doi.org/10.1038/nrm.2017.135>
153. Zhao S, Allis CD, Wang GG. The language of chromatin modification in human cancers. *Nat Rev Cancer* [Internet]. 2021;0123456789. Available from: <http://dx.doi.org/10.1038/s41568-021-00357-x>
154. Bannister AJ, Kouzarides T. Regulation of chromatin by histone modifications. *Cell Res*. 2011;21(3):381–95.
155. Hyun K, Jeon J, Park K, Kim J. Writing, erasing and reading histone lysine methylations. *Exp Mol Med*. 2017;49(4).
156. Landt SG, Marinov GK, Kundaje A, Kheradpour P, Pauli F, Batzoglou S, et al. ChIP-seq guidelines and practices of the ENCODE and modENCODE consortia. *Genome Res* [Internet]. 2012 Sep 1;22(9):1813–31. Available from: <http://genome.cshlp.org/cgi/doi/10.1101/gr.136184.111>
157. Donaldson-Collier MC, Sungalee S, Zufferey M, Tavernari D, Katanayeva N, Battistello E, et al. EZH2 oncogenic mutations drive epigenetic, transcriptional, and structural changes within chromatin domains. *Nat Genet* [Internet]. 2019;51(3):517–28. Available from: <http://dx.doi.org/10.1038/s41588-018-0338-y>
158. Rowley MJ, Corces VG. Organizational principles of 3D genome architecture. *Nat Rev Genet* [Internet]. 2018;19(12):789–800. Available from: <http://dx.doi.org/10.1038/s41576-018-0060-8>
159. Rao SSP, Huntley MH, Durand NC, Stamenova EK, Bochkov ID, Robinson JT, et al. A 3D map of the human genome at kilobase resolution reveals principles of chromatin looping. *Cell* [Internet]. 2014;159(7):1665–80. Available from: <http://dx.doi.org/10.1016/j.cell.2014.11.021>
160. Guo Y, Xu Q, Canzio D, Shou J, Li J, Gorkin DU, et al. CRISPR Inversion of CTCF Sites Alters Genome Topology and Enhancer/Promoter Function. *Cell* [Internet]. 2015;162(4):900–10. Available from: <http://dx.doi.org/10.1016/j.cell.2015.07.038>
161. Kane L, Williamson I, Flyamer IM, Kumar Y, Hill RE, Lettice A, et al. Cohesin is required for long-range enhancer action. *bioRxiv* [Internet]. 2021; Available from: <https://www.biorxiv.org/content/10.1101/2021.06.24.449812v1>
162. Magaña-Acosta M, Valadez-Graham V. Chromatin Remodelers in the 3D Nuclear Compartment [Internet]. Vol. 11, *Frontiers in Genetics*. Frontiers Media S.A.; 2020 [cited 2021 Jun 14]. p. 600615. Available from: www.frontiersin.org
163. Mikkelsen TS, Ku M, Jaffe DB, Issac B, Lieberman E, Giannoukos G, et al. Genome-wide maps of chromatin state in pluripotent and lineage-committed

- cells. *Nature* [Internet]. 2007;448(7153):553–60. Available from: <http://www.nature.com/doifinder/10.1038/nature06008>
164. Buenrostro JD, Giresi PG, Zaba LC, Chang HY, Greenleaf WJ. Transposition of native chromatin for fast and sensitive epigenomic profiling of open chromatin, DNA-binding proteins and nucleosome position. *Nat Methods* [Internet]. 2013 Oct 6 [cited 2021 Jun 8];10(12):1213–8. Available from: <http://www.nature.com/doifinder/10.1038/nmeth.2688>
 165. Corces MR, Buenrostro JD, Wu B, Greenside PG, Chan SM, Koenig JL, et al. Lineage-specific and single-cell chromatin accessibility charts human hematopoiesis and leukemia evolution. *Nat Genet* [Internet]. 2016 Aug 15;48(10):1193–203. Available from: <http://www.nature.com/doifinder/10.1038/ng.3646>
 166. Moskowitz DM, Zhang DW, Hu B, Le Saux S, Yanes RE, Ye Z, et al. Epigenomics of human CD8 T cell differentiation and aging. *Sci Immunol* [Internet]. 2017;2(8):eaag0192. Available from: <http://immunology.sciencemag.org/lookup/doi/10.1126/sciimmunol.aag0192>
 167. Ho L, Crabtree GR. Chromatin remodelling during development. *Nature* [Internet]. 2010;463(7280):474–84. Available from: <http://www.nature.com/doifinder/10.1038/nature08911>
 168. Yu VWC, Yusuf RZ, Oki T, Wu J, Saez B, Wang X, et al. Epigenetic Memory Underlies Cell-Autonomous Heterogeneous Behavior of Hematopoietic Stem Cells. *Cell* [Internet]. 2016 Nov 17;167(5):1310–1322.e17. Available from: <http://dx.doi.org/10.1016/j.cell.2016.10.045>
 169. Wei G, Wei L, Zhu J, Zang C, Hu-Li J, Yao Z, et al. Global Mapping of H3K4me3 and H3K27me3 Reveals Specificity and Plasticity in Lineage Fate Determination of Differentiating CD4+ T Cells. *Immunity* [Internet]. 2009;30(1):155–67. Available from: <http://dx.doi.org/10.1016/j.immuni.2008.12.009>
 170. Kloetgen A, Thandapani P, Ntziachristos P, Ghebrechristos Y, Nomikou S, Lazaris C, et al. Three-dimensional chromatin landscapes in T cell acute lymphoblastic leukemia. *Nat Genet*. 2020;52(4):388–400.
 171. Zhang JA, Mortazavi A, Williams BA, Wold BJ, Rothenberg E V. Dynamic transformations of genome-wide epigenetic marking and transcriptional control establish T cell identity. *Cell* [Internet]. 2012;149(2):467–82. Available from: <http://dx.doi.org/10.1016/j.cell.2012.01.056>
 172. Knoechel B, Roderick JE, Williamson KE, Zhu J, Lohr JG, Cotton MJ, et al. An epigenetic mechanism of resistance to targeted therapy in T cell acute lymphoblastic leukemia. *Nat Genet* [Internet]. 2014 Apr 2;46(4):364–70. Available from: <http://dx.doi.org/10.1038/ng.2913>
 173. Murtaugh LC, Stanger BZ, Kwan KM, Melton DA. Notch signaling controls multiple steps of pancreatic differentiation. *Proc Natl Acad Sci U S A* [Internet]. 2003 Dec 9;100(25):14920–5. Available from: <http://www.ncbi.nlm.nih.gov/pubmed/14657333>

174. Kühn R, Schwenk F, Aguet M, Rajewsky K. Inducible gene targeting in mice. *Science* (80-) [Internet]. 1995 Sep 8 [cited 2021 Jun 8];269(5229):1427–9. Available from: <https://science.sciencemag.org/content/269/5229/1427>
175. Brault V, Moore R, Kutsch S, Ishibashi M, Rowitch DH, McMahon AP, et al. Inactivation of the β -catenin gene by Wnt1-Cre-mediated deletion results in dramatic brain malformation and failure of craniofacial development. *Development*. 2001 Apr 15;128(8):1253–64.
176. Woodford-Thomas T, Thomas ML. The leukocyte common antigen, CD45 and other protein tyrosine phosphatases in hematopoietic cells. *Semin Cell Dev Biol*. 1993 Jan 1;4(6):409–18.
177. Pritchard CEJ, Kroese LJ, Huijbers IJ. Direct generation of conditional alleles using CRISPR/Cas9 in mouse zygotes. In: *Methods in Molecular Biology* [Internet]. Humana Press Inc.; 2017 [cited 2021 Jun 8]. p. 21–35. Available from: https://link.springer.com/protocol/10.1007/978-1-4939-7169-5_2
178. Yang H, Wang H, Shivalila CS, Cheng AW, Shi L, Jaenisch R. XOne-step generation of mice carrying reporter and conditional alleles by CRISPR/cas-mediated genome engineering. *Cell*. 2013 Sep 12;154(6):1370.
179. Heigwer F, Kerr G, Boutros M. E-CRISP: Fast CRISPR target site identification [Internet]. Vol. 11, *Nature Methods*. Nature Publishing Group; 2014 [cited 2021 Jun 8]. p. 122–3. Available from: <http://www.e-crisp.org/>.
180. Wilson A, MacDonald HR, Radtke F. Notch 1–Deficient Common Lymphoid Precursors Adopt a B Cell Fate in the Thymus. *J Exp Med* [Internet]. 2001 Oct 1 [cited 2021 Jun 8];194(7):1003–12. Available from: <http://www.jem.org/cgi/content/full/194/7/1003>
181. Naviaux RK, Costanzi E, Haas M, Verma IM. The pCL vector system: rapid production of helper-free, high-titer, recombinant retroviruses. *J Virol* [Internet]. 1996 Aug [cited 2021 Jun 8];70(8):5701–5. Available from: <https://journals.asm.org/journal/jvi>
182. Wendorff AA, Koch U, Wunderlich FT, Wirth S, Dubey C, Brüning JC, et al. Hes1 is a critical but context-dependent mediator of canonical notch signaling in lymphocyte development and transformation. *Immunity*. 2010;33(5):671–84.
183. Liu Z, Chen O, Wall JBJ, Zheng M, Zhou Y, Wang L, et al. Systematic comparison of 2A peptides for cloning multi-genes in a polycistronic vector. *Sci Rep* [Internet]. 2017 Dec 1 [cited 2021 Jun 8];7(1):1–9. Available from: www.nature.com/scientificreports/
184. Giambra V, Jenkins CR, Wang H, Lam SH, Shevchuk OO, Nemirovsky O, et al. NOTCH1 promotes T cell leukemia-initiating activity by RUNX-mediated regulation of PKC- θ and reactive oxygen species. *Nat Med* [Internet]. 2012 Nov [cited 2021 Jun 8];18(11):1693–8. Available from: <https://pubmed.ncbi.nlm.nih.gov/23086478/>
185. Barde I, Salmon P, Trono D. Production and Titration of Lentiviral Vectors. In: *Current Protocols in Neuroscience* [Internet]. John Wiley & Sons, Inc.; 2010 [cited 2021 Jun 8]. p. 4.21.1–4.21.23. Available from: <http://www.addgene.org>

186. Ruedl C, Khameneh HJ, Karjalainen K. Manipulation of immune system via immortal bone marrow stem cells. *Int Immunol* [Internet]. 2008 Jul 3 [cited 2021 Jun 8];20(9):1211–8. Available from: <https://academic.oup.com/intimm/article-lookup/doi/10.1093/intimm/dxn079>
187. Corces MR, Trevino AE, Hamilton EG, Greenside PG, Sinnott-Armstrong NA, Vesuna S, et al. An improved ATAC-seq protocol reduces background and enables interrogation of frozen tissues. *Nat Methods* [Internet]. 2017 Oct 1 [cited 2021 Jun 8];14(10):959–62. Available from: <https://www.nature.com/articles/nmeth.4396>
188. Mellacheruvu D, Wright Z, Couzens AL, Lambert JP, St-Denis NA, Li T, et al. The CRAPome: A contaminant repository for affinity purification-mass spectrometry data. *Nat Methods* [Internet]. 2013 Aug 7 [cited 2021 Jun 20];10(8):730–6. Available from: <http://www.crapome.org/>
189. Robinson JT, Turner D, Durand NC, Thorvaldsdóttir H, Mesirov JP, Aiden EL. Juicebox.js Provides a Cloud-Based Visualization System for Hi-C Data. *Cell Syst*. 2018 Feb 28;6(2):256-258.e1.
190. Al Ait L, Yamak Z, Morgenstern B. DIALIGN at GOBICS--multiple sequence alignment using various sources of external information. *Nucleic Acids Res* [Internet]. 2013 [cited 2021 Jun 8];41(Web Server issue). Available from: <https://pubmed.ncbi.nlm.nih.gov/23620293/>
191. Siepel A, Bejerano G, Pedersen JS, Hinrichs AS, Hou M, Rosenbloom K, et al. Evolutionarily conserved elements in vertebrate, insect, worm, and yeast genomes. *Genome Res* [Internet]. 2005 Aug 1 [cited 2021 Jun 8];15(8):1034–50. Available from: www.genome.org
192. Letunic I, Bork P. Interactive tree of life (iTOL) v3: an online tool for the display and annotation of phylogenetic and other trees. *Nucleic Acids Res* [Internet]. 2016 Jul 8 [cited 2021 Jun 8];44(W1):W242–5. Available from: <http://itol.embl.de>
193. Kim D, Paggi JM, Park C, Bennett C, Salzberg SL. Graph-based genome alignment and genotyping with HISAT2 and HISAT-genotype. *Nat Biotechnol* [Internet]. 2019 Aug 1 [cited 2021 Jun 8];37(8):907–15. Available from: <https://doi.org/10.1038/s41587-019-0201-4>
194. Controlling the False Discovery Rate: A Practical and Powerful Approach to Multiple Testing on JSTOR [Internet]. [cited 2021 Jun 8]. Available from: https://www.jstor.org/stable/2346101?seq=1#metadata_info_tab_contents
195. Subramanian A, Tamayo P, Mootha VK, Mukherjee S, Ebert BL, Gillette MA, et al. Gene set enrichment analysis: A knowledge-based approach for interpreting genome-wide expression profiles. *Proc Natl Acad Sci U S A* [Internet]. 2005 Oct 25 [cited 2021 Jun 8];102(43):15545–50. Available from: www.pnas.org/cgi/doi/10.1073/pnas.0506580102
196. Li H. Aligning sequence reads, clone sequences and assembly contigs with BWA-MEM. 2013 Mar 16 [cited 2021 Jun 8]; Available from: <http://arxiv.org/abs/1303.3997>
197. Zhang Y, Liu T, Meyer CA, Eeckhoutte J, Johnson DS, Bernstein BE, et al. Model-based analysis of ChIP-Seq (MACS). *Genome Biol* [Internet]. 2008 Sep

- 17 [cited 2021 Jun 8];9(9):1–9. Available from: <http://genomebiology.com/2008/9/9/R137>
198. Didion JP, Martin M, Collins FS. Atropos: Specific, sensitive, and speedy trimming of sequencing reads. *PeerJ* [Internet]. 2017 Aug 30 [cited 2021 Jun 8];2017(8):e3720. Available from: <https://github.com/jdidion/atropos>.
199. Parmentier R, Moussy A, Chantalat S, Racine L, Ravi S, Gao NP, et al. Selective silencing rather than targeted activation of gene expression underlies fate choice in human hematopoietic stem cells. *bioRxiv* [Internet]. 2020 Sep 10 [cited 2021 Jun 8];2020.09.09.289751. Available from: <https://europepmc.org/article/ppr/ppr212210>
200. Bentsen M, Goymann P, Schultheis H, Klee K, Petrova A, Wiegandt R, et al. ATAC-seq footprinting unravels kinetics of transcription factor binding during zygotic genome activation. *Nat Commun* [Internet]. 2020 Dec 1 [cited 2021 Jun 8];11(1):1–11. Available from: <https://doi.org/10.1038/s41467-020-18035-1>
201. Fornes O, Castro-Mondragon JA, Khan A, Van Der Lee R, Zhang X, Richmond PA, et al. JASPAR 2020: Update of the open-Access database of transcription factor binding profiles. *Nucleic Acids Res* [Internet]. 2020 Jan 1 [cited 2021 Jun 8];48(D1):D87–92. Available from: <https://academic.oup.com/nar/article/48/D1/D87/5614568>
202. Frankish A, Diekhans M, Ferreira AM, Johnson R, Jungreis I, Loveland J, et al. GENCODE reference annotation for the human and mouse genomes. *Nucleic Acids Res* [Internet]. 2019 Jan 8 [cited 2021 Jun 8];47(D1):D766–73. Available from: <https://academic.oup.com/nar/article/47/D1/D766/5144133>
203. Stark R, Brown G. DiffBind: Differential binding analysis of ChIP-Seq peak data.
204. Gu Z, Eils R, Schlesner M, Ishaque N. EnrichedHeatmap: An R/Bioconductor package for comprehensive visualization of genomic signal associations. *BMC Genomics* [Internet]. 2018 Apr 4 [cited 2021 Jun 8];19(1):1–7. Available from: <https://doi.org/10.1186/s12864-018-4625-x>
205. Maintainer G, Gu Z. Package “rGREAT” Type Package Title Client for GREAT Analysis [Internet]. 2021 [cited 2021 Jun 8]. Available from: <https://git.bioconductor.org/packages/rGREAT>
206. Durand NC, Shamim MS, Machol I, Rao SSP, Huntley MH, Lander ES, et al. Juicer Provides a One-Click System for Analyzing Loop-Resolution Hi-C Experiments. *Cell Syst* [Internet]. 2016 Jul 27 [cited 2021 Jun 8];3(1):95–8. Available from: <http://dx.doi.org/10.1016/j.cels.2016.07.002>
207. Chen C, Yu W, Tober J, Gao P, He B, Lee K, et al. Spatial Genome Reorganization between Fetal and Adult Hematopoietic Stem Cells. *Cell Rep*. 2019 Dec 17;29(12):4200–4211.e7.
208. Dixon JR, Jung I, Selvaraj S, Shen Y, Antosiewicz-Bourget JE, Lee AY, et al. Chromatin architecture reorganization during stem cell differentiation. *Nature* [Internet]. 2015 Feb 19 [cited 2021 Jun 8];518(7539):331–6. Available from: <https://www.nature.com/articles/nature14222>
209. Schmitt AD, Hu M, Ren B. Genome-wide mapping and analysis of chromosome

- architecture. *Nat Rev Mol Cell Biol* [Internet]. 2016 Nov 21 [cited 2021 Jun 8];17(12):743–55. Available from: <http://www.nature.com/doi/10.1038/nrm.2016.104%5Cnhttp://www.ncbi.nlm.nih.gov/pubmed/27580841>
210. Bailey TL, Boden M, Buske FA, Frith M, Grant CE, Clementi L, et al. MEME Suite: Tools for motif discovery and searching. *Nucleic Acids Res* [Internet]. 2009 Jul 1 [cited 2021 Jun 8];37(SUPPL. 2):W202–8. Available from: https://academic.oup.com/nar/article/37/suppl_2/W202/1135092
 211. Quinlan AR, Hall IM. BEDTools: A flexible suite of utilities for comparing genomic features. *Bioinformatics* [Internet]. 2010 Jan 28 [cited 2021 Jun 8];26(6):841–2. Available from: <https://pubmed.ncbi.nlm.nih.gov/20110278/>
 212. Ramírez F, Ryan DP, Grüning B, Bhardwaj V, Kilpert F, Richter AS, et al. deepTools2: a next generation web server for deep-sequencing data analysis. *Nucleic Acids Res* [Internet]. 2016 Jul 8 [cited 2021 Jun 8];44(W1):W160–5. Available from: <https://www.encodeproject.org>.
 213. Greenwald WW, Li H, Benaglio P, Jakubosky D, Matsui H, Schmitt A, et al. Subtle changes in chromatin loop contact propensity are associated with differential gene regulation and expression. *Nat Commun* [Internet]. 2019 Dec 1 [cited 2021 Jun 8];10(1):1–17. Available from: <https://doi.org/10.1038/s41467-019-08940-5>
 214. Greenwald WW, Li H, Smith EN, Benaglio P, Nariai N, Frazer KA. Pgltools: A genomic arithmetic tool suite for manipulation of Hi-C peak and other chromatin interaction data. *BMC Bioinformatics* [Internet]. 2017 Apr 7 [cited 2021 Jun 8];18(1):1–6. Available from: www.github.com/billgreenwald/pgltools,
 215. Cadigan KM, Waterman ML. TCF/LEFs and Wnt signaling in the nucleus. *Cold Spring Harb Perspect Biol* [Internet]. 2012 Nov [cited 2021 Jun 30];4(11). Available from: <http://pmc/articles/PMC3536346/>
 216. Hosokawa H, Ungerback J, Wang X, Matsumoto M, Nakayama KI, Cohen SM, et al. Transcription Factor PU.1 Represses and Activates Gene Expression in Early T Cells by Redirecting Partner Transcription Factor Binding. *Immunity* [Internet]. 2018 Jun 19 [cited 2021 Jun 17];48(6):1119–1134.e7. Available from: <https://pubmed.ncbi.nlm.nih.gov/29924977/>
 217. Mansur MB, Ford AM, van Delft FW, Gonzalez D, Emerenciano M, Maia RC, et al. Occurrence of identical NOTCH1 mutation in non-twin sisters with T-cell acute lymphoblastic leukemia. *Leukemia* [Internet]. 2011 Aug 10 [cited 2021 Jun 17];25(8):1368–70. Available from: <http://www.nature.com/leu>
 218. Rivera R, Murre C. The regulation and function of the Id proteins in lymphocyte development. *Oncogene* [Internet]. 2001 Dec 5 [cited 2021 Jun 24];20(58):8308–16. Available from: www.nature.com/onc
 219. Dunham I, Kundaje A, Aldred SF, Collins PJ, Davis CA, Doyle F, et al. An integrated encyclopedia of DNA elements in the human genome. *Nature* [Internet]. 2012 Sep 6 [cited 2021 Jun 17];489(7414):57–74. Available from: <http://encodeproject.org/ENCODE/>
 220. Heilmann AM, Schrock AB, He J, Nahas M, Curran K, Shukla N, et al. Novel

- PDGFRB fusions in childhood B-And T-Acute lymphoblastic leukemia [Internet]. Vol. 31, Leukemia. Nature Publishing Group; 2017 [cited 2021 Jun 17]. p. 1989–92. Available from: <https://www.nature.com/articles/leu2017161>
221. Wang H, Zang C, Taing L, Arnett KL, Wong YJ, Pear WS, et al. NOTCH1-RBPJ complexes drive target gene expression through dynamic interactions with superenhancers. *Proc Natl Acad Sci U S A* [Internet]. 2014;111(2):705–10. Available from: <http://www.pnas.org/content/111/2/705.long>
 222. Richter-Pechańska P, Kunz JB, Hof J, Zimmermann M, Rausch T, Bandapalli OR, et al. Identification of a genetically defined ultra-high-risk group in relapsed pediatric T-lymphoblastic leukemia. *Blood Cancer J* [Internet]. 2017 Feb 3 [cited 2021 Jun 17];7(2):523. Available from: www.nature.com/bcj
 223. Li X, Gounari F, Protopopov A, Khazaie K, von Boehmer H. Oncogenesis of T-ALL and nonmalignant consequences of overexpressing intracellular NOTCH1. *J Exp Med* [Internet]. 2008;205(12):2851–61. Available from: <http://www.ncbi.nlm.nih.gov/pubmed/18981238>
 224. Gekas C, Altri TD, Aliqué R, González J, Espinosa L, Bigas A. β -Catenin is required for T-cell leukemia initiation and MYC transcription downstream of Notch1. *Nat Publ Gr*. 2016;(May):2002–10.
 225. Guo Z, Dose M, Kovalovsky D, Chang R, O'Neil J, Look AT, et al. β -Catenin stabilization stalls the transition from double-positive to single-positive stage and predisposes thymocytes to malignant transformation. *Blood* [Internet]. 2007 Jun 15 [cited 2021 Jul 19];109(12):5463–72. Available from: <http://ashpublications.org/blood/article-pdf/109/12/5463/1480990/zh801207005463.pdf>
 226. Bigas A, Guillén Y, Schoch L, Arambilet D. Revisiting β -Catenin Signaling in T-Cell Development and T-Cell Acute Lymphoblastic Leukemia. *BioEssays*. 2020;42(2):1–10.
 227. Steinke FC, Yu S, Zhou X, He B, Yang W, Zhou B, et al. TCF-1 and LEF-1 act upstream of Th-POK to promote the CD4⁺ T cell fate and interact with Runx3 to silence Cd4 in CD8⁺ T cells. *Nat Immunol* [Internet]. 2014 May 18 [cited 2021 Jul 7];15(7):646–56. Available from: <http://www.nature.com/doifinder/10.1038/ni.2897>
 228. Wang F, Qi Z, Yao Y, Yu G, Feng T, Zhao T, et al. Exploring the stage-specific roles of Tcf-1 in T cell development and malignancy at single-cell resolution. *Cell Mol Immunol* 2020 183 [Internet]. 2020 Aug 31 [cited 2021 Jul 7];18(3):644–59. Available from: <https://www.nature.com/articles/s41423-020-00527-1>
 229. Zmuidzinis A, Fischer KD, Lira SA, Forrester L, Bryant S, Bernstein A, et al. The vav proto-oncogene is required early in embryogenesis but not for hematopoietic development in vitro. *EMBO J*. 1995;14(1):1–11.
 230. Perez-Cunningham J, Boyer SW, Landon M, Forsberg EC. Hematopoietic stem cell-specific GFP-expressing transgenic mice generated by genetic excision of a pan-hematopoietic reporter gene. *Exp Hematol*. 2016 Aug 1;44(8):755–764.e1.
 231. Ferrero I, Koch U, Claudinot S, Favre S, Radtke F, Luther SA, et al. DL4-

- mediated Notch signaling is required for the development of fetal $\alpha\beta$ and $\gamma\delta$ T cells. *Eur J Immunol* [Internet]. 2013 Nov 1 [cited 2021 Aug 2];43(11):2845–53. Available from: <https://onlinelibrary.wiley.com/doi/full/10.1002/eji.201343527>
232. Ciofani M, Zúñiga-Pflücker JC. Notch promotes survival of pre-T cells at the β -selection checkpoint by regulating cellular metabolism. *Nat Immunol* 2005 69 [Internet]. 2005 Jul 31 [cited 2021 Jul 22];6(9):881–8. Available from: <https://www.nature.com/articles/ni1234>
 233. Aster JC, Pear WS, Blacklow SC. Notch signaling in leukemia. *Annu Rev Pathol* [Internet]. 2008 Feb;3(1):587–613. Available from: <http://www.annualreviews.org/doi/10.1146/annurev.pathmechdis.3.121806.154300>
 234. Fowlkes BJ, Robey EA. A Reassessment of the Effect of Activated Notch1 on CD4 and CD8 T Cell Development. *J Immunol* [Internet]. 2002 Aug 15 [cited 2021 Jul 13];169(4):1817–21. Available from: <https://www.jimmunol.org/content/169/4/1817>
 235. Chiang MY, Xu L, Shestova O, Histen G, L'Heureux S, Romany C, et al. Leukemia-associated NOTCH1 alleles are weak tumor initiators but accelerate K-ras-initiated leukemia. *J Clin Invest* [Internet]. 2008 Sep 2 [cited 2021 Jul 13];118(9):3181–94. Available from: <http://www.jci.org>
 236. Aster JC, Xu L, Karnell FG, Patriub V, Pui JC, Pear WS. Essential Roles for Ankyrin Repeat and Transactivation Domains in Induction of T-Cell Leukemia by Notch1. *Mol Cell Biol* [Internet]. 2000 Oct 15 [cited 2021 Jul 13];20(20):7505–15. Available from: <https://journals.asm.org/journal/mcb>
 237. Ding J, Cardoso AA, Yoshimoto M, Kobayashi M. The Earliest T-Precursors in the Mouse Embryo Are Susceptible to Leukemic Transformation. *Front Cell Dev Biol* [Internet]. 2021 Apr 29 [cited 2021 Jul 13];9:1018. Available from: www.frontiersin.org
 238. Sheridan C. Grail of RAS cancer drugs within reach. *Nat Biotechnol*. 2020 Jan 1;38(1):6–8.
 239. Doroshow JH, Kummur S. Translational research in oncology—10 years of progress and future prospects. *Nat Rev Clin Oncol* 2014 1111 [Internet]. 2014 Oct 7 [cited 2021 Jul 22];11(11):649–62. Available from: <https://www.nature.com/articles/nrclinonc.2014.158>
 240. Dragani TA, Castells A, Kulasingam V, Diamandis EP, Earl H, Iams WT, et al. Major milestones in translational oncology. *BMC Med* 2016 141 [Internet]. 2016 Jul 28 [cited 2021 Jul 22];14(1):1–13. Available from: <https://bmcmmedicine.biomedcentral.com/articles/10.1186/s12916-016-0654-y>
 241. Workman P, Kaye SB. Translating basic cancer research into new cancer therapeutics. *Trends Mol Med* [Internet]. 2002 Apr 1 [cited 2021 Jul 22];8(4):S1–9. Available from: <http://www.cell.com/article/S1471491402023195/fulltext>
 242. Sivakumar A, de las Heras JI, Schirmer EC. Spatial Genome Organization: From Development to Disease. *Front Cell Dev Biol* [Internet]. 2019 Mar 21 [cited 2021 Jul 13];7(MAR):18. Available from: www.frontiersin.org

243. Acton SE, Astarita JL, Malhotra D, Lukacs-Kornek V, Franz B, Hess PR, et al. Podoplanin-Rich Stromal Networks Induce Dendritic Cell Motility via Activation of the C-type Lectin Receptor CLEC-2. *Immunity*. 2012;37(2):276–89.
244. Palomero T, Lim WK, Odom DT, Sulis ML, Real PJ, Margolin A, et al. NOTCH1 directly regulates c-MYC and activates a feed-forward-loop transcriptional network promoting leukemic cell growth. *Proc Natl Acad Sci [Internet]*. 2006 Nov 28 [cited 2021 Jul 23];103(48):18261–6. Available from: <https://www.pnas.org/content/103/48/18261>
245. Sanchez-martin M, Ferrando A, Author C. The NOTCH1-MYC highway towards T-cell acute lymphoblastic leukemia. *Blood [Internet]*. 2017 Jan 23; Available from: c
246. Elnitski L, Ovcharenko I. The hypothesis of ultraconserved enhancer dispensability overturned. *Genome Biol* 2018 191 [Internet]. 2018 May 8 [cited 2021 Jul 24];19(1):1–3. Available from: <https://genomebiology.biomedcentral.com/articles/10.1186/s13059-018-1433-1>
247. Ru B, Sun J, Tong Y, Wong CN, Chandra A, Tang ATS, et al. CR2Cancer: a database for chromatin regulators in human cancer. *Nucleic Acids Res [Internet]*. 2018 Jan 4 [cited 2021 Jul 14];46(D1):D918–24. Available from: <https://academic.oup.com/nar/article/46/D1/D918/4316101>
248. Krönke J, Udeshi ND, Narla A, Grauman P, Hurst SN, McConkey M, et al. Lenalidomide Causes Selective Degradation of IKZF1 and IKZF3 in Multiple Myeloma Cells. *Science [Internet]*. 2014 [cited 2021 Jul 14];343(6168):301. Available from: <https://pmc/articles/PMC4077049/>
249. Holoch D, Moazed D. RNA-mediated epigenetic regulation of gene expression. *Nat Rev Genet [Internet]*. 2015 Jan 2;16(2):71–84. Available from: <http://dx.doi.org/10.1038/nrg3863>
250. Liu X, Zhang Y, Chen Y, Li M, Zhou F, Li K, et al. In Situ Capture of Chromatin Interactions by Biotinylated dCas9. *Cell [Internet]*. 2017 Aug;170(5):1028-1043.e19. Available from: <https://linkinghub.elsevier.com/retrieve/pii/S0092867417308917>

Acknowledgments

With the completion of this thesis, it is the most appropriate time to acknowledge, first, Prof. Freddy Radtke. Since the very first discussions during hiring days, it has been a pleasure to talk to you, be guided by you, and discuss with you not only about the project. Even though we had to completely change my Ph.D. project shortly after beginning, you have always provided useful insights and kept reminding us about priorities and the big picture.

Secondly, I have to thank Dr. Ute Koch, she was my partner in crime from the very first minutes of my time in the lab and was deeply involved in most of the aspects of my lab career. Thank you Ute for having a tremendous amount of patience, understanding and compassion! And of course for all the snacks and drinks that we shared.

Then, a huge thank you to Christelle Dubey and Marianne Nkosi. Both were not only excellent technicians in the lab, but more importantly kind, supportive and fun people to have around. It has been a pleasure to work with you on daily basis! Every after-work game night, or just drink night, with you was pure fun. And there is no better person to finish the parties with than Christelle!

It was a genuine pleasure to work in Freddy's lab thanks to all the lab members. Great bunch of people, always up for a chat or a get-together outside the lab. Tara Sugrue, Alain Kfoury and Markus Germann taught me a lot during the first weeks and months in the lab. Charlotte Urech and Michele Vigolo were always helpful and tremendously kind, even after 'graduating' from the lab. Delphine Tardivon was the best deskmate ever, a huge supporter of snacking in the afternoon. Linlin Cao was a great co-junior Ph.D. student to share the burdens with. Morgane Fournier spread the joy in the lab, quite often in French – forcing me to passively learn multiple expressions. Jelena Zaric shared with everyone not only lab tricks or ancient and foolproof protocols, but also her big heart. Pasqualina Magliano – a beautiful Italian spirit that sometimes 'sacrificed' herself to genotype without me, just to help me out. Erta Xhafa and Jessica Hacheney brought a fresh perspective and energy into our bay.

Next, close collaboration with Nadine Fournier made this project possible. Thank you for all your work, multiple long meetings (over chocolate) and e-mails that allowed us to have all the genomic data analyzed. It has been a pleasure to balance daily struggles with nightly drinks with you.

Thank you to all the collaborators that helped with the project since the generation of the mouse model many years ago. Core facilities at EPFL, especially Valérie, Hervé, Pierre and Margaux from CPG provided great service throughout the years. The amazing Danny Labes from Flow Cytometry Facility at UNIL filled in the shoes for a top-notch FACS facility. The brilliant labs of Andrew P. Weng, Adolfo A. Ferrando and Laura Belver shared their time and resources with us.

Completion of the Ph.D. is never a success of only one person. It is possible thanks to all the friends and colleagues that are part of our lives, sharing moments of struggles and happiness. That is why I am overwhelmingly grateful to all my friends, those back in Poland – you know who you are. In Lausanne, thank you to all my colleagues and friends for being there. However, the Swiss support group has been dominated by two individuals. Dear Amber and Frédérica, thank you for everything: proofreading, hiking, cooking, eating, watching movies in Locarno, sightseeing and many more uncountable moments. It has been a blessing to have you around.

Thank you to all members of the jury: Prof. Elisa Oricchio, Prof. Elisa Laurenti, Prof. Bart Deplancke and Prof. Jules Meijerink for your time and insightful comments.

Przez ostatnie pięć lat, całość tego naukowego przedsięwzięcia była możliwa tylko dzięki zaangażowaniu kilku najważniejszych osób – mojej rodziny! – od młodzieniaszków do seniorów. Dziękuję Wam z całego serca za wsparcie i nieustającą motywację, nawet w nieco gorszych dniach czy chwilach. Wiem, że to nie jest oczywisty wybór w naszej rodzinie by kontynuować karierę naukową. Tym bardziej, że wiąże się to z pobytem za granicą. Jednak dzięki Wam wszystkim, utrzymanym kciukom, pomyślnym myślom i wszelakiemu dobru, nauka (czy raczej sztuka, w końcu to biologia a nie fizyka czy chemia) nie jest taka zła.

Curriculum Vitae

Mateusz Antoszewski

e-mail: mw.antoszewski@gmail.com

Education

- 2016-2021 Ph.D. in Molecular Life Sciences – EPFL, Lausanne, Switzerland
Promoter: Prof. Freddy Radtke
- 2014-2016 Master of Biomedical Sciences, graduated with Magna cum laude –
KU Leuven, Leuven, Belgium.
Promoter: Prof. Massimiliano Mazzone
- 2010-2014 Bachelor of Engineering in Biotechnology – Poznan University of Life
Sciences, Poznan, Poland.

Research

- 2016-2021 **‘Tcf-1 is an essential epigenetic regulator of Notch1-driven T-ALL’**
Doctoral project supervised by Prof. Freddy Radtke at the Swiss Institute
for Experimental Cancer Research (ISREC), School of Life Sciences
(SV), EPFL, Lausanne, Switzerland.
- 2015-2016 **‘Role of macrophage-derived podoplanin in breast cancer
progression’**
Master thesis supervised by Prof. Massimiliano Mazzone at
VIB-KU Leuven Center for Cancer Biology, KU Leuven,
Leuven, Belgium.
- 2013-2014 **‘Bioengineered spider silk spheres as a new drug carrier’**
Internship supervised by Prof. Andrzej Mackiewicz at Department of
Cancer Diagnostics and Immunology at Greater Poland Cancer Centre,
Poznan University of Medical Sciences, Poznan, Poland.

Publications

‘Notch Signaling Promotes Disease Initiation and Progression in Murine
Chronic Lymphocytic Leukemia’ Tardivon D., Antoszewski M., Zangger
N., Nkosi M.,..., Koch U., Radtke F., Blood, June 3, 2021

'Tcf1 is essential for initiation of oncogenic Notch1-driven chromatin topology in T-ALL' Antoszewski M., Fournier N.,..., , Ferrando A.A., Weng A.P., Koch U., Radtke F., Blood, *in revision*

International presentations

- | | |
|---------------|---|
| 21.04.2021 | Poster presentation at the VKS Hematopoiesis symposium (online)

<u>'Tcf1 epigenetically regulates Notch1-driven T-ALL induction at the hematopoietic progenitor level'</u> |
| 28.05.2020 | Oral presentation at the Blood and Bone Seminar (via Zoom)

<u>'Tcf-1 Regulates Epigenetic Landscape in Notch1-driven T-ALL'</u> |
| 06-10.10.2019 | Oral presentation at The Notch Meeting XI, Athens, GR

<u>'Tcf-1 Epigenetically Regulates Initiation of Notch1-driven T-ALL'</u> |
| 08-11.09.2018 | Poster presentation at the ISREC-SCCL Symposium 2018 'Horizons of Cancer Biology and Therapy 2018', Lausanne, CH

<u>'Tcf-1 Mediates Essential Epigenetic Response to Leukemic Notch1 Signalling'</u> |

Extracurricular activity

- | | |
|-----------|---|
| 2020-2021 | <i>Member</i> Gender Equality Committee

School of Life Sciences (SV), EPFL, Lausanne, Switzerland |
| 2020-2021 | <i>Board Member</i> Association of Doctoral Students in Life Sciences

EPFL, Lausanne, Switzerland |
| 2006-2016 | <i>National President, Board Member</i> Leo Clubs Poland and Leo Club Poznan

Lions Clubs International District 121 Poland |
| 2012-2016 | <i>Executive board member</i> Charity Fashion Show Leofashion

Poznan, Poland |